THE DEVELOPMENT OF A COMPLEX CONTINUOUS WAVELET

TRANSFORM BASED HARMONIC ANALYSIS AND DYNAMIC WAVEFORM

RECONSTRUCTION ALGORITHMS

A thesis submitted to

CITY UNIVERSITY

for the Degree of

DOCTOR OF PHILOSOPHY

by

TSE CHUNG FAI, NORMAN

School of Engineering and Mathematical Sciences

City University
Northampton Square
London EC1V 0HB
United Kingdom

JUNE 2007

Abstract

The wide spread use of power electronic equipment has been causing serious current harmonics in electrical power distribution system. Harmonic currents that flow in the electrical power distribution system would cause extra copper loss and immature operation of overcurrent protection devices. Voltage distortion due to harmonic voltage drop in the electrical power distribution system impairs the operation of voltage sensitive equipment. The harmonic distortion of the current and voltage waveforms can be caused by sub-harmonics, integer harmonics and inter-harmonics. Traditionally harmonic distortions are predominately caused by integer harmonics. With the advance of power electronic technology, the amount of sub-harmonics and inter-harmonics are rising and cause problems not experienced before.

In order to improve the electrical power quality and reduce energy wastage in the electrical power distribution system, especially under the deregulated environment, the nature of the harmonics must be identified so that the causes and effects of the harmonics would be studied. Moreover corrective measures cannot be easily implemented without knowing the characteristics of the harmonics existing in the electrical power distribution system.

Power harmonic analysis in electrical power distribution system is essentially related to the topic of waveform distortion analysis commonly encountered in signal processing. Waveform distortion analysis relates to the identification of all harmonics components, including sub-harmonics, integer harmonics and inter-harmonics. Harmonics identification consists of identifying harmonic frequencies, amplitudes and instantaneous phases. In classical signal processing, waveforms are classified into stationary (time-invariant) waveforms and non-stationary (time-variant) waveforms. For non-stationary waveforms, time information is also required.

Traditionally Discrete Fourier Transform (DFT) implemented with Fast Fourier Transform (FFT) is used to analyze stationary waveform distortions with integer harmonics. DFT is not suitable for analyzing waveform distortions caused by sub-harmonics and inter-harmonics. Short-time Fourier Transform (STFT) and Gabor Transform (GT) which are windowed version of DFT were developed for the analysis of time-variant waveforms. These methods have their own usages and limitations. With STFT, one must compromise frequency resolution with time resolution, or vice versa. With GT, the accuracy lies in selecting the right time and frequency parameters, which cannot be done wisely without a prior knowledge of the waveform characteristics.

This thesis reports on the development of a new approach for harmonic analysis which is able to analyze distorted waveforms containing sub-harmonics, integer harmonics and inter-harmonics by identifying their respective harmonics frequencies, amplitudes and instantaneous phases. Wavelet Transform (WT) is used for the new approach. WT is a comparatively new mathematical tool originally developed for signal analysis, which have found applications in many areas of science and engineering. WT makes use of a wavelet which is an oscillating waveform of short duration with magnitudes decaying quickly to zero at both ends. WT is performed by shifting and dilating a mother wavelet. Dilating a mother wavelet varies the frequency of oscillation and time duration simultaneously, while the time duration of DFT is fixed. Shifting the dilated wavelet captures time information of the waveform. With these properties, the WT is most suitable for harmonic analysis. In particular, Continuous Wavelet Transform (CWT) is used for harmonic analysis because of its ability to identify harmonic frequencies accurately.

The simplified Complex Morlet Wavelet (CMW) is selected for the new approach introduced in this thesis. CMW is basically a sinusoid-modulated Gaussian function with harmonic-like shape and smooth decaying magnitudes. CMW achieves the best compromise between time and frequency localization, and therefore can identify frequency information and time information reasonably accurate. A modified CMW is introduced in this thesis which is better suited for harmonics analysis.

A WT-based harmonic analysis algorithm is developed based on the modified CMW, with detailed study on settings of the modified CMW parameters for discriminating adjacent frequencies, determining minimum sampling frequency and minimum harmonic signal

duration. The proposed WT-based harmonic analysis algorithm is tested with synthesized waveforms and field harmonic waveforms vigorously. Harmonic analysis results obtained from DFT implemented with FFT are used to compare with the results obtained from the proposed WT-based algorithm.

Overall, the proposed algorithm is able to identify all harmonic components including integer, non-integer and sub-harmonics. Comparing with DFT, the proposed algorithm achieves exact estimation of the harmonic frequency, amplitude and phase of the harmonic components in power harmonic signals. The power harmonic signal length required by the proposed algorithm is much shorter than the DFT-based algorithm.

The thesis also reports on the development of a WT-based dynamic waveform reconstruction algorithm which is able to identify amplitude variations of harmonic components of the distorted waveform in the examined period. The performance of the WT-based waveform reconstruction algorithm is compared with the performance of the Discrete Waveform Transform based techniques which is used to reconstruct the fundamental frequency component only. It is found that the proposed algorithm is more accurate in reconstructing the waveform of the fundamental frequency component and can be used to reconstruct waveforms of any harmonic components.

Summary of Original Contributions

The following summarizes the original contributions made in this thesis.

1. Development of a Wavelet Transform-based harmonic analysis algorithm by using filter banks generated from modified Complex Morlet Wavelet implemented by Complex Continuous Wavelet Transform. The WT-based approach is capable of identifying sub-harmonics, inter-harmonics and integer harmonics (Chapter 5).

2. Modification of the Complex Morlet Wavelet for the detection of harmonics with very small amplitudes. The filter banks generated by the dilation of the modified Complex Morlet Wavelet have equal lobe height in the frequency domain (Chapter 5).

3. The adoption of the wavelet ridges for estimating harmonic frequencies and amplitudes based on the modified Complex Morlet Wavelet (Chapter 5).

4. Determination of the centre frequency and bandwidth parameter of the modified Complex Morlet Wavelet with respect to the minimum frequency separation between adjacent harmonic frequencies (Chapter 6).

5. Determination of the minimum sampling frequency for the proposed WT-based harmonics analysis algorithm to avoid aliasing (Chapter 6).

6. Determination of the minimum harmonic signal length for the proposed WT-based harmonics analysis algorithm for accurate harmonics detection (Chapter 6).

7. Development of computational formulae for the estimation of the initial phases of harmonics and the phase difference between signals of the same frequency from wavelet coefficients (Chapter 6).

8. Development of a computational algorithm for the WT-based harmonic analysis implemented with FFT. The minimum scale of the decomposition is determined from

the minimum sampling frequency. The maximum scale of decomposition is determined by the length of the signal sufficiently long enough to get rid of edge effects at data ends. The dilation step is determined by the accuracy required in harmonic frequency estimation (Chapter 7).

9.   Testing of the proposed WT-based harmonic algorithm with synthesized harmonic signals and field harmonic signals. The field harmonic signals include input current waveform to VSD and input phase current waveform to a single phase circuit containing nonlinear loads (Chapter 8).

10. Development of a WT-based dynamic waveform reconstruction algorithm for reconstruction of time-variant harmonics waveforms. The algorithm is capable of showing the variation of amplitudes of harmonics over time. The waveform reconstruction algorithm was tested with synthesized harmonic signals and field harmonic signals (Chapter 9).

List of Published Papers

Norman C. F. Tse, *"Practical application of wavelet to power quality analysis,"* Proceedings of the 2006 IEEE Power Engineering Society General Meeting, IEEE Catalogue Number 06CH37818C, June 2006, CD ROM.

Norman C. F. Tse and L. L. Lai, *"Wavelet-based algorithm for detection of voltage fluctuation,"* The 7th International Conference on Advances in Power System Control, Operation and Management, IET Hong Kong APSCOM2006, Oct. 2006, CD-ROM (Paper - APSCOM2006-509).

Norman C. F. Tse and L. L. Lai, *"Wavelet-based algorithm for signal analysis,"* EURASIP Journal on Advances in Signal Processing, vol. 2007, Article ID 38916.

Norman C. F. Tse, *"Wavelet Based Algorithm for Power Quality Analysis,"* accepted to be published in the 2007 IEEE Power Engineering Society General Meeting, June 2007, (Paper 07GM0496).

Acknowledgments

First of all, I would like to express my sincere gratitude to my PhD supervisor Professor L. L. Lai, DSc FIEEE. Without Professor Lai, my PhD study is hardly able to be finished. Many times when my research was stuck by difficult mathematics, unexpected simulation results, or unclear way forward, Professor Lai's encouragements and insightful advices often came just in time and helped to raise my aspirations and to restore my confidence. I am indebted to Professor Lai for his valuable time and effort amid his busy schedule.

My research topic on power harmonics analysis by wavelet transform was inspired by Professor Lai. The topic was certainly a timely issue, and received much attention worldwide in recent years. Through years of study and the scrutiny of thousands of academic and professional papers, I have acquainted myself with the topic both academically and technically. An extra benefit I have gained is the ability to use wavelet transform for mathematical and computational analysis. To me the PhD study is not only meant for attending a qualification, but also a new page in professional development. Professor Lai has indeed inspired me to explore in this direction which I certainly would continue after my PhD degree attainment.

During the critical period of my research study, I had the privilege to have a home stay at Professor Lai's house. I was under a round-the-clock supervision by Professor Lai at that time, and was served with warm reception of his family and delicious meals cooked by Mrs. Lai. That really added colour, taste and good memory to my PhD study and was an experience unforgettable.

I must also thank my local PhD supervisor Dr. Albert So. He provided me with all equipment I needed to conduct testing and furnished me with the necessary data for analysis. He has also given me inspirations and encouragement all along.

My heartfelt thank goes to my wife Rebecca. I really appreciate Rebecca for her support, patience, sacrifice, understanding and prayer. I owe Rebecca thousands of weekends spent in my research study in office in the past six years instead of family gatherings. Without Rebecca's consent, I simply did not have the luxury to take up a tremendous task such as a PhD degree study.

I am sure that my two lovely daughters, Long Ling and Long Ching, will join me in celebrating the end of a stage of academic development and we envisage together for a new phase in life. I have promised them a long vacation holiday after my PhD study!

"For I know the plans I have for you," declares the LORD, "plans to prosper you and not to harm you, plans to give you hope and a future".

Jeremiah 29:11
The Holy Bible

COPYRIGHT DECLARATION

Tse Chung Fai, Norman

Hong Kong, June 2007

Table of Contents

Chapter 10

Conclusions ⋯⋯⋯⋯⋯⋯⋯⋯⋯⋯⋯⋯ 143

References ⋯⋯⋯⋯⋯⋯⋯⋯⋯⋯⋯⋯ 147

Glossary

Abbreviations

ANN	Artificial Neural Network
CMW	Complex Morlet Wavelet
CWT	Continuous Wavelet Transform
D-CWT	Discretised Continuous Wavelet Transform
DFT	Discrete Fourier Transform
DSP	Digital Signal Processing
DTFT	Discrete Time Fourier Transform
DWT	Discrete Wavelet Transform
FFT	Fast Fourier Transform
FS	Fourier Series
HF	High-Pass
IDFT	Inverse Discrete Fourier Transform
LF	Low-Pass
LVQ	Learning Vector Quantization
MCMW	Modified Complex Morlet Wavelet
N-DFT	N-Point Discrete Fourier Transform
QMF	Quadrature Mirror Filter
STFT	Short-Time Fourier Transform
VSD	Variable Speed Drive
WBTA	Wavelet-Based Transient Analysis
WT	Wavelet Transform

Mathematical Notations

$\Delta\omega$	Frequency localization or angular frequency spread
$\varphi(t)$	Wavelet function
E	Energy of a function
$|\varphi(t)|$	Absolute value of a wavelet function
$\Phi(f)$	Fourier transform of a wavelet function
$\hat{g}$	Fourier transform of a function
C_g	Admissibility constant
φ^*	Complex conjugate of the wavelet function
a	Dilation or scale
u	Location parameter
T	Time period
Z	The set of positive integers
$C_{m,n}$	Discrete wavelet coefficients at m, n
N	Number of data points in a wavelet or signal
$Re[\ ]$	Real part of a complex function
$Im[\ ]$	Imaginary part of a complex function
$x[i]$	Discrete time domain series
$X[k]$	Discrete frequency domain series
Δf	Frequency resolution
f_s	Sampling frequency
$f(t)$	Time function
Δt	Time spread
$W_H(t)$	Hamming window function
$Wf(u,a)$	Wavelet transform of a function f at location u and scale a
$P_w f$	Energy function, also called scalogram for wavelet transform
ε	Error term
f_b	Complex Morlet Wavelet bandwidth parameter
f_c	Complex Morlet Wavelet centre frequency
ω_c	Complex Morlet Wavelet angular centre frequency
$\ln$	Natural logarithm

ω	Angular frequency
A / $A(t)$	Amplitude / Amplitude function
ϕ / $\phi(t)$	Phase / Phase function
f_H	Highest frequency
f_L	Lowest frequency
v / $v(t)$	Voltage / Voltage signal function
i / $i(t)$	Current / Current signal function
θ	Initial phase angle
θ_w	Instantaneous phase angle
n	n^{th} data in a discrete time series
f_{sep}	Frequency separation between two adjacent frequencies
a_{min}	Minimum scale
$\langle \ \rangle$	Convolution of the functions

Definition of Common Terms

Harmonics of a signal are the frequency components of the signal.

Sub-harmonics of a signal are frequency components of the signal with frequencies below the fundamental frequency.

Inter-harmonics of a signal are frequency components of the signal with frequencies not integer multiples of the fundamental frequency.

Integer harmonics of a signal are frequency components of the signal with frequencies equal to integer multiples of the fundamental frequency

Stationary or time-invariant signal is a signal for which the signal properties such as amplitude and frequency do not vary with time.

Non-stationary or time-variant signal is a signal for which the signal properties such as amplitude and frequency vary with time.

Beat frequency is equal to the absolute value of the difference in frequency of two waveforms.

High-pass filter is a filter that allows all signals above a given frequency to pass.

Low-pass filter is a filter that allows only frequencies below a given frequency to pass.

Bandpass filter is a filter that allows a given band of frequencies to pass while attenuating all others.

Q-factor of filter is defined as the ratio of the peak frequency to bandwidth of the filter.

Mainlobe height is the peak magnitude of a window function in frequency domain.

Voltage sag is an RMS reduction in the ac voltage at the power frequency, for durations from a half cycle to a few seconds.

List of Figures and Tables

List of Figures

List of Tables

Chapter 1

Introduction

1.1 Motivation for the Research

Power quality [1] has become a major concern for utility, facility and consulting engineers in recent years. International as well as local standards have been formulated to address the power quality issues [2-5]. To the facility managers and end users, frequent complaints by tenants/customers on occasional power failures of computer and communication equipment, and the energy inefficiency of the LV electrical distribution system are on the management's agenda. Harmonic currents produced by nonlinear loads would cause extra copper loss in the distribution network, which on one hand will increase the energy cost and on the other hand would increase the electricity tariff charge. The benefits of using power electronic devices in the LV distribution system in buildings, such as switch mode power supplies, variable speed drive units, etc. to save energy are sometimes offset by the increased energy loss in the distribution cables by current harmonics and the cost of remedial measures required. Voltage harmonics caused by harmonic voltage drops in the distribution cables are affecting the normal operation of voltage sensitive equipment as well.

Although the distorting frequency components are predominantly integer harmonics [6], the amount of sub-harmonics and inter-harmonics are increasing and turning into a major issue. Other power quality issues such as transients, voltage sag and swell, waveform distortion, power frequency variations, etc. are experienced by electricity users frequently.

In order to improve electric power quality and energy efficiency, the nature of harmonics must be identified and studied before appropriate corrective or mitigating actions [7,8] can be taken.

1.2 Power Harmonics Analysis

Power harmonics analysis in electrical power systems is essentially related to the topic of waveform distortion analysis commonly encountered in signal processing. Waveform distortion analysis relates to the identification of all harmonics components, including sub-harmonics, integer harmonics, and inter-harmonics. Any harmonic waveforms can be characterised by their frequencies, amplitudes and instantaneous phases. Time information is required for non-stationary (time-variant) waveforms.

A traditional approach is to use Discrete Fourier Transform (DFT) to analyse harmonics contents of a power signal. The DFT which is implemented by FFT has many attractive features. That theory of FFT has been fully developed and well known; scientists and engineers are familiar with the computation procedures and find it convenient to use as many standard computation tools are readily available. Short-time Fourier Transform (STFT) and Gabor Transform (GF) were developed for estimating time-variant harmonic information. These methods have certain limitations, which will be discussed in detail in Chapter 3.

1.3 Objectives of the Study

The first objective is to develop a robust, reliable and accurate method for waveform distortion analysis which should be able to overcome the limitations of the traditional Discrete Fourier Transform implemented with Fast Fourier Transform. The new method should be able to identify the frequencies, amplitudes and phase information of all distortion harmonic components, including integer harmonics, sub-harmonics and inter-harmonics. It should also be suitable for analysing non-stationary and time-variant waveforms.

The new waveform distortion analysis method is developed from Wavelet Transform. Wavelet transform is a newly developed signal analysis mathematical tool. It has many

practical applications in science, engineering and mathematical fields in recent years. Unlike the Fourier Transform with sinusoidal waveforms as the basis, wavelets are oscillating waveforms of short duration with fast decaying magnitudes. In Wavelet Transform, a so-called mother wavelet is dilated to vary its centre frequency and time duration. A dilated wavelet is shifted along and superimposed onto the signal waveform under analysis to generate the transform coefficients. The dilation and translation processes are important features for analyzing non-stationary waveforms and waveforms containing harmonic frequencies not related by integer multiplication.

Although wavelets are fast-decaying and oscillating waveforms, their lengths are still finite, and a finite length of distortion waveform is required for conducting the analysis. The length of the distortion waveform to be used is dependent on the separation between adjacent frequencies and the frequency resolution required. This will be discussed in detail in Chapter 6.

The second objective of the study is to develop a Wavelet Transform-based method to reconstruct all the harmonic components of the distorted waveform. The new method for harmonic component waveform reconstruction is useful in revealing the variation of waveform amplitudes within the period of analysis of the distortion waveform, which can be adopted for the analysis of time-variant waveforms.

1.4   Organisation of the Thesis

This thesis summarizes the research study findings undertaken to achieve the above two objectives. The thesis consists of the following chapters.

Chapter 2 describes backgrounds on power system waveform problems. It presents the common definitions of power harmonics issues. The causes and origins of power system waveform distortions are discussed and the effects of the distortions are also presented.

Chapter 3 describes the history of Wavelet Transform development. Since Wavelet Transform is a comparatively new tool for power signal analysis, this chapter briefly describes the origin of invention and the definitions of Wavelet Transform. The recent applications of WT in power engineering are also discussed.

Chapter 4 introduces the Fourier Transform. Fourier Transform is a frequency domain analytical tool specifically useful for stationary harmonic analysis. In particular the Discrete Fourier Transform implemented with Fast Fourier Transform is described thoroughly because of its fast and efficient computation capability for harmonic analysis. The underlying principles, assumptions, and the limitations of Discrete Fourier Transform are also presented.

Chapter 5 describes a new approach for harmonic analysis. This approach is based on Continuous Wavelet Transform which does not have the limitations of Fourier Transform-based harmonic analysis. The Continuous Wavelet Transform is used to transform a time signal into a time-frequency representation. Both time information and frequency information are contained in the wavelet coefficients.

The simplified Complex Morlet Wavelet is chosen for the Continuous Wavelet Transform for harmonic analysis. The simplified Complex Morlet Wavelet is a sinusoid-modulated Gaussian function with a smooth declining waveform, which is best suited for harmonic analysis.

Wavelet ridges are used to extract frequency information from the complex wavelet coefficients. The amplitudes of harmonics are readily available in the process of generating the scalogram.

Chapter 6 further introduces a modified Complex Morlet Wavelet to better suit for harmonic analysis and discusses the application of the modified Complex Morlet Wavelet from the perspective of filter banks for harmonics detection. Based on the filter banks generated by the modified Complex Morlet Wavelet, the minimum sampling frequency for representing the harmonic signal is estimated so that aliasing would be avoided.

The shortest time width of the modified Complex Morlet Wavelet, and hence the harmonic signal length required for harmonic analysis, is found to be dependent on the centre frequency and bandwidth of the modified Complex Morlet Wavelet, and the period of the lowest harmonic frequency in the signal. The time width of the CMW should be chosen such that the mean value of the CMW should be close to zero.

This chapter also defines initial phase, instantaneous phase and phase difference from the perspective of wavelet-based harmonic analysis. The complex wavelet coefficients obtained from Continuous Wavelet Transform based on the modified Complex Morlet Wavelet contains the instantaneous phase information. From the instantaneous phase information, the initial phases of the harmonics in the harmonic signal can be estimated. The phase difference between any two harmonics of the same frequency can be calculated from the wavelet coefficients as well.

The proposed wavelet-based harmonic analysis method can be used to detect any frequency components in a signal, including sub-harmonics, integer harmonics, inter-harmonics.

Chapter 7 discusses practical issues related to the implementation of the proposed wavelet-based harmonic analysis algorithm. A computation formula for the estimation of the minimum sampling frequency without aliasing is proposed. The signal time signal is determined mathematically by considering the lowest harmonic frequencies and the separation between adjacent harmonic frequencies in the harmonic signal.

The accuracy in harmonics amplitudes estimation is found to be dependent on the time width of the modified Complex Morlet Wavelet and hence the harmonic signal length used in the harmonic analysis. The setting of the centre frequency and bandwidth of the CMW is dependent on the harmonic frequencies in the signal and the required separation between adjacent harmonic frequencies.

The detection of the initial phases of harmonics requires that the number of data points used in the WT-based estimation algorithm should be an odd number.

The minimum and maximum dilation scales to be used in the Wavelet Transform are discussed and estimated. It is suggested that instead of dilating the CMW by incrementing scales, it would be more convenient and accurate to determine the dilation scales by the frequency range and frequency resolution specified.

Chapter 8 presents the application studies by using the proposed WT-based algorithm for waveform distortion analysis. The robustness of the algorithm is verified using highly

distorted synthesized waveforms containing sub-harmonics, integer harmonics and inter-harmonics. The sensitivity of the WT-based algorithm to harmonics with very small amplitudes is also estimated. The algorithm is then applied to two real field harmonic signals. The first field harmonic signal is obtained from line current input to three-phase variable speed drive and the second field harmonic signal is obtained from the line current input to a group of single-phase loads.

Chapter 9 discusses the development of a WT-based waveform reconstruction algorithm for reconstructing the harmonic waveforms from the complex CWT coefficients. This is useful for identifying the amplitude variations of the harmonic frequency over the estimation time period.

The WT-based reconstruction algorithm is tested with synthesized waveforms and field harmonic waveforms. The tests revealed that the WT-based harmonic waveform reconstruction algorithm is able to reconstruct any harmonic waveforms accurately. The reconstruction accuracy is higher than that produced by Discrete Wavelet Transform (DWT). The reconstruction algorithm is able to display waveform variations of a cycle short. The WT-based reconstruction algorithm is time-invariant and therefore is able to preserve the phase information of the harmonic waveform.

Chapter 10 summarises the work done in the research study. Further improvements and developments areas are suggested.

Chapter 2

Power System Harmonics Problem

2.1 Introduction

Defining the nature and characteristics of a problem is the first step in any problem solving process. This Chapter gives a review of the power system harmonics problems [9]. The evaluation of harmonic distortion is becoming increasingly important for a number of reasons. An increasing percentage of building load consisted of electronic equipment supplied by switched-mode power supplies. These power supplies can have input currents with very high harmonic content. New high-efficiency fluorescent luminaries use electronic ballasts and can have higher harmonic contents than conventional fluorescent luminaries using magnetic ballasts. Much of the HVAC load in buildings is being controlled by variable speed drives in order to improve overall efficiency. These drives together with the drives for electric traction lift systems produce significant harmonic currents.

The overall harmonic levels depend on how the individual harmonics from these loads combine together [10]. In fact, there is usually significant harmonic cancellation in commercial facilities due to the variety of load types. Most harmonic problems are localized to low voltage systems that supply a significant percentage of single phase electronic load. The harmonic current limits specified in IEEE 519-1992 [5] for the overall facility are usually not exceeded.

The voltage distortion levels depend on the circuit impedances as well as the harmonic generation characteristics. The circuit impedance is usually dominated by the step down

transformers and conductor impedances. The current harmonics may also cause resonance with power factor correction capacitors resulting in capacitor breakdown.

2.2 Definitions of Harmonics

Electricity supply is represented in the form of voltage and current. Both the voltage and current are sinusoidal waveforms if the power supply system consists of linear components, collectively represented as resistors, inductors and capacitors. For a steady state power supply analysis, electrical quantities are described by phasor representation, and root-mean-square (RMS) value is conveniently used for power calculation. The phasor representation and the RMS value are valid as long as the voltage and the current are strictly sinusoidal with a constant supply frequency, normally 50Hz or 60Hz, depending on the country of use. However if the loads are nonlinear, the supply current will become non-sinusoidal even though the supply voltage is still sinusoidal [3].

By traditional Fourier Transform analysis, any periodic waveform can be represented by the sum of sinusoids of higher frequencies, which are related to the fundamental frequency by integer multiples. The individual frequency components of the distorted waveform can be described in terms of the harmonic order, magnitude and phase of each component.

Distorted voltage or current waveforms containing periodic distortions of a sinusoidal nature that are not integer multiples of the fundamental supply frequency are termed inter-harmonics.

Flicker is a term used to describe the visual effect of small voltage variations on electrical lighting equipment. The frequency range of disturbances affecting lighting appliances, which are detectable by the human eye, is 1-30Hz, which is also one type of sub-harmonics.

In steady state condition, the periodic non-sinusoidal waveform is time-invariant, harmonics would have a constant magnitude. The magnitude of the harmonics would change due to changes in system configuration or load conditions.

2.3 Sources of Harmonics

Harmonic current is produced by nonlinear circuit components. Harmonic voltage is produced by the harmonic current flow through impedances of the power supply distribution system. Power supply components are connected either in series or in parallel. Current harmonics are produced by parallel elements, and therefore are normally end-user loads. Voltage harmonics are produced by harmonic current flow in the series elements, and are attributed to cables and power distribution equipment such as step up/down transformers [11].

Switched mode electronic power supplies commonly used for electronic equipment are rectifier-inverter bridges for controlling DC or AC motor drives. In both cases, the high peak charging current for the large smoothing capacitor contains a correspondingly higher harmonic content.

With the increasing use of office equipment such as personal computer, printers, copiers and other electronic devices, current harmonics generated is inevitably increasing. Electronic ballasts newly developed to replace the magnetic ballasts for fluorescent luminaries are main sources of harmonics in commercial buildings.

Variable speed drives are used extensively in buildings' water supply systems, air-conditioning systems and electric traction lift system. Variable speed drives use three-phase power converters consisting of six-pulse or twelve-pulse rectifier, which produces harmonics that cause serious problems. As air-conditioning loads and lighting loads together account for 70% of total electrical load of a typical commercial building, power harmonics are no wonder common concerns of building operators and system designers [12].

Saturation effects in transformer and shunt reactors (i.e. parallel inductor) can produce steady-state harmonics, as well as transient harmonics and temporary over-voltage. Magnetization current of a transformer contains even harmonics, although in an amount far below the fifth and the seventh harmonics.

Discharge lamps produce third-harmonic current that may be as high as 30% of the

fundamental and add up to 90% in the neutral wire. Lamp ignition occurs during each half cycle when the applied AC voltage reaches the required firing angle. During conduction, the lamp exhibits a negative resistive characteristic, and a nonlinear ballast circuit is placed in series with the lamp to limit the current.

Arcs in furnaces are significant sources of a wide range of frequency harmonics. A particular feature of the operation of electric arc-furnaces is the frequent recurrence of short circuits between the electrodes and the scrap-metal charge. Often when the molten scrap metal drops away from an electrode the arc will extinguish and no current will flow. During the melt-down period there will thus be random current changes with two or three phases short-circuited, or one phase on open circuit. The swing from short circuit to open circuit produces violent current fluctuations. These result in large voltage variations being impressed on the supply voltage.

2.4 Effects of Harmonic Distortion

In most cases, the presence of harmonics may lead to aging of electrical appliances and damages to electrical apparatus [13-15].

Conductor overheating can be caused by harmonic current larger than the expected fundamental magnitude; a common case is overloading the neutral of a three-phase system. Harmonics orders that are odd multiples of three are called the 'triplen' harmonics and they are additive in the neutral. The neutral currents are dominated by third harmonic components from single phase electronic loads.

Electrical equipment can be overheated by distorted load current that cause higher eddy current losses inside the equipment. At the frequency of the third harmonics, skin effect and proximity effect cause harmonic current to flow non-uniformly across the entire cross-sectional area of the winding conductor of transformers. In the total copper loss, both the true RMS value current as well as the a.c. resistance increase. In addition, losses will be increased because of the circulating current in the delta connection of transformers.

Transformer losses include DC and AC resistance in the winding, eddy currents in the windings and core, and hysteresis losses in the core. All other losses are called stray losses.

An eddy current is produced by the voltage induced by the magnetic field that surrounds each winding conductor and all other metallic materials permeated by the field. These eddy currents must be dissipated as heat by the windings and associated insulating materials. It is known that eddy current losses are proportional to the square of the frequency.

Vibrations and periodic rasping sounds from induction motors are due to harmonic currents. Harmonic torque is produced having both positive and negative rotational directions; when summed these almost cancel each other leaving the net rotational torque virtually unaltered. Interaction of harmonic currents with the fundamental flux results in possibly troublesome pulsating harmonic torque components.

The interaction between capacitive and inductive devices at some harmonic frequency causes unexpected large circulating current in some parts of the circuit [16]. Over-voltage and excessive current lead to failure of capacitor banks. Power factor correction capacitors with cable or apparatus inductance may set up current-amplifying resonance. These resonant loop current paths may raise local conductor heat loss and destroy the capacitors.

Harmonic currents and voltages in power system lines due to the power electronic equipment can impair the performance of telecommunication systems by virtue of their proximity, exposure, and susceptibly to the disturbance. For harmonic voltages, the interference is due to the electrostatic induction which acts through the capacitive coupling between the supply and communication circuits. For the harmonics current, the electromagnetic induction applies.

Many electrical measuring meters are designed to respond to average value or peak value rather than true RMS value. For sinusoidal waveform, a constant ratio exists between average (or peak) and RMS values. The meter can then be calibrated to indicate RMS value. With the presence of harmonics, the ratio changes which will throw off the calibration to an unknown extent. In the case of energy or kWhr meters, the meters may not be able to respond to high frequency components. Thus, readings may be lower in most cases.

Solid-state electronic relays used to protect motor circuits can be fooled by waveform distortion. In the case of overcurrent relay, the RMS value of the pick-up current may be increased. The static under-frequency relay is very sensitive to voltage sub-harmonics and

therefore such harmonics should be limited. For the moulded-case circuit breaker or miniature circuit breaker containing a thermal trip element, the element may heat up more rapidly at high harmonic frequency than at the fundamental frequency. The breaker may be cheated by opening at an overall current well under its normal trip setting. In magnetic-trip breakers, operation depends upon electromagnetic force which is proportional to the square of peak current [17]. Hence, a high third harmonic current with abnormally high overall peak could open the breaker at an over-ampere value lower than its preset tripping point. Large harmonic components in the current waveform can affect the interruption capability of the switchgear. The presence of harmonics affects the rate of rise of the transient recovery voltage across the break, and the voltage may be higher than normal and cause dielectric failure.

The definition for active, reactive, and apparent powers that are currently used are based on sinusoidal quantities with constant frequency. Such definitions are to be reviewed and redefined for distorted voltage and current waveforms [18]. IEEE 1459-2000 'Definitions for the Measurement of Electric Power Quantities under Sinusoidal, Non-sinusoidal, Balanced or Unbalanced Conditions' [30] has a detailed description on the new power definitions taking into account distorted voltage and current waveforms [19-21].

2.5 Power Harmonics Mitigation Measures

There are a number of ways to overcome the problems caused by harmonics. The simplest way is to design and build equipment that would tolerate more harmonics. The common measures are over-sizing the power supply cable and in some cases use double-neutral. Transformer overheating would be reduced by employing appropriate k-rated transformers.

The mutual coupling between power circuits and communication circuits can be reduced by earthed shielding. Harmonics can also be reduced or eliminated through transformer connections. A separate delta-connected tertiary winding is usually wound on large power transformers to provide a path for circulating triplen harmonics to flow. However, losses increase because of circulating current in the delta connection.

Power harmonics filters are developed to mitigate the amount of harmonics in the power distribution system. Harmonic filters can be passive and active, and can be connected in

series or shunt. The purpose of installing shunt power harmonic filters at the connection of power electronic equipment to the power system is to bypass the harmonic current generated by the equipment from entering the power system. Power factor correction capacitors would be used to improve the power factor of the power supply system. Line reactors limit harmonic current flow and do so at the expense of voltage distortion. The output voltage of the line reactor will show distinct waveform distortion and the peak voltage will often be limited. Active filters sense voltage and current harmonics, and generate offsetting harmonics to cancel out the unwanted harmonics [22].

2.6 Current Power Harmonics Analysis Methods

Before any power harmonics mitigation measures can be implemented, the nature and characteristics of the distorted waveforms should be analyzed. Traditionally power harmonic analysis makes use of Fourier series and Discrete Fourier Transform. The method assumes that the harmonics are integer multiples of the supply frequency. Non-integer harmonics are dealt with by using multiple periods of sampling for estimating harmonic magnitudes.

There are practical cases in which the DFT cannot be used with confidence to identify the harmonic components. There are sub-harmonics and inter-harmonics. Incorrect selection of the distorted waveform length would also result in spectral leakage. As a result, the detected fundamental frequency deviates from the actual value.

In practical applications, the distorted waveform changes over time due to changes in system configuration or load demand. Windowed discrete Fourier transform, Short time Fourier Transform and Gabor transform are commonly used to analyze time-varying harmonics. The effectiveness of these methods lie with the appropriate selection of the window length.

The DFT is liable to errors caused by aliasing, spectra leakages and picket-fence effect. There are measures proposed by engineers and academics to improve the accuracy of the DFT. Some of the measures are using a non-rectangular window to reduce spectra leakages and to increase the fft no. in the FFT to achieve a better frequency resolution for a particular window width. Chapter 3 will discuss the properties of DFT and the various

methods to improve its accuracy. The improvement measures have advantages and disadvantages. The search for better methods continues to be a research area worth exploring.

2.7 Conclusion

This Chapter gives an overview of the many issues related to power system harmonics problems. Definitions of integer harmonics, sub-harmonics and inter-harmonics are given. The common sources of power harmonics, the effects of power harmonics and mitigation measures are investigated. Limitations of existing analysis techniques and the needs for new techniques of harmonic analysis are presented.

Chapter 3

The Developments of Wavelet Transform

3.1 Introduction

Wavelet transform (WT) is a new mathematical tool in the field of signal processing, especially in dealing with image processing, data compression and transmission. This Chapter presents a brief theoretical background of WT to serve as an introduction to the development of a WT-based algorithm for harmonic analysis. The development of wavelet transform follows a path of coincidences, and some coincidences constituted the emergence of wavelet transform in many fields of science and engineering. Reviewing the history of wavelet transform development does provide some insights and aspirations.

3.2 The Developments of Wavelet Transform [23-25]

The written record of wavelets linked to a man named Alfred Haar in 1909. It was mentioned in the appendix of a thesis he had written for his doctoral degree. Alfred Haar was born on October 11, 1885 in Budapest, Hungary. In 1904, Haar took his study at Gottingen, Germany under Hilbert. Haar's study at that time was on the orthogonal systems of functions. Haar's contribution to wavelets is very evident and an entire wavelet family named after him. The Haar wavelets are known to be the simplest of the wavelet families. The concept of a wavelet family is easy to understand. They all start with the scaling function called the father wavelet. Through scaling and shifting the father wavelet, one obtains the mother wavelet, daughters, sons, granddaughters, grandsons, etc.

A long gap of time elapsed after Haar's contribution to wavelets during which no advances have been made on wavelet mathematics, until a man named Paul Levy. Paul Levy was

born on September, 15, 1886 in Paris, France. He has a strong family background on mathematics. His grandfather was a mathematics professor; his father wrote geometry papers for Ecole Polytechnique, which is a school of higher education (indeed a university) in Paris, France. However, Levy did not only win awards in the field of mathematics, but also in the fields of chemistry and physics. He attended the prestigious school of Ecole Polytechnique, there he also taught later in life till retirement. Levy used wavelet mathematics to carry out his research in Brownian motion. He found that the scale-varying basis functions created by Haar (i.e. Haar wavelets) were a better basis than the Fourier basis functions. Unlike the Haar basis function, which can be chopped up into different intervals such as the interval from 0 to 1 or the interval from 0 to ½ and ½ to 1, the Fourier basis functions have only one interval. Therefore, the Haar wavelets can be used to precisely model a function. Levy therefore used the Haar basis to deal with the small details in Brownian motion.

After Levy, there were slight advances in the field of wavelets from the 1930s to the 1970s. The next major advancements were started by Jean Morlet around 1975. In fact, Morlet was the first researcher to use the term "wavelet" to describe his functions. Before 1975, many researchers had considered the idea of Windowed Fourier Analysis (mainly a man named Dennis Gabor). This concept allowed researchers to consider phenomena in terms of both time and frequency. Windowed Fourier Analysis was used to study the frequencies of a signal piece by piece (or window by window). These windows helped to make the time variable discrete or fixed. Different oscillating functions of varying frequencies could therefore be looked at in these windows. Morlet, also a graduate of Ecole Polytechnique, explored with the Windowed Fourier Analysis while working for an oil company. Customarily underground oil farm was explored by sending impulses into the ground and analyzing their echoes. With suitable analytical tools, these echoes could tell how thick a layer of underground oil would be. Fourier Analysis and Windowed Fourier Analysis were used to analyze these echoes. It was later found that Fourier Analysis was too time-consuming for this purpose. Morlet began to look for an alternative solution. When he worked with Windowed Fourier Analysis he discovered that keeping the window fixed was not the right approach and so he turned to the opposite. He kept the frequency of the function (number of oscillations) constant and changed the window width. He discovered that stretching the window stretched the function and squeezing the window compressed the function. In fact, a close resemblance could be seen between the sine functions used in

Fourier Analysis and the Morlet wavelets. In 1981, Morlet met another man named Alex Grossman. Morlet and Grossman worked on an idea that Morlet discovered while experimenting on a basic calculator. The idea was that a signal could be transformed into wavelet form and then transformed back into the original signal without any information being lost. This process is thus lossless. Morlet and Grossman's efforts with this concept were a complete success. Since wavelets deal with both time and frequency, they thought a double integral would be needed to transform wavelet coefficients back into the original signal. However, in 1984, Grossman found that a single integral was all that was needed. They also discovered another interesting thing:- making a small change in the wavelets only causes a small change in the original signal. This is an important feature of modern wavelets. In data compression, small wavelet coefficients are changed to zero to allow for a higher compression and when the signal is recomposed the new signal is only slightly different from the original. Without this property, data compression today would be a much more difficult task.

The next two important contributors to the field of wavelets were Yves Meyer and Stephane Mallat. Although Meyer is a mathematics professor working in France and Mallat was a graduate of Ecole Polytechnique where Meyer used to teach, they first met in the United States in 1986. Mallat was very intrigued by a paper Meyer had written about his orthogonal wavelets. They spent three days researching on works done on wavelets in many applied fields and eventually created the multi-resolution analysis for wavelets. Multi-resolution analysis was a big step in the research of wavelets. It was in this perspective that the scaling function of wavelets was first mentioned, and which allowed researchers and mathematicians to construct their own family of wavelets.

More importantly, multi-resolution analysis led to a simple and recursive filtering algorithm to compute the wavelet decomposition of a function from its finest scale approximation. The use of filters in wavelet decompositions led to the merging of sub-band filtering of electrical engineering and wavelet mathematics.

Electrical engineers have been accustomed to the idea of grouping frequencies together in bands with a width proportional to the average frequency in that band. This is called constant relative-bandwidth or constant-Q filtering. One way to obtain such a splitting is to work iteratively. Firstly the full range of frequencies is halved by applying two filters: one

high-pass (HF) one low-pass (LF). The lower frequency half can then be halved again, and so forth. Different sections that result from this procedure have different bandwidths; they correspond to different Nyquist sampling rate. An easy way to obtain the correctly sampled versions of all the components is to retain only half the output samples at every filtering step. Such steps would also produce aliasing due to imperfect filter characteristics. In 1970s, A. Groisier and his colleagues discovered a design procedure, which uses a quadrature mirror filter (QMF) in the decomposition structure to cancel out the aliasing. Ten years later in 1983, M. Smith and T. Barnwell and independently F. Mintzner, discovered QMF-like pairs that were capable of exact reconstruction. The quadrature filter pairs were exactly the types of filter pairs that researchers in search of orthonormal wavelet bases would discover later from a completely different approach.

The latest wavelet researcher worth mentioning is Ingrid Daubechies, who is currently a professor at Princeton University. She was born in Houthalen, Belgium and earned her PhD in Physics in 1980. Around 1988, Daubechies made use of the idea of multi-resolution analysis to create her own family of wavelets. These wavelets were later named the Daubechies Wavelets. Daubechies wavelet family satisfies a number of wavelet properties. They have compact support, orthogonality, regularity, and continuity. The property of orthogonality is satisfied because the inner products of all of the various translations of the Daubechies wavelets are zero. The regularity property is satisfied because the Daubechies wavelets can reproduce linear functions. Finally, the continuity property is satisfied because the Daubechies wavelet functions are continuous even though they are not very smooth and not differentiable everywhere.

3.3   Wavelet Basics

The background theory of WT can be found in [25-29]. WT is a mathematical tool similar to Windowed Fourier Transform. The Short Time Fourier Transform uses a window to section the signal into portions that can be assumed as stationary, FFT is then performed on each section. A choice of window function has to be made and the window size remains constant for the duration of the analysis; this gives poor frequency resolution for non-stationary signals.

The Gabor transform is a windowed Fourier Transform with a Gaussian window, the window width being constant. As before the transform is meaningful only if there is at least one complete cycle of the frequency of interest in the window of observation.

The Gaussian window determines the localization properties of the Gabor transform and as the width of the window remains constant for all frequencies, the variance of the time localization will be the same for all frequencies and by Heisenberg uncertainty principle the frequency localization will also be the same for all frequencies. The Gabor transform therefore has constant size localization cells in the time-frequency plane; the absolute accuracy of frequency localization ($\Delta\omega$) is limited by characteristics of the Gaussian window.

The Wigner-Ville distribution gives excellent frequency resolution but for multi-component signals its quadratic nature produces interference (cross terms), these cross-terms are oscillatory and may have magnitudes in excess of the auto-terms for each component, also the transform output is not necessarily non-negative as investigated in [25].

3.4   Definitions of Wavelet Transform

The Wavelet Transform is a method of converting a function into another form. For time signal, the WT is able to convert the function into a time-frequency plane. A wavelet is needed to perform the WT. The wavelet should be localized in time.

In order to be called a wavelet, a function must satisfy certain mathematical criteria. These are:

1)   A wavelet must have finite energy:

$$E = \int_{-\infty}^{+\infty} \left| \varphi(t) \right|^2 dt < \infty . \tag{3.1}$$

2)   Given the FT of the function $|\varphi(t)|$,

$$\Phi(f) = \int_{-\infty}^{+\infty} \varphi(t)e^{-j(2\pi f)t}dt .$$ (3.2)

Then the following condition must hold:

$$C_g = \int_{0}^{+\infty} \frac{|\Phi(f)|^2}{f} df < \infty .$$ (3.3)

This implies that the wavelet has non-zero frequency component,

$$\Phi(0) = 0 ,$$ (3.4)

or the wavelet must have a zero mean. (3.3) is known as the admissibility condition and Cg is called the admissibility constant. The value of Cg depends on the chosen wavelet.

3)   An additional criterion that must hold for complex wavelets is that the FT of the wavelet must be real and be vanished for negative frequencies.

Wavelets satisfying the admissibility condition are in fact bandpass filters.

3.5   The Continuous Wavelet Transform (CWT)

The Continuous Wavelet Transform of a continuous signal, f(t), is defined as [28]

$$Wf(u,a) = \langle f, \varphi_{u,a} \rangle = \int_{-\infty}^{+\infty} f(t)\frac{1}{\sqrt{a}}\varphi^*(\frac{t-u}{a})dt,$$ (3.5)

The $\frac{1}{\sqrt{a}}$ in (3.5) is the normalization factor of the wavelet so that if $\varphi(t)$ has a unit length, then its scaled version also has a unit length.

At a=1 and u=1, the wavelet is called the analyzing wavelet or mother wavelet. Wavelets produced by other values of a and u are called baby wavelets as they come from the same mother wavelet.

As can be seen in (3.5), wavelets are families of functions generated from one single function, called an analyzing wavelet or mother wavelet, by means of scaling and translating operations. The scaling operation is nothing more than performing 'stretching' and 'compressing' operations on the mother wavelet, which in turn can be used to obtain the different frequency information of the function to be analyzed. The compressed version is used to satisfy the high frequency needs, and the dilated version is used to meet low frequency requirements. Then, the translated version is used to obtain the time information of the function to be analyzed. In this way, a family of scaled and translated wavelets is created and serves as the bases, the building blocks, for representing the function to be analyzed.

The wavelet coefficients thus generated by the dilation and translation measures the correlation between the signal and each wavelet function.

As with its Fourier counterpart, there is an inverse wavelet transform, defined as

$$f(t) = \frac{1}{C_g} \int\limits_{-\infty}^{+\infty}\int\limits_{-\infty}^{+\infty} Wf(u,a)\varphi\left(\frac{t-u}{a}\right)\frac{da\,du}{a^2}.$$ (3.6)

This allows the original signal to be recovered from its wavelet transform by integrating over all scales and locations. The existence of the inverse wavelet transform is essential; this means that the function can be uniquely reconstructed from the transform coefficients. Otherwise one function can have more than one set of transform coefficients. The proof of the invertability of the CWT can be found in [27].

The main advantage of WT as compared with STFT is that the size of the analysis window is not constant; it varies in inverse proportion to the frequency. Since the traditional FT cannot simultaneously achieve good localization in both time and frequency for a signal, the name of the game in time-frequency analysis is to trade one type of localization for the

other. Other conventional time-frequency methods are much less suited to the analysis of short duration signals. WT can offer a better compromise in terms of localization.

3.6 The Discrete Wavelet Transform (DWT)

Instead of continuous dilation and translation, the mother wavelet may be dilated and translated discretely by selecting $a = a_o^m$ and $u = u_o a_o^m$ in (3.5), where a_o and u_o are fixed values with $a_o > 1$ and $u_o > 0$, m, n, k $\in$ Z, and Z is the set of positive integers [30, 31]. Then the discretized mother wavelet becomes

$$\varphi_{m,n}(t) = a_o^{-m/2} \varphi(\frac{kT - nu_o a_o^m}{a_o^m}),$$ (3.7)

the corresponding discrete wavelet transform is given by

$$DWT_\varphi f(m,n) = \langle f, \varphi_{m,n} \rangle = \int_{-\infty}^{+\infty} f(kT)\varphi_{m,n}^*(t)dt .$$ (3.8)

DWT provides a decomposition of a signal into sub-bands with a bandwidth that increases linearly with frequency. In the case of dyadic transform (a_o=2 and u_o=1), each spectral band is approximately one octave side. In this form, DWT can be viewed as a special kind of spectral analyzer.

It is possible to obtain a signal f through wavelet series reconstruction by setting

$$f = \sum_m \sum_n c_{m,n} \varphi_{m,n} ,$$ (3.9)

and

$$c_{m,n} = \langle f, \varphi_{m,n}^* \rangle .$$ (3.10)

The same as DFT implemented with the FFT for fast and efficient implementation, DWT can be implemented efficiently and fast by the discrete wavelet transform filter bank.

However the wavelets used for DWT must be real wavelets. That means DWT is not suitable for phase estimation.

3.7 Types of Wavelets

Wavelets come in many shapes and sizes. They must satisfy the admissibility condition and have zero dc component [32-34]. As long as these criteria are met, any functions can be used as wavelets. Broadly speaking, wavelets can be classified according to their mathematical properties as follows:

1) compactly support or not;
2) symmetrical or asymmetrical;
3) real valued or complex valued;
4) can be used for Continuous Wavelet Transform and/or Discrete Wavelet Transform.

Nearly all wavelets can offer the exact reconstruction property, except discrete approximation of Meyer wavelet and Morlet wavelet. The complex version of the Morlet wavelet has the exact reconstruction property. Complex valued wavelet transform should be implemented with complex valued wavelets.

Haar wavelet is compactly supported in time domain, of symmetrical shape and can be used for CWT and DWT. Real valued Morlet wavelet is not compactly supported, of symmetrical shape and can only be used for CWT. Complex valued Morlet wavelet has the same properties as the real valued version, and can be used for complex continuous wavelet transform. Shannon wavelets are not compactly supported, of symmetrical shape and are complex valued, which can be used for complex continuous wavelet transform only. Daubechies wavelets are compactly supported, of asymmetrical shape and can be used for CWT and DWT. However the wavelets used for DWT must be real wavelets.

3.8 Applications of Wavelet Transform in Power Engineering

The applications of the WT in power engineering are mostly related to power disturbances and cover the following major areas [35-37]:

3.8.1   Power Disturbance Detection and Localization

Power disturbances include fast voltage fluctuations, short and long voltage duration variations, and harmonic distortion [38-42]. They are caused by transmission line switching, capacitor switching, lightning strikes, faulty conductors and equipment failures. Harmonic distortion is mostly caused by nonlinear loads. WT is used to detect and localize these disturbances.

3.8.2   Power Disturbance Data Compression and Storage

Power disturbance phenomena cover a broad frequency spectrum, power quality monitoring devices usually are set at very high sampling frequency in order to capture as many information as possible, resulting in huge amount of data to be stored [42-45]. WT is being used to compress power disturbance signals based on the properties of decomposition and reconstruction. The magnitudes of the wavelet transform coefficients are inspected; those below a certain threshold are discarded. It has been tested that a compression ratio of 3 to 6 times can be achieved.

3.8.3   Power Disturbance Identification and Classification

Using the properties of WT and the features of the decomposed waveform along with a special type of Artificial Neural Network (ANN), called the Learning Vector Quantization (LVQ) network, it is possible to extract important information from a disturbance signal and determine what type of disturbance has caused a power quality problem to occur [46-51].

3.8.4   Power Devices Protection

WT has been using in the detection of transformer inrush current and motor terminal voltage waveform during switching surges in real-time [52-54]. WT may be useful for the design of a fast relay algorithm.

3.8.5   Power Disturbance Network/System Analysis

A method called Wavelet-Based Transient Analysis (WBTA) has been developed for power disturbance analysis based on wavelet domain equivalents of power system components such as resistors, inductors, and capacitors [55-57]. This method offers a systematic way to analyze power system disturbance problems.

3.9   Applications of Wavelet Transform for Harmonics Analysis

On the research area of power disturbance detection and localization, many researches have been done on transient analysis. As mentioned before, conventionally power analysis is based on the FT which is able to provide frequency information only. WT offers the possibility of time-frequency analysis, opening a new avenue in power transient detection and localization. Moreover, DWT implemented with the discrete wavelet transform filter bank is a fast and efficient algorithm similar to FFT, thus attracting a lot of researches in this area. As discussed in Section 3.5, the compressed mother wavelet has a higher frequency in a shorter window, while the stretched version has a lower frequency in a larger window. This best suits power disturbance analysis in which power transient is of short duration at high frequency, and harmonics and voltage fluctuations are of low frequency at a longer duration. The time-frequency representation by WT is particularly useful for slow voltage fluctuation analysis. However, few researches have been published on harmonic analysis [58-60, 81]. It may be that harmonic analysis has been considered as a frequency domain analysis, and FFT has offered a fast and efficient algorithm to deal with the problem.

With the advances in the application of power electronics in power engineering, harmonic analysis is no longer confining to identification of integer harmonics. There are inter-harmonics and sub-harmonics as well as non-stationary harmonics found in the power systems. WT is more suitable for harmonic analysis in modern power system than the traditional FT-based methods.

The wavelet transform is an inner product between an analyzing wavelet at a given scale and the signal under analysis; the wavelet coefficients combine both the information of the signal and the wavelet. The choice of the transform, orthogonal or not, and of the

appropriate wavelet is thus an important issue which depends on the kind of information one want to extract from the signal. For analyzing purposes the continuous wavelet transform is better suited because its redundancy allows good legibility of the signal's information content. For compression or modeling purposes, the orthogonal wavelet transform or the newly developed wavelet packet technique is preferable because they decompose the signal into a minimal number of independent coefficients.

With the discrete wavelet transform, one has lost the covariance by dilation and translation of the continuous wavelet transform and the redundancy of the wavelet coefficients, both properties can be very useful for signal analysis and signal processing.

3.10 Conclusion

The development of wavelet transform has been briefly introduced. The emergence of wavelet transform and the related wavelet analysis has a strong link to applications and was developed originally for solving engineering problems. The development of wavelet theories can be seen as concerted contributions from many fields of sciences and engineering. The idea of a fast and efficient algorithm for the implementation of DWT was inspired by the filter theories. Based on the previous work, a complete set of wavelet mathematics was developed and the mathematical properties of wavelet theory were established and theorized. Researchers are even able to construct their own wavelets with desirable properties.

The recent applications of WT in power engineering have been briefly discussed. Moreover, wavelet transform has been used in many other areas of science and engineering, for example, structural vibration studies, electrical power disturbance analysis, machine vibration analysis, acoustical analysis, data and image compression, etc [61]. With the popularity of wavelet analysis and readily available software for easy implementation, it is very tempting to use standard wavelet analysis algorithm and tries to fit it to a problem. On the contrary, one should start with a problem in mind, defining the characteristics of the problem and the expected outcomes, and then devise a custom-made wavelet analysis tool for the application. In other words, wavelet analysis tool development should be problem-driven. Furthermore, the choice of a suitable wavelet(s) has a deterministic effect on the outcomes.

It can be seen that CWT is most suitable for harmonic analysis. Chapter 5 will discuss in detail the underlying theories of the wavelet transform, the choice of an appropriate wavelet and the other considerations.

Chapter 4

Discrete Fourier Transform and Limitations

4.1 Introduction

Fourier Transform has been the major analytical tool for harmonic analysis. Discrete Fourier Transform implemented with Fast Fourier Transform offers a fast and efficient algorithm for harmonic analysis. Basically Fourier Transform is a frequency domain analysis tool. The following sections give an introduction to Fourier Transform, the underlying principles, assumptions, and the limitations.

4.2 Fourier Transforms (FT)

A signal can be either *continuous* or *discrete*, and it can be either *periodic* or *aperiodic*. The combination of these two features generates the four categories of Fourier Transform [62].

4.2.1 Aperiodic-Continuous Signals (Fourier Transform, FT)

This includes, for example, decaying exponentials and the Gaussian curve. These signals extend to both positive and negative infinity without repeating in a periodic pattern, i.e., the signal is continuous and aperiodic. The Fourier Transform for this type of signal is simply called the **Fourier Transform**.

4.2.2 Periodic-Continuous Signals (Fourier Series, FS)

Here the examples include: sine waves, square waves, and any waveform that repeats

itself in a regular pattern from negative to positive infinity, i.e. the signal is continuous and periodic. This version of the Fourier Transform is called the **Fourier Series**.

4.2.3   Aperiodic-Discrete Signals (Discrete Time Fourier Transform, DTFT)

These signals are only defined at discrete points between positive and negative infinity, and do not repeat themselves in a periodic fashion, i.e., the signal is discrete and aperiodic. This type of Fourier Transform is called the **Discrete Time Fourier Transform.**

4.2.4   Periodic-Discrete Signals (Discrete Fourier Transform, DFT)

These are discrete signals that repeat themselves in a periodic fashion from negative to positive infinity, i.e., the signal is discrete and periodic. This class of Fourier Transform is sometimes called the Discrete Fourier Series, but is most often called the **Discrete Fourier Transform.**

These four classes of signals all extend to positive and negative infinity. Examples are sine and cosine waves which are extending from negative infinity to positive infinity. One cannot use a group of infinitely long signals to synthesize something finite in length. The way around this dilemma is to make the finite data look like an infinite length signal. This is done by imagining that the signal has an infinite number of samples on the left and right of the actual points. If all these "imagined" samples have a value of zero, the signal looks discrete and aperiodic, and the Discrete Time Fourier Transform applies. The method is like applying a rectangular window to the signal before conducting DFT. The rectangular window has unity amplitude.

As an alternative, the imagined samples can be a duplication of the actual points. In this case, the signal looks discrete and periodic, with a period equal to the number of the actual points. This calls for the Discrete Fourier Transform to be used. As it turns out, an infinite number of sinusoids are required to synthesize a signal that is aperiodic. This makes it impossible to calculate the Discrete Time Fourier Transform in a computer algorithm. By elimination, the only type of Fourier transform that can be used in DSP is the DFT. In other words, digital computers can only work with information that is

discrete and finite in length. The key point to understand is that this periodicity is invoked in order to use a mathematical tool, i.e., the DFT. It is usually meaningless in terms of where the signal originated or how it was acquired.

The sine and cosine waves used in the DFT are commonly called the DFT basis functions. In other words, the output of the DFT is a set of numbers that represent amplitudes. The basis functions are a set of sine and cosine waves with unity amplitude.

Let X[k] is the frequency domain representation of the time domain function x[n]. With a complex DFT notation, X[k] has real part and imaginary part denoted as ReX[k] and ImX[k] respectively. The DFT basis functions are generated from the equations:

$$c_k[i] = cos(2\pi i \frac{k}{N} f_s)$$
(4.1)

$$s_k[i] = sin(2\pi i \frac{k}{N} f_s)$$
(4.2)

where i=0 to N-1; and k=0 to N/2 which determines the frequency of the wave.

The $c_k[\ ]$ is the cosine wave for the amplitude held in the real part of X[k], and $s_k[\ ]$ is the sine wave for the amplitude held in the imaginary part of X[k].

4.3   Inverse Discrete Fourier Transform

The synthesis equations for conducting the IDFT are [63]

$$x[i] = \sum_{k=0}^{\frac{N}{2}} Re\,\overline{X}[k]\,cos(2\pi i \frac{k}{N} f_s) + \sum_{k=0}^{\frac{N}{2}} Im\,\overline{X}[k]\,sin(2\pi i \frac{k}{N} f_s)$$
(4.3)

where

$$Re\,\overline{X}[k] = \frac{Re\,X[k]}{\frac{N}{2}} \quad ; \quad Re\overline{X}[0] = \frac{ReX[0]}{N}$$

$$Im\,\overline{X}[k] = -\frac{Im\,X[k]}{\frac{N}{2}} \quad Re\overline{X}[\frac{N}{2}] = \frac{ReX[\frac{N}{2}]}{N}$$

This is called a rectangular notation. Alternatively the frequency domain can be expressed in polar form. The magnitude and phase are a pair-for-pair replacement for the real and imaginary parts. In other words, DFT can be used to estimate signal frequencies, amplitudes and phase angles.

However the phase calculated by DFT can be erroneous for various reasons, such as

* divide by zeros;
* incorrect arctan;
* phase of very small magnitudes; and
* spikes between π and $-\pi$.

The DFT can be calculated in three completely different ways. The first method is by using a set of simultaneous equations. This method is too inefficient to be of practical use. The second method is correlation. This is based on detecting a known waveform in another signal. The third method, called the Fast Fourier Transform (FFT) is an ingenious algorithm that decomposes a DFT with N points, into N DFTs each with a single point. In actual practice, correlation is the preferred technique if the DFT has less than about 32 points, otherwise the FFT is used.

The FFT assumes periodicity in all cases. The FFT assumes that the windowed data repeats with a period equal to the window time. Thus, there are many assumed windows extending to either side of the physical window, and each is an exact duplicate of the physical one.

4.4 The Sampling Frequency

A classical sampling theorem is that a continuous signal can be correctly represented in discrete form provided the number of samples per cycle should be at least two [63]. In other words the sampling frequency should be at least twice the highest frequency contained in the signal. In practice, an absolutely stable sampling may not be easily achieved. A sampling frequency three or more times higher than the highest frequency is desirable.

4.5 Time Resolution and Frequency Resolution

Given that a signal is sampled at f_s, and with a N-point FFT, the frequency resolution is given by [62]

$$\Delta f = \frac{f_s}{N}.$$

(4.4)

The number of data points is equal to the number of points of the FFT.
The time window (T) is

$$T = \frac{N}{f_s}$$

(4.5)

As seen from the above expressions, frequency resolution is improved at the expense of time resolution. This is an inherent property of DFT. By referring to the underlying principles of DFT, the basis functions are extending from negative infinity to positive infinity. Therefore periodicity is assumed in DFT implemented with FFT. The DFT is therefore only suitable for analyzing stationary signals. Furthermore a very large window must be used to achieve a high frequency resolution.

Consider a simulated signal represented as

$$f(t) = \cos(2\pi 50t) + \cos(2\pi 100t) + \cos(2\pi 150t) + \cos(2\pi 200t) + \cos(2\pi 250t).$$

(4.6)

The simulated signal is sampled at f_s = 1000Hz with a signal length (T) of 0.2s. The fft no. is set as 200 to achieve a frequency resolution of 5Hz. Fig. 4.1 shows the frequency spectrum produced by FFT.
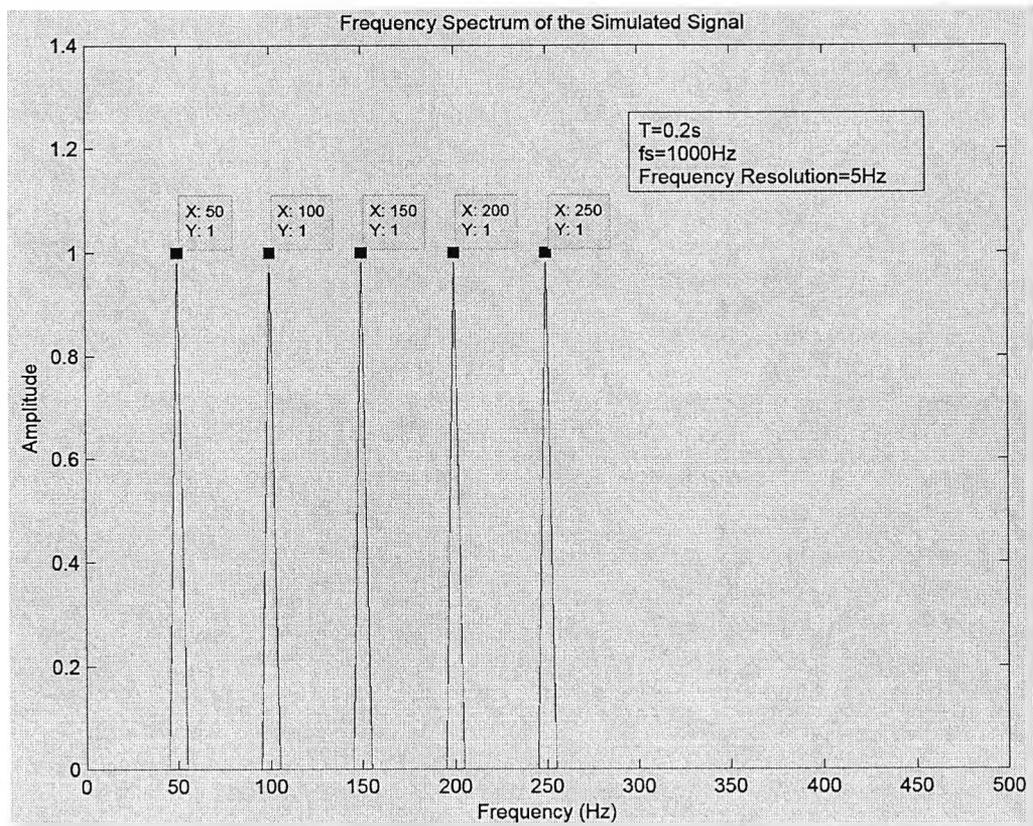
Fig. 4.1 Frequency spectrum by FFT

The FFT is able to estimate the frequencies and amplitudes of the harmonics in the signal accurately.

Consider the signal

$$f(t) = \cos(2\pi51t)+\cos(2\pi102t)+\cos(2\pi153t)+\cos(2\pi204t)+\cos(2\pi255t). \qquad (4.7)$$

The harmonics are still an integer multiples of the fundamental. The simulated signal is sampled at f_s = 1000Hz with a signal length (T) of 0.2s. The fft no. is set as 200 with a frequency resolution of 5Hz. Fig. 4.2 shows the frequency spectrum produced by FFT.
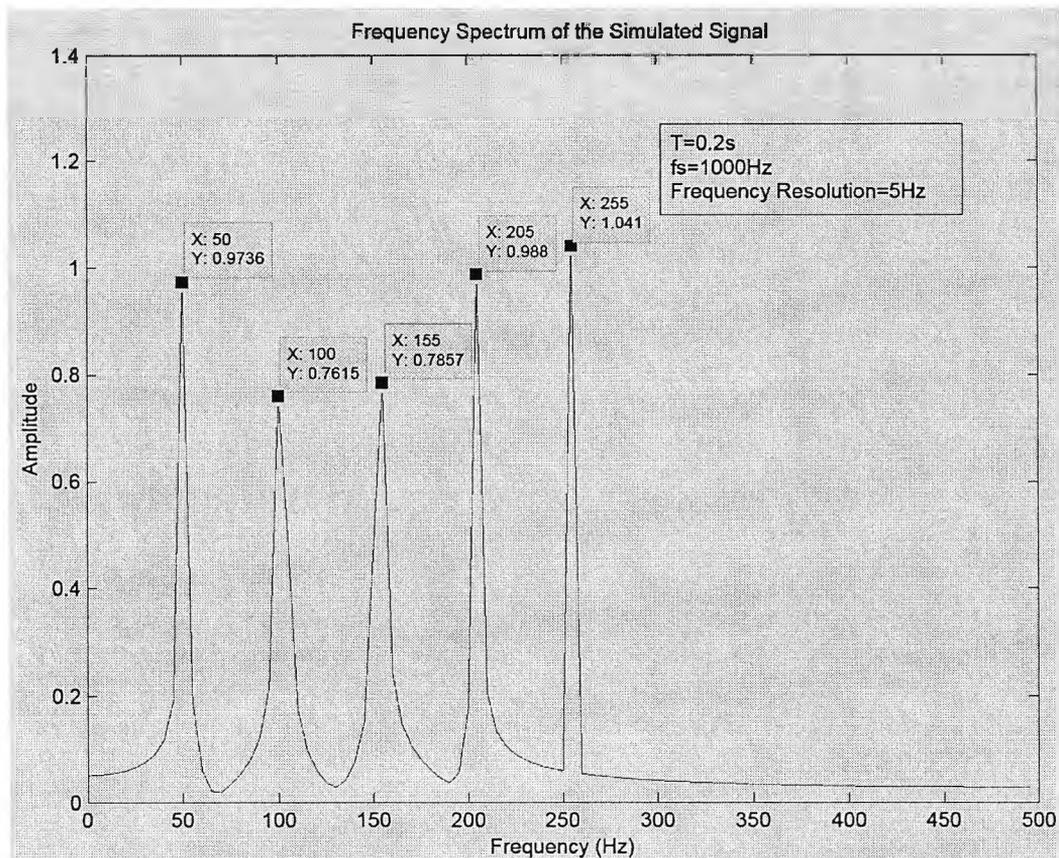
Fig. 4.2   Frequency spectrum by FFT with coarse Δf

It can be seen that the frequency resolution is not high enough to detect the harmonic frequencies. Also there are leakages seen around the detected frequencies due to the reason to be discussed in Section 4.6 [64].

To achieve accurate frequency detection, the frequency resolution should be increased to 1Hz. With f_s = 1000Hz, the signal length (T) should be at least 1s to give 1000 data points. The fft no. is therefore set as 1000 which is equal to the number of data points. Fig. 4.3 shows the frequency spectrum produced by FFT.
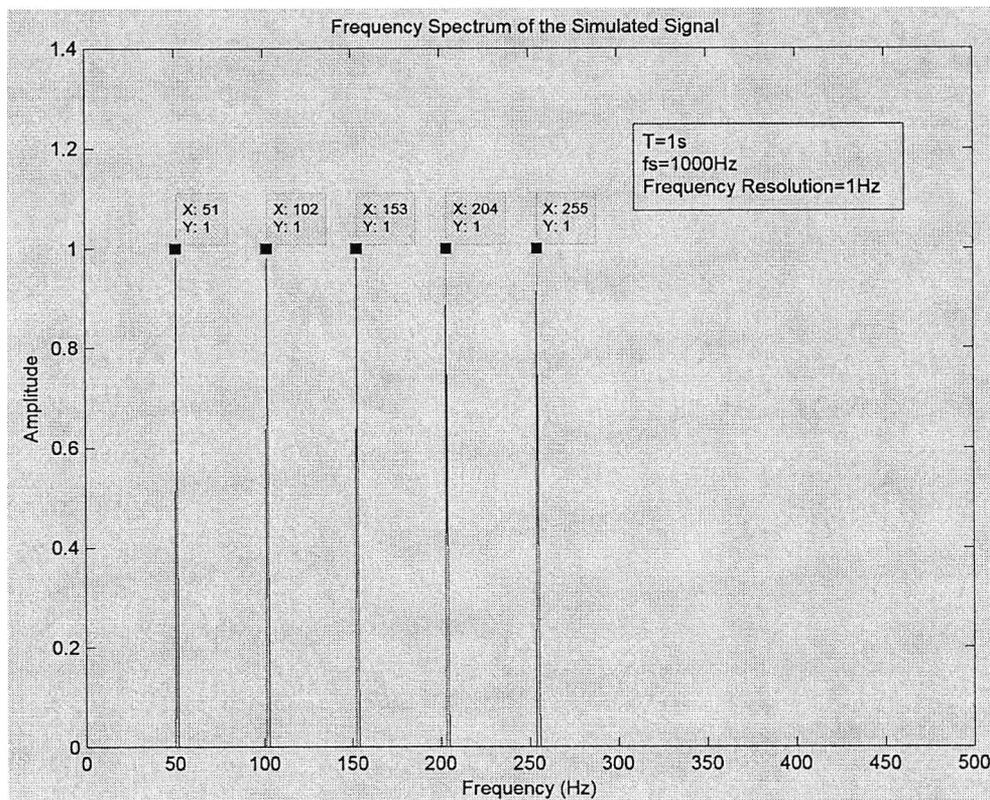
Fig. 4.3   Frequency spectrum by FFT with fine Δf

With the fft no. and no. of data points increased, the FFT is able to estimate accurately the frequencies and amplitudes of the harmonics in the signal.

4.6   Frequency Leakages

The term 'leakage' refers to the apparent spreading of energy from one frequency into adjacent ones [63,65]. It arises due to the truncation of the time sequence such that a fraction of a cycle exists in the waveform that is subjected to the FFT. This comes about because the FFT assumes that the truncated window repeats itself from negative infinity to positive infinity. If an incomplete cycle of the signal is contained in the window, jump discontinuities are produced at the data window and the imaginary repeating windows, violating the assumption that the signal is periodic.

Leakage is not a universal problem. It does not affect transient data as long as the transient is fully contained in the window. Leakage only occurs when the FFT is used to estimate the discrete line spectra associated with periodic and almost periodic signals.

Almost periodic signals have line spectra, but the components are not harmonically related. The actual source of leakage is the window used in acquiring the waveform. The amount of leakage depends upon the window shape and how the waveform fits into the window.

If the rectangular acquisition window exactly collects an integer number of cycles, leakage will not occur. However there are too many variables involved in the process to obtain exactly an integer number of cycles in a window so that leakages are unavoidable in practice.

It can be seen that with a time window of T, the frequency resolution is 1/T. The Heisenberg Uncertainty Principle states that [28]

$$\Delta t \, x \, \Delta \omega \geq \frac{1}{2}. \tag{4.8}$$

The Heisenberg box for DFT is

$$\Delta t \, x \, \Delta \omega = T \, x \, \frac{1}{T} \, x \, 2\pi = 2\pi. \tag{4.9}$$

One can see that the DFT has a Heisenberg box of a rather large area. DFT would be set to provide a high accuracy in frequency resolution, but time resolution would be very poor. It can be said that DFT is only useful for analyzing stationary and periodic signals.

4.7 Windowing

To reduce the effect of leakage which happens in practice, a way to reduce discontinuities at the window edges, and thus reduce leakage to a tolerable level, is to taper the rectangular window [62,63,66]. In short, this is to get rid of the abrupt edges by making them fall off smoothly to zero. One can do this by multiplying the acquired data with a window function.

Window functions exhibit various mainlobe widths and sidelobe magnitudes. In general, the lower the sidelobes, the less leakage or skirts will be in the frequency domain of the windowed data. However lowering the sidelobes also results in more energy being concentrated in widening the mainlobe. Lowering sidelobes therefore widens the bandwidth. The exception to this is the hamming window, which has a comparatively narrow mainlobe for its sidelobe level.

In terms of line spectra, the greater the window's bandwidth, the less resolution it provides. In other words equal-amplitude and adjacent frequencies become more difficult to distinguish. On the other hand, as the sidelobes decrease, selectivity increases. This means one has increased ability to distinguish adjacent frequency components of unequal amplitudes. The use of windowing and the choice of windows require some prior knowledge of the signal to be windowed.

Consider the signal represented in (4.7), a hamming window is applied to the signal before conducting FFT. The hamming window is represented as

$$W_H(t) = 0.54 - 0.46\cos(\frac{2\pi t}{T}).$$
(4.10)

Since the hamming window has a mainlobe height of 0.54, the amplitudes estimated by FFT should be scaled by 1/0.54. Fig. 4.4 shows the frequency spectrum produced by FFT. It can be seen that leakages are greatly reduced.
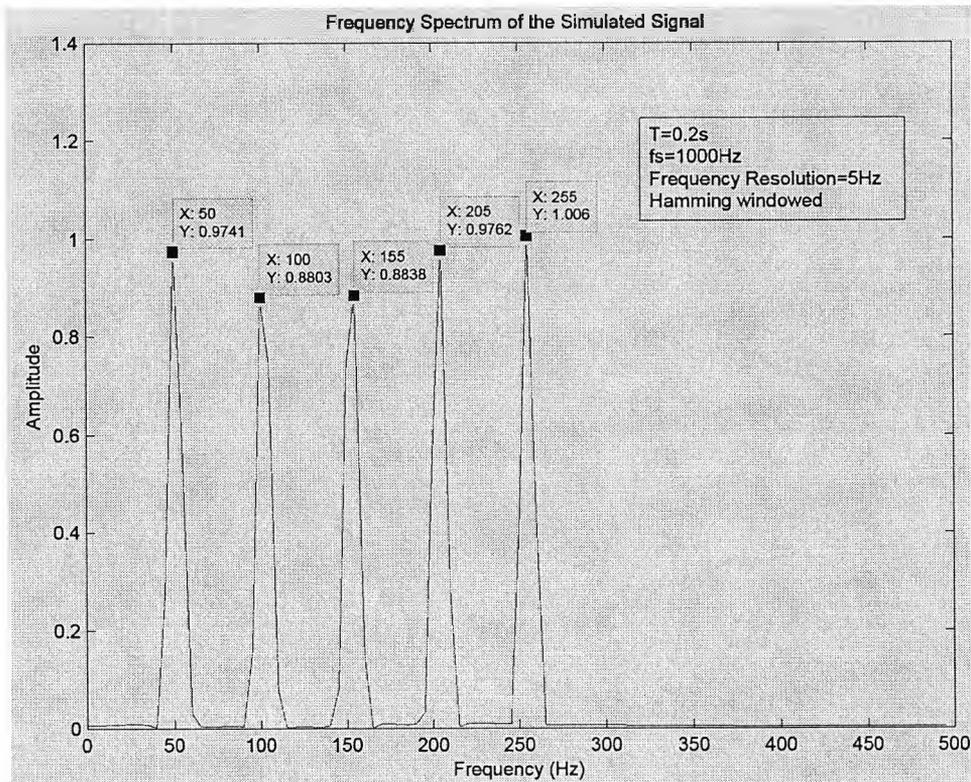
Fig. 4.4   Frequency spectrum by FFT (using Hamming window)

4.8   Picket-Fence Effect

If the analyzed waveform has frequencies which are integral numbers of the original window length T, the FFT will yield the appropriate amplitudes at the appropriate frequencies and zero at others. The picket-fence effect occurs if the analyzed waveform includes a frequency which is not one of the integer multiples of the fundamental [62-63,65-66]. A frequency lying between the adjacent harmonics would affect primarily the magnitudes of the two adjacent frequencies and secondarily the magnitude of all other harmonics. This frequency can cause leakage which in turn may cause pseudoaliasing.

4.9   Adjustment of FFT Number for Better Frequency Resolution

From the underlying principles of the FFT based DFT, the number of fft points should be equal to the number of data points for a correct estimation of the harmonic frequencies and amplitudes. That requirement implies that a longer signal length is required for a higher frequency resolution. However it has been found that the fft no. would be set to be

larger than the number of data in the signal to be analyzed. The amplitudes estimated by the FFT would need to be scaled by the ratio of fft no. to the no. of data points of the signal [67].

Using the simulated signal in (4.7), the frequency resolution is increased to 1Hz by setting the fft no. to 1000. The number of sampled data used is kept as 200. The scaling factor for the amplitude is 1000/200. Fig. 4.5 shows the frequency spectrum produced by FFT.
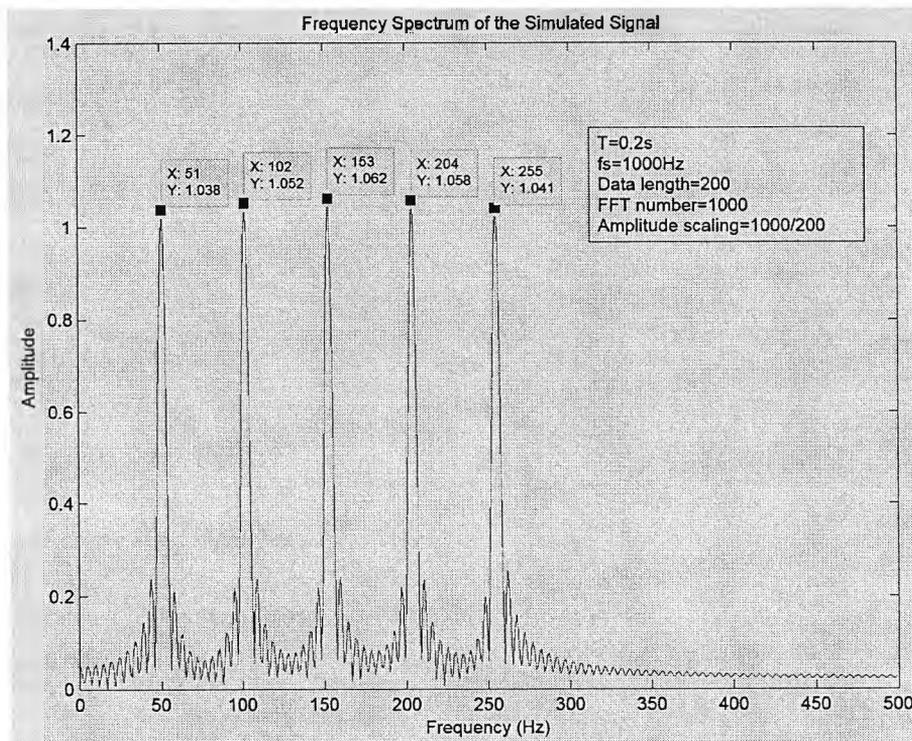
Fig. 4.5   Frequency spectrum by FFT (fft no. > N)

The hamming window in (4.10) is further applied to the sampled data representing the simulated signal. Fig. 4.6 shows the frequency spectrum produced by FFT.
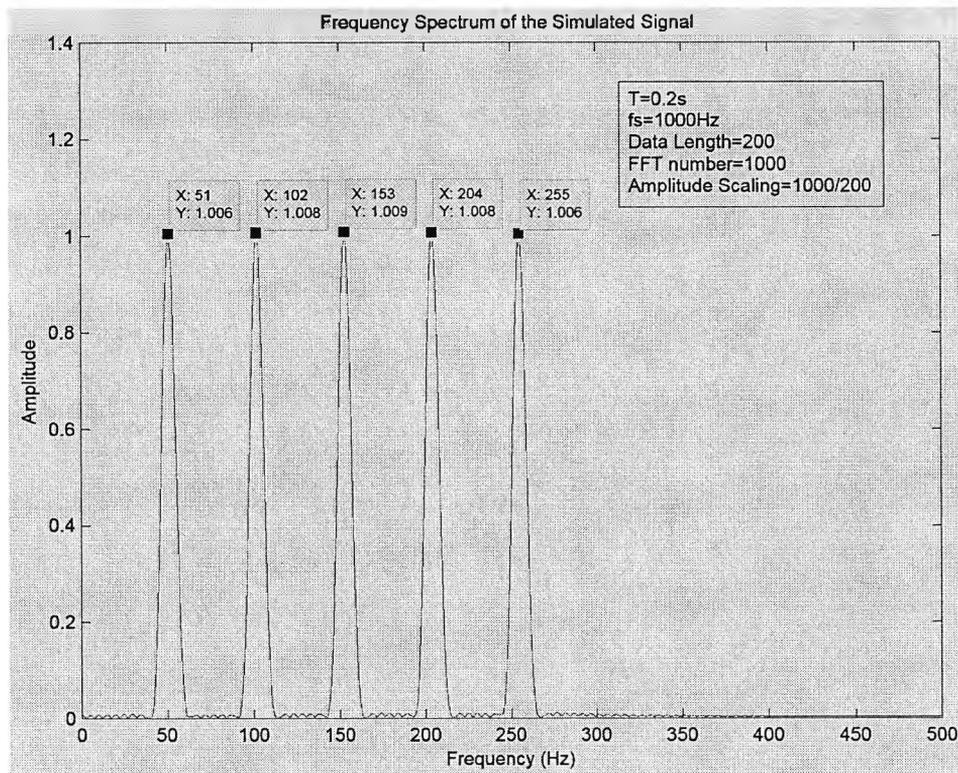
Fig. 4.6   Frequency spectrum by FFT (fft no. > N & using Hamming window)

It can be seen that the combination of using a hamming window to condition the harmonic signal and conducting the FFT by using a higher fft no. would effect a quite satisfactory harmonic analysis results.

4.10 Instantaneous Phase Estimation

DFT is able to preserve the phase information of a signal [62,68]. Consider the simulated signal in (4.7) with phase angle introduced as follows.

$$f(t) = \cos(2\pi 51t) + \cos(2\pi 102t + 20^\circ) + \cos(2\pi 153t - 10^\circ) + \cos(2\pi 204t + 15^\circ)$$
$$+ \cos(2\pi 255t - 25^\circ). \tag{4.11}$$

The f_s is set as 1000Hz, the signal length is 0.2s, and the number of sampled data is 200. In order to have a frequency resolution of 1Hz, the fft no. should be set to 1000. The scaling factor for the amplitude is 1000/200. Fig. 4.7 shows the phase spectrum by FFT.
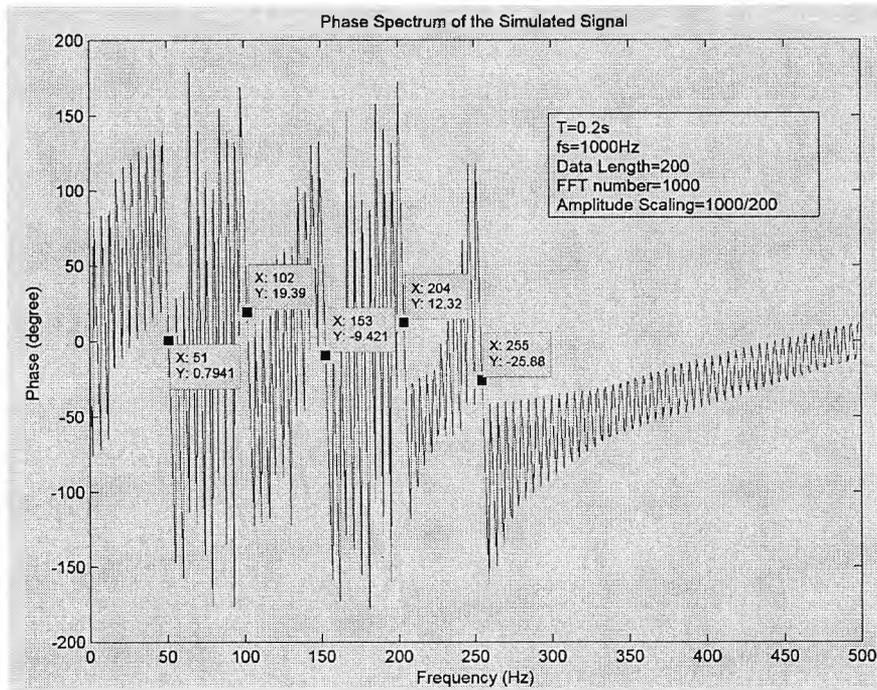
Fig. 4.7   Phase spectrum by FFT (fft no. > N)

It can be seen that the phase estimation is not accurate due to frequency leakages. With the hamming window in (4.10) applied, Fig. 4.8 shows the phase spectrum by FFT.
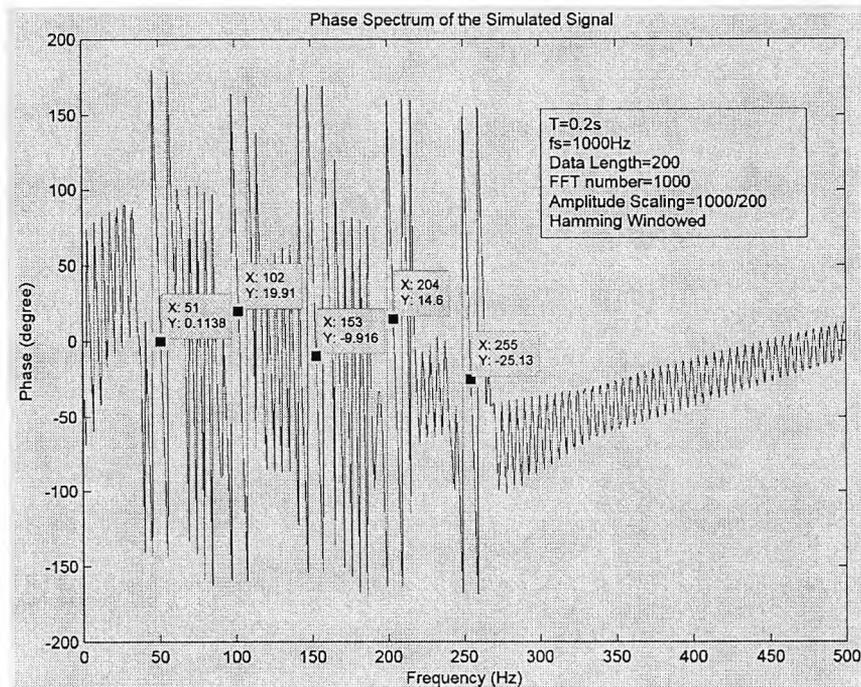
Fig. 4.8   Phase spectrum by FFT (fft no. > N & using Hamming window)

It can be seen that the phases estimated are better with the hamming window applied. To achieve a better phase estimation, the fft no. used is set to 1000. The number of data points used is therefore equal to 1000 and the minimum signal length required is 1s. Fig. 4.9 shows the phase spectrum by FFT.
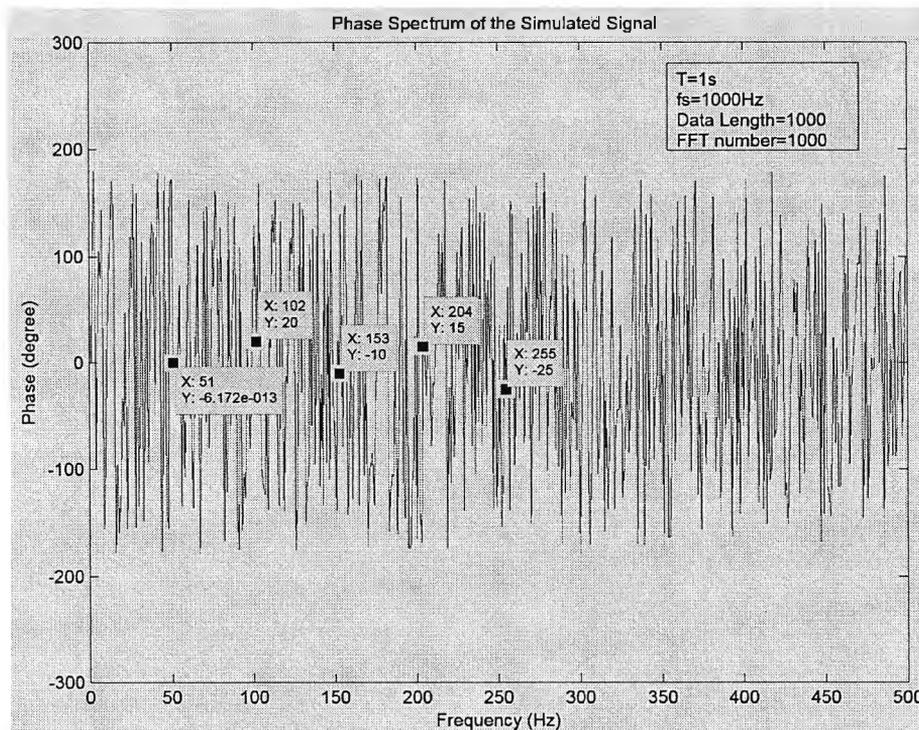
Fig. 4.9   Phase spectrum by FFT (fft no. = N & using Hamming window)

Table 4.1 shows the comparison of the phase estimation results with different fft no., different signal data no. and with or without hamming window, as in Fig. (4.9), (4.10) and (4.11).

Table 4.1 Comparison of phases estimated by FFT

Set Frequency (Hz)	Set Phase Angle (deg.)	Estimated Phase(deg.) T = 0.2s Data Length = 200 FFT no. = 1000	Estimated Phase (deg.) T = 0.2s Data Length=200 FFT no. = 1000 Hamming window	Estimated Phase (deg.) T = 1s Data Length = 1000 FFT no. = 1000
51	0	0.7941	0.1138	0
102	20	19.39	19.91	20
153	-10	-9.421	-9.916	-10
204	15	12.32	14.6	15
255	-25	-25.88	-25.13	-25

It can be seen from Table 4.1 that with a sufficiently long signal length such that the number of data points is equal to the required fft no. to achieve the frequency resolution, the phases estimated by FFT is very accurate. On the other hand, applying the hamming window and using a larger fft no. would improve the accuracy in phase estimations, but the phases estimated are still erroneous.

4.11 Conclusion

Periodicity of the signal is assumed when implementing DFT. DFT is therefore only suitable for analyzing stationary signals. Furthermore a very long signal must be used to achieve a high frequency resolution. The frequency resolution is determined by the number of points in the DFT which in turn is to be equal to the number of signal data. The DFT number can be set to a desirable value to achieve a higher frequency resolution in regardless of the number of signal data. The amplitudes of the harmonics estimated would need to be scaled by the ratio of the DFT number to signal data number. However the amplitudes of the harmonics estimated are not exact. The instantaneous phases of the harmonics estimated by this method would exhibit large errors.

Furthermore, the DFT assumes that the period of the signal is equal to the length of the window. If the time window contains a fraction of cycles of the harmonics in the signal, discontinuities at window edges would result in leakages. Various window shapes would be used to get rid of the abrupt edges by making them to fall off smoothly to zero. The use of windowing and the choice of windows require some prior knowledge of the signal to be windowed. If the chosen frequency resolution is not high enough to correctly detect the harmonics in the signal, picket fence effect would result. All the magnitudes of the harmonic frequencies estimated would be affected.

Chapter 5

Continuous Wavelet Transform and Harmonics Analysis

5.1 Introduction

This Chapter describes a new approach for harmonic analysis. This approach is based on Continuous Wavelet Transform (CWT) which does not have the limitations of FT-based harmonic analysis. The CWT is used to transform a time-based signal into a time-frequency representation. Both time information and frequency information are contained in the wavelet coefficients.

5.2 Limitations of DFT for Harmonics Analysis

DFT assumes that the signal is infinitely long and is strictly periodic. There is no such signal exists in real life. For a real time signal, a portion of it is sampled and taken for harmonic analysis. Therefore windowing is normally applied resulting in so called Short Time Fourier Transform. With the windowing approach, DFT regards each windowed time period of the signal would repeat itself outside the window, extending to negative infinity and positive infinity.

To distinguish two sinusoids of frequencies f_1 and f_2 respectively, the window length T must not be less than one cycle of the beat frequency [26], i.e.,

$$T \geq \frac{1}{|f_1 - f_2|}. \tag{5.1}$$

The frequency resolution of the DFT in detecting the exact frequency of a sinusoid is

related to DFT number which is be determined by the number of data in the windowed signal, as given in (4.5), i.e.,

$$N = T \times f_s.$$

Therefore the frequency resolution is given by

$$\Delta f = \frac{f_s}{N} = \frac{f_s}{T \times f_s} = \frac{1}{T}. \tag{5.2}$$

For example, with T=0.2s, the frequency resolution is 5Hz. The frequency spectrum has a step size of 5Hz only.

One of the techniques to increase the frequency resolution is to set the DFT number to be a multiple of the DFT number calculated from T and fs, the amplitudes thus estimated should be scaled accordingly. That would increase the frequency resolution but the detection of the amplitude would not be improved much. A large time window would still be required to achieve high frequency resolution.

The power supply authority declares that the nominal frequency of the supply voltage has a variation ±2%, i.e., from 49Hz to 51Hz for some countries. To detect a supply source of 49.5Hz, the frequency resolution requires a minimum time window size of 2 seconds.

Because of periodicity requirement of the DFT, frequency leakage around the harmonic frequencies is unavoidable. The use of a time window other than a rectangular window would reduce the edging effect. Yet the choice of time window is also related to the properties of the time signal to be analyzed.

It can be seen that the selection of DFT number (or the data length), time window width and a proper window shapes would have profound effects on the DFT results and this cannot be done appropriately without a prior knowledge of the signal characteristics.

5.3 Harmonic Identification using Continuous Wavelet Transform

The wavelet transform of a continuous signal, f(t), is defined in (3.5) as

$$Wf(u,a) = \langle f, \varphi_{u,a} \rangle = \int_{-\infty}^{+\infty} f(t) \frac{1}{\sqrt{a}} \varphi^* (\frac{t-u}{a}) dt.$$

The $\frac{1}{\sqrt{a}}$ in (3.5) is the normalization factor of the wavelet so that if $\varphi(t)$ has a unit length, then its scaled version also has a unit length.

There are four ways to view the integral operation of the CWT formula [26]:

1. it computes the inner product, or the cross-correlation of the signal f(t) with $\varphi(\frac{t}{a})/\sqrt{a}$ at shift u/a. It therefore computes the 'similarity' between f(t) and $\varphi(\frac{t}{a})/\sqrt{a}$, or the component of f(t) that is 'common' to $\varphi(\frac{t}{a})/\sqrt{a}$;

2. it is the output of a bandpass filter of impulse response $\varphi(\frac{-t}{a})/\sqrt{a}$, of input f(t), at the instant u/a;

3. it also computes the inner product or the cross-correlation of a scaled signal f(at) with $\sqrt{a}\varphi(t)$, at shift u/a; and

4. it follows that the CWT is also the output of a bandpass filter of impulse response $\sqrt{a}\varphi(-t)$ of input f(at), at the instant u/a.

The main distinction is that in one case, the cross-correlation is between f(t) and the baby wavelets and is equivalent to finding the output of a bank of bandpass filters, of impulse responses $\varphi(\frac{-t}{a})/\sqrt{a}$ and input f(t). In the other, successively scaled versions of f(t) are

passed through identical bandpass filters to give the transform. The latter seems easier to implement if there is a simple way to scale f(t).

Based on this, the dilation operation and the translation operation of the CWT measure the similarities between the wavelets for various frequencies controlled by the dilated centre frequency of the wavelet and at various instants. In this way, both frequency information and time dependent occurrences can be measured by the CWT. Fig. 5.1 illustrates the dilations of the real part of the Complex Morlet wavelet.
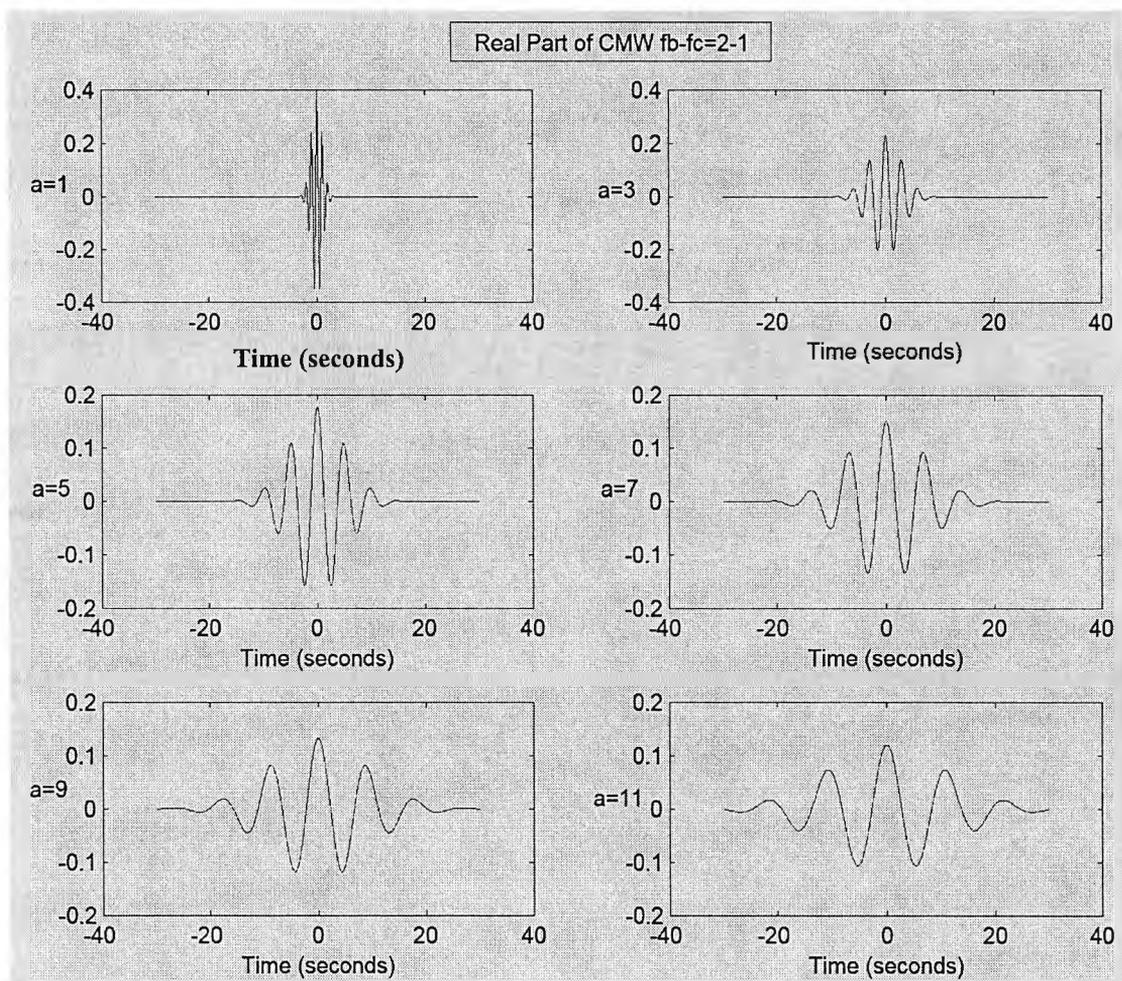
Fig. 5.1 Real part of CMW for various scales

It can be seen that unlike STFT where changing the window size would change number of oscillations in the window, dilation of the wavelet would change the time window size but the no. of oscillations in the time window remain the same. The frequency of oscillations is however changed accordingly.

Moreover at higher scale a which represents lower frequency, the wavelet length is longer. Therefore the higher the frequency, the better would be the time localization.

5.4 The Selection of Wavelets for Harmonics Analysis

For harmonic analysis on power signals, the main parameters to be estimated are harmonic frequencies, their amplitudes and phase angles. Complex continuous wavelet transform must be used for phase detection. This is one of the reasons why CWT is preferred to DWT for harmonic analysis. The simplified Complex Morlet Wavelet (CMW) is chosen for harmonic analysis [60,69-71]. CMW is smooth with harmonic-like waveform. It is represented as

$$\varphi(\frac{t}{a}) = \frac{1}{\sqrt{a}} \frac{1}{\sqrt{\pi f_b}} e^{-(\frac{t}{a})^2 / f_b} e^{j 2\pi f_c (\frac{t}{a})} . \tag{5.3}$$

The CMW in (5.3) is essentially a sinusoid-modulated Gaussian function. Because of the analytic nature, CMW is able to separate amplitude and phase information.

5.5 Properties of the Complex Morlet Wavelet

Strictly speaking, the mean of the simplified CMW [25,72] is not equal to zero as illustrated in

$$\int_{-\infty}^{+\infty} \varphi(\frac{t}{a}) dt = \frac{1}{\sqrt{a}} \frac{1}{\sqrt{\pi f_b}} \int_{-\infty}^{+\infty} e^{-(\frac{t}{a})^2 / f_b} e^{j 2\pi f_c (\frac{t}{a})} dt = \sqrt{a} e^{-\pi^2 f_b f_c^2} . \tag{5.4}$$

However, the mean of the CMW can be made arbitrarily small by setting the f_b and f_c parameters large enough [61]. For example, the mean of the CMW with f_b=2 and f_c=1 at a=1 is 2.753×10^{-9}, which is practically equal to zero. Many literatures recommend that the minimum setting should not be smaller than f_b=2 f_c=0.8.

The FT of the CMW is given as

$$\Phi(af) = \sqrt{a} e^{-\pi^2 f_b (af - f_c)^2} . \tag{5.5}$$

Substitute f=0 into (5.5) gives,

$$\Phi(0) = \sqrt{a}e^{-\pi^2 f_b(0-f_c)^2} = \sqrt{a}e^{-\pi^2 f_b f_c^2}.$$ (5.6)

Again the FT of the wavelet at negative frequencies is not strictly equal to zero. For example, with f = -1, a = 1, fb=2 and fc=1, (5.5) gives

$$\Phi(-1) = \sqrt{1}e^{-\pi^2 2(-1-1)^2} = 5.1225x10^{-35}.$$ (5.7)

However practically speaking, the CMW is qualified to be a wavelet.

5.6 Filter Banks

Fig. 5.2 shows the filter banks produced for the CMW, with fb=2 fc=1 and for a=1 to 501.
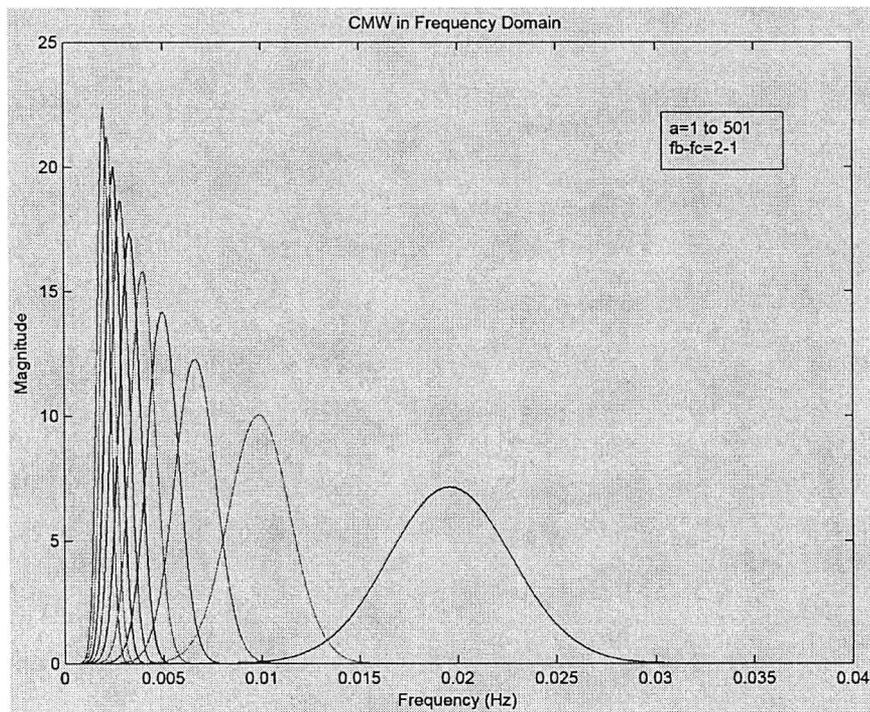
Fig. 5.2 Filter banks by CMW

It can be seen from Fig. 5.2 that the filter has very good frequency localization at low frequencies. The frequency localization is poorer as the wavelet centre frequency increases.

In (5.3), the wavelet centre frequency at scale a can be interpreted as

$$\omega = \frac{\omega_c}{a}.$$

(5.8)

5.7 The Heisenberg Uncertainty Principle

The Heisenberg uncertainty principle addresses the problem of the simultaneous localization in time and frequency that can be attained when measuring a signal [28,61]. More precisely, the Heisenberg uncertainty principle says that for any normalized wave function f(t) such that

$$\int_{-\infty}^{\infty} \left| f(t) \right|^2 dt = 1;$$

(5.9)

the product of the spread in time and the spread in frequency is at least 1/2 as given in (4.8), i.e.,

$$\Delta t \, x \, \Delta \omega \geq \frac{1}{2}.$$

If Δt is the side of a rectangle and $\Delta \omega$ is the other side, then the product of Δt and $\Delta \omega$ gives the area of the rectangle. The rectangular box formed by Δt and $\Delta \omega$ is called the Heisenberg Box. The Heisenberg uncertainty principle actually says that a signal itself cannot be concentrated simultaneously in time and frequency. The best localization that can be achieved should be at least equal to 1/2. This requirement applies to any time-frequency transforms in signal processing. The DFT has a Heisenberg box area of 2π.

The first moment in time provides a measure of where the wavelet is centred along the time axis and is defined as [28]

$$t_o = \frac{\int_{-\infty}^{\infty} t \left| \varphi(t) \right|^2 dt}{\int_{-\infty}^{\infty} \left| \varphi(t) \right|^2 dt}.$$

(5.10)

The first moment in frequency provides a measure of where $\Phi(\omega)$ is centered along the frequency axis and is defined as [28]

$$\omega_o = \frac{\int\limits_{-\infty}^{\infty} \omega |\Phi(\omega)|^2 \, d\omega}{\int\limits_{-\infty}^{\infty} |\Phi(\omega)|^2 \, d\omega} . \qquad (5.11)$$

A measure of the duration of the wavelet or the spread in time is defined as [28]

$$\Delta t^2 = \frac{\int\limits_{-\infty}^{\infty} (t - t_o)^2 |\varphi(t)|^2 \, dt}{\int\limits_{-\infty}^{\infty} |\varphi(t)|^2 \, dt} . \qquad (5.12)$$

This is called root mean square (rms) duration or the second moment in time.

The rms bandwidth is similarly defined as [28]

$$\Delta\omega^2 = \frac{\int\limits_{-\infty}^{\infty} (\omega - \omega_o)^2 |\Phi(\omega)|^2 \, dt}{\int\limits_{-\infty}^{\infty} |\Phi(\omega)|^2 \, dt} . \qquad (5.13)$$

5.8   Heisenberg Box of the Complex Morlet Wavelet

From (5.10), the first moment in time of the CMW is calculated as

$$\int\limits_{-\infty}^{\infty} \left| \varphi(\frac{t}{a}) \right|^2 \, dt = \frac{1}{\sqrt{2\pi f_b}} , \qquad (5.14)$$

and

$$\int\limits_{-\infty}^{\infty} t \left| \varphi(\frac{t}{a}) \right|^2 \, dt = 0 . \qquad (5.15)$$

Therefore $t_o = 0$. The CMW is centred at zero on the time axis.

The second moment in time domain of the CMW is calculated as

$$\int_{-\infty}^{\infty} (t - t_o)^2 \left| \varphi(\frac{t}{a}) \right|^2 dt = \frac{a^2 f_b}{4\sqrt{2\pi f_b}}.$$ (5.16)

Therefore from (5.12),

$$\Delta t^2 = \frac{\dfrac{a^2 f_b}{4\sqrt{2\pi f_b}}}{\dfrac{1}{\sqrt{2\pi f_b}}} = \frac{a^2 f_b}{4}.$$ (5.17)

The spread in time is equal to

$$\Delta t = \frac{a\sqrt{f_b}}{2}.$$ (5.18)

Now consider the first moment in frequency of the Complex Morlet Wavelet,

$$\int_{-\infty}^{\infty} |\Phi(a\omega)|^2 d\omega = \sqrt{\frac{2\pi}{f_b}},$$ (5.19)

and

$$\int_{-\infty}^{\infty} \omega |\Phi(a\omega)|^2 d\omega = \frac{\omega_c}{a} \sqrt{\frac{2\pi}{f_b}}.$$ (5.20)

Therefore from (5.11),

$$\omega_o = \frac{\dfrac{\omega_c}{a}\sqrt{\dfrac{2\pi}{f_b}}}{\sqrt{\dfrac{2\pi}{f_b}}} = \frac{\omega_c}{a}. \tag{5.21}$$

The CMW has a centre frequency of ω_c/a on the frequency axis.

For the second moment in frequency of the Complex Morlet Wavelet,

$$\int_{-\infty}^{\infty} a(\omega - \frac{\omega_c}{a})^2 e^{-\frac{f_b}{2}(a\omega - \omega_c)^2} \, d\omega = \frac{1}{a^2 f_b}\sqrt{\frac{2\pi}{f_b}}. \tag{5.22}$$

From (5.13), then

$$\Delta\omega^2 = \frac{\displaystyle\int_{-\infty}^{\infty}(\omega - \omega_o)^2 |\Phi(\omega)|^2 \, dt}{\displaystyle\int_{-\infty}^{\infty}|\Phi(\omega)|^2 \, dt} = \frac{\dfrac{1}{a^2 f_b}\sqrt{\dfrac{2\pi}{f_b}}}{\sqrt{\dfrac{2\pi}{f_b}}} = \frac{1}{a^2 f_b}. \tag{5.23}$$

Therefore the spread in frequency is given as

$$\Delta\omega = \frac{1}{a\sqrt{f_b}}. \tag{5.24}$$

From (5.18) and (5.23),

$$\Delta t \times \Delta\omega = \frac{a\sqrt{f_b}}{2} \times \frac{1}{a\sqrt{f_b}} = \frac{1}{2}. \tag{5.24}$$

(5.24) reveals that the CMW has the smallest Heisenberg box area [71]. Compared with DFT, CWT with CMW would give the best time-frequency localization.

From (5.23),

$$\frac{\Delta\omega}{\omega_o} = \frac{1}{a\sqrt{f_b}} x \frac{a}{\omega_c} = \frac{1}{\omega_c\sqrt{f_b}} .$$

(5.25)

A property of the wavelet transform described by (5.25) is that while the spread in frequency $\Delta\omega$ is dependent on the scale, the relative spread $\Delta\omega/\omega_o$ about the centre frequency remains constant for a given ω_c and f_b, and the transform is often called a constant Q filter. Increasing either f_b or ω_c improves the frequency localization of the wavelet transform.

Q-factor is defined as the ratio of the centre frequency to the bandwidth. From (5.25),

$$Q = \frac{\omega_o}{\Delta\omega} = \omega_c\sqrt{f_b} = 2\pi f_c\sqrt{f_b} .$$

(5.26)

The Q-factor of CMW is therefore determined by the bandwidth parameter f_b and the centre frequency f_c. The Q-factor has a significant contribution to the frequency and time localization. The higher the Q factor, the better would be the frequency localization and the poorer the time localization, and vice versa. From Section 5.5, fb $\geq$ 2 and fc $\geq$ 0.8 are necessary for a zero mean of the CMW, which requires that fc√fb $\geq$ 1.14 and Q $\geq$ 7.2. By adjusting the Q-factor and therefore the f_b and f_c of the CMW, one can control the frequency localization and time localization accordingly.

5.9 Heisenberg Boxes of the Complex Morlet Wavelet on the Time-Frequency Plane

From (5.8), the frequency ω of a sinusoidal signal is related to the scale and the centre frequency of the mother CMW by $a = \frac{\omega_c}{\omega}$. Substitute (5.8) into (5.18) and (5.23),

$$\Delta\omega = \frac{1}{a\sqrt{f_b}} = \frac{\omega}{\omega_c}\frac{1}{\sqrt{f_b}} = \left(\frac{1}{\omega_c\sqrt{f_b}}\right)\omega ,$$

(5.27)

$$\Delta t = \frac{a\sqrt{f_b}}{2} = \frac{\omega_c}{\omega} x \frac{\sqrt{f_b}}{2} = \left(\frac{\omega_c\sqrt{f_b}}{2}\right)\frac{1}{\omega}. \qquad (5.28)$$

For a given CMW with a bandwidth parameter f_b and centre frequency f_c, dilating the CMW (large a) would increase the spread in time and decrease the spread in frequency, while compressing the CMW (small a) would decrease the spread in time and increase the spread in frequency. Fig 5.3 shows the Heisenberg boxes of the CMW at various scales [61].
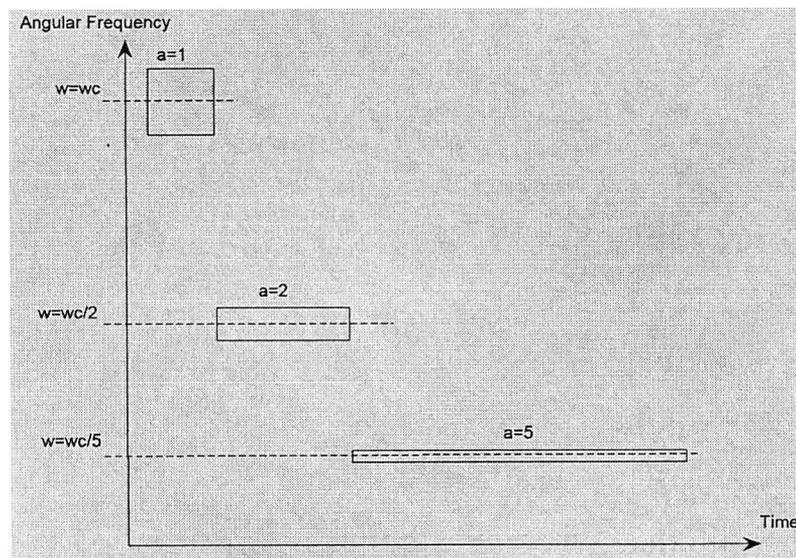
Fig. 5.3 Heisenberg boxes of the CMW

CMW has high frequency localization at low frequency corresponding to large scale, while the time localization is comparatively poorer. At small scale representing high frequency, CMW has poorer frequency localization and a better time localization. This property of the wavelet is very suitable for power disturbance analysis, because transients are of high frequency and a very short duration, while power harmonics are of low frequency and last longer.

From (5.27), with a fixed bandwidth $\Delta\omega$ for all frequencies, it is demanded that

$$\Delta\omega = \left(\frac{1}{\omega_c\sqrt{f_b}}\right)\omega = \text{constant},$$

which requires that

$$\frac{\omega_c}{\omega} = \text{constant} = a \,.$$

From (5.24), a fixed bandwidth $\Delta\omega$ would give a constant time spread Δt.

$$\Delta t = \frac{1}{2\Delta\omega} = \text{constant} \,.$$

The centre frequency ω_c of the CMW can be adjusted in accordance with harmonic frequency ω for harmonic frequency detection so that the corresponding Heisenberg box has a constant spread in time and frequency. Fig 5.4 shows the Heisenberg boxes of the CMW at various centre frequencies [61].
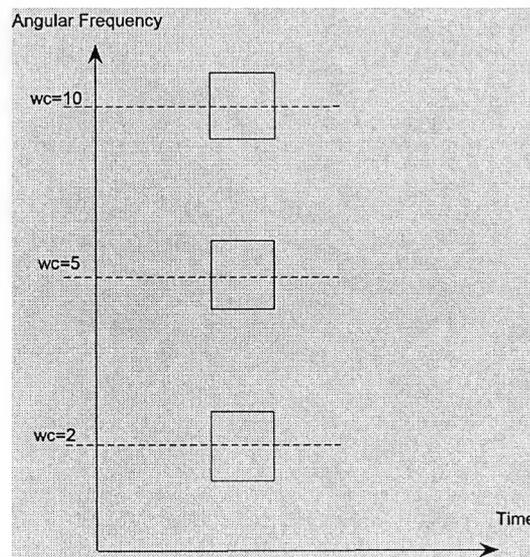
Fig. 5.4 Heisenberg boxes of the CMW for different centre frequencies

5.10 Modified Complex Morlet Wavelet with Constant Lobe Height

As shown in (5.5) and Fig. (5.2), the bandpass filters produced by increasing dilations of the Complex Morlet Wavelet would have increasing lobe heights in frequency domain , in accordance with the factor $\sqrt{a}$. This is not a desirable feature for harmonic analysis. The

power harmonics found in electrical power system normally have lower magnitudes at higher frequencies. If the bandpass filters used have lobe heights inversely proportional frequencies, the small magnitudes of high frequency harmonics would further be scaled by the magnitudes of the bandpass filters, making the identification of higher harmonics very difficult and erroneous. It would be desirable to have equal lobe heights for all dilations of the wavelet. This can be achieved by modifying the definition of the CMW shown in (5.3) slightly, with the scaling factor $1/\sqrt{a}$ changed to $1/a$, as in (5.29) below.

$$\varphi(\frac{t}{a}) = \frac{1}{a}\frac{1}{\sqrt{\pi f_b}}e^{-(\frac{t}{a})^2/f_b}e^{j2\pi f_c(\frac{t}{a})}.$$ (5.29)

The Fourier transform of (5.29) is therefore equal to

$$\Phi(af) = e^{-\pi^2 f_b(af-f_c)^2}.$$ (5.30)

The importance of the modification to the CMW is that the bandpass filters generated by dilations of the modified mother CMW would have the same lobe height for all harmonic frequencies. Fig. 5.5 shows the filter banks generated from the modified CMW.
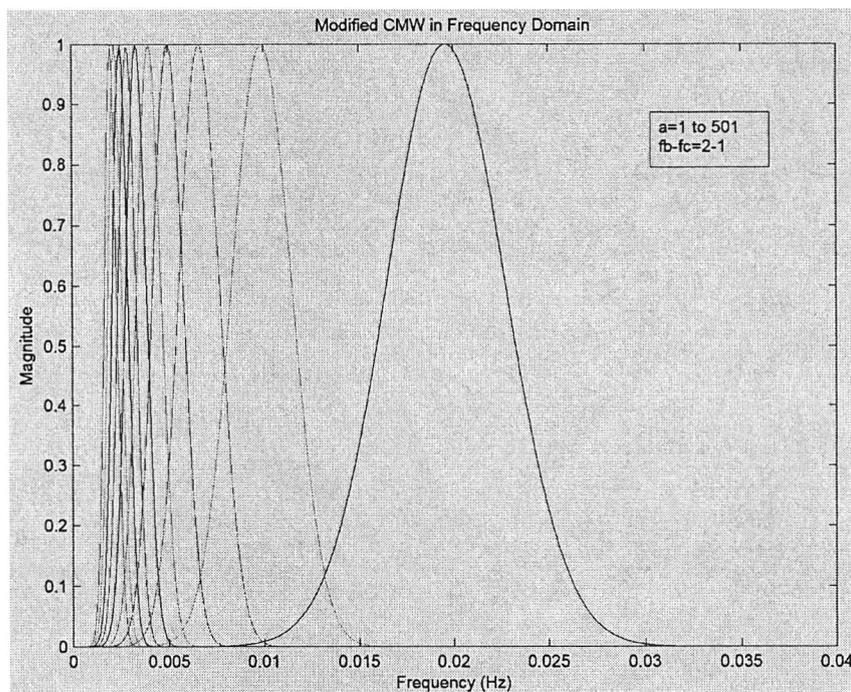
Fig. 5.5 Filter banks of the modified CMW

The time spread and frequency spread of the modified CMW (MCMW) are the same as the original CMW. (5.29) is adopted for the subsequent harmonic analysis applications.

5.11 Frequency and Amplitude Estimation by Wavelet Ridges

Given a signal f(t) represented as

$$f(t) = A(t)\cos\phi(t). \tag{5.31}$$

The wavelet function in (5.3) can be represented as [25,28]

$$\varphi(t) = g(t)e^{j\omega_c t}. \tag{5.32}$$

The dilated and translated wavelet families are represented as [25,28]

$$\varphi_{u,a}(t) = \frac{1}{\sqrt{a}}\varphi\left(\frac{t-u}{a}\right) = e^{-j\omega u}g_{a,u,\omega}(t), \tag{5.33}$$

where $\omega = \dfrac{\omega_c}{a}$ $g_{a,u,\omega}(t) = \sqrt{a}\,g\left(\dfrac{t-u}{a}\right)e^{j\omega t}$.

The wavelet transform of the signal function f(t) in (5.31) is given as

$$Wf(u,a) = \frac{\sqrt{a}}{2}A(u)e^{j\phi(u)}\{\hat{g}(a[\omega - \phi'(u)]) + \varepsilon(u,\omega)\}, \tag{5.34}$$

where $\hat{g}(\omega)$ represents the Fourier Transform of the function g(t).

The error term $\varepsilon(u,\omega)$ in (5.34) is negligible if A(t) and $\phi'(t)$ in (5.31) have small variations over the support of $\varphi_{u,a}$ in (5.33) and if $\phi'(u) \geq \dfrac{\Delta\omega}{a}$. If a power signal contains only a single frequency, the corrective term can be neglected safely. However for a power signal containing harmonics from low frequency to high frequency, the error term will

contribute to the wavelet coefficients, making the frequency detection not as straightforward.

The instantaneous frequency is measured from wavelet ridges defined over the wavelet transform. The normalised scalogram defined by

$$\frac{1}{a}P_W f(u,\omega) = \frac{|Wf(u,a)|^2}{a},$$ (5.35)

is calculated with

$$\frac{1}{a}P_W f(u,\omega) = \frac{1}{4}A^2(u)\left|\hat{g}(\omega_c[1-\frac{\phi'(u)}{\omega}]) + \varepsilon(u,\omega)\right|^2.$$ (5.36)

Since $|\hat{g}(\omega)|$ in (5.36) is maximum at $\omega = 0$, if one neglect $\varepsilon(u,\omega)$, (5.36) shows that the scalogram is maximum at

$$\frac{\omega_c}{a(u)} = \omega(u) = \phi'(u).$$ (5.37)

The corresponding points $(u,\omega(u))$ calculated by (5.37) are called wavelet ridges. For the CMW, g(t) in (5.32) is a Gaussian function. Since the FT of a Gaussian function is also a Gaussian function, the wavelet ridge plot exhibits a Gaussian shape.

Once the harmonic frequencies contained in the harmonic signal are determined by the wavelet ridges, the corresponding harmonics amplitudes would be determined readily by

$$A(u) = \frac{2\sqrt{\frac{1}{a}P_W f(u,\omega)}}{|\hat{g}(0)|} = \frac{2\sqrt{\frac{|Wf(u,a)|^2}{a}}}{1} = \frac{2|Wf(u,a)|}{\sqrt{a}}.$$ (5.38)

The values of $\dfrac{2|Wf(u,a)|}{\sqrt{a}}$ in (5.38) are produced in the process of generating the scalogram.

With the MCMW suggested in (5.29), where the dilated wavelet is defined as

$$\varphi(\frac{t}{a}) = \frac{1}{a}\frac{1}{\sqrt{\pi f_b}}e^{-(\frac{t}{a})^2/f_b}\, e^{j2\pi f_c(\frac{t}{a})}\;;$$

the amplitude can be calculated directly as

$$A(u) = 2\left|Wf(u,a)\right|. \tag{5.39}$$

This is another reason for adopting the MCMW.

The wavelet ridges plot is customarily produced in accordance with scales. For harmonics estimation, it would be more convenient to generate the wavelet ridges plot in terms of frequency. This will be discussed in Chapter 7.

5.12 Conclusion

The simplified Complex Morlet Wavelet is chosen for the Continuous Wavelet Transform for harmonic analysis. It is able to extract frequency, amplitude and phase angle information from the signal. The simplified Complex Morlet Wavelet is a sinusoid-modulated Gaussian function with a smooth harmonic waveform, which is best suited for harmonic analysis. As long as the Q factor of the wavelet is large enough ($f_b=2$, $f_c \geq 0.8$, $Q \geq 7.11$), the Simplified Complex Morlet Wavelet is qualified to be a wavelet in practical sense.

The simplified Complex Morlet Wavelet has the smallest Heisenberg box area, which is able to achieve the best time-frequency localization. The time-frequency localization of the wavelet can be controlled by the Q-factor which in turn is determined by the bandwidth parameter and the centre frequency of the simplified Complex Morlet Wavelet. As harmonic signals are normally of equal frequency distribution and a fixed time length is

normally used for harmonic analysis, a constant time-frequency localization wavelet can also be constructed by appropriately varying the centre frequency of the wavelet in accordance with the harmonic frequency to be detected.

The simplified Complex Morlet Wavelet is further modified to have constant lobe height for all dilations, so that the errors in detecting the amplitudes of higher harmonics would be reduced.

Wavelet ridges are used to extract frequency information from the complex wavelet coefficients [73-76]. The amplitudes of harmonics are readily available in the process of generating the scalogram.

Chapter 6

The Use of Modified Complex Morlet Wavelet for Harmonics Analysis

6.1 Introduction

As discussed in Section 5.6, a set of frequency filter banks would be produced by the dilations of the MCMW. The filter banks are Gaussian function in both time and frequency domain. Dependent on the filter parameters, adjacent filter banks overlap with each other in frequency domain. Errors would be produced in signal frequency estimation when the signals contain frequencies in close proximity. This Chapter will investigate the application of the MCMW from the perspective of filter banks for harmonics detection.

6.2 Q-Factor and the Shape of the Modified Complex Morlet Wavelet

The time width of the MCMW is dependent on the Q-factor of the MCMW. MCMW with different settings of centre frequency f_c and bandwidth f_b but with the same Q-factor would have the same shape, same oscillation and time width. Fig. 6.1 shows two MCMWs with different f_b and f_c values. Fig. 6.1(a) is a MCMW with f_b-f_c = 2-1 and Fig. 6.1(b) is a MCMW with f_b-f_c = 1-$\sqrt{2}$. The $f_c\sqrt{f_b}$ which is equivalent to $Q/(2\pi)$ is equal to $\sqrt{2}$ in both MCMWs. As seen from Fig. 6.1, they have the same time width, oscillation and shape.
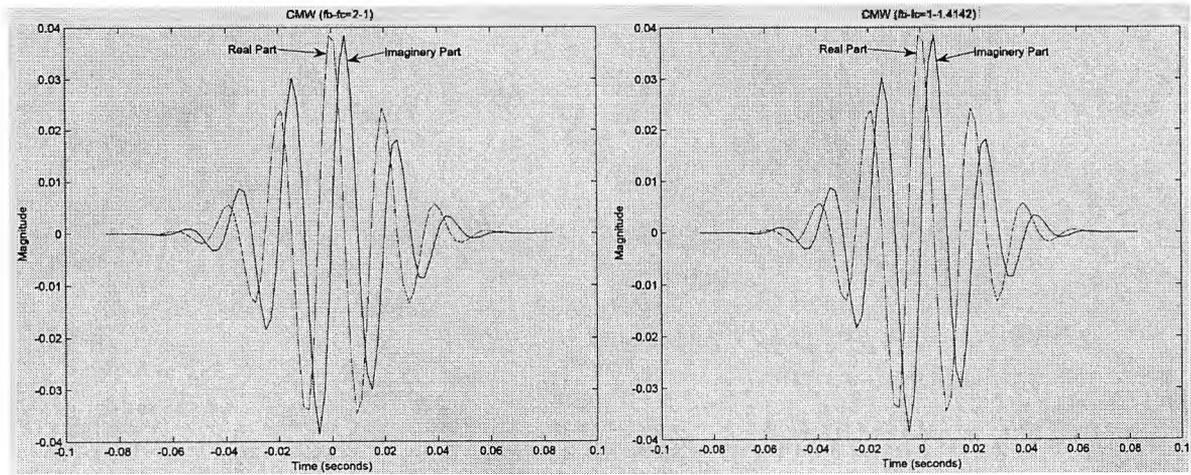
(a) f_b-f_c=2-1   (b) f_b-f_c=1-$\sqrt{2}$

Fig. 6.1 Modified CMW with f_b-f_c=2-1 & 1-$\sqrt{2}$

Fig. 6.2 shows another two MCMWs with f_b-f_c = 16-1 and f_b-f_c = 4-2 respectively. The $f_c\sqrt{f_b}$ values in both MCMWs are the same and are equal to 4. It can be seen that the two MCMWs are exactly the same.
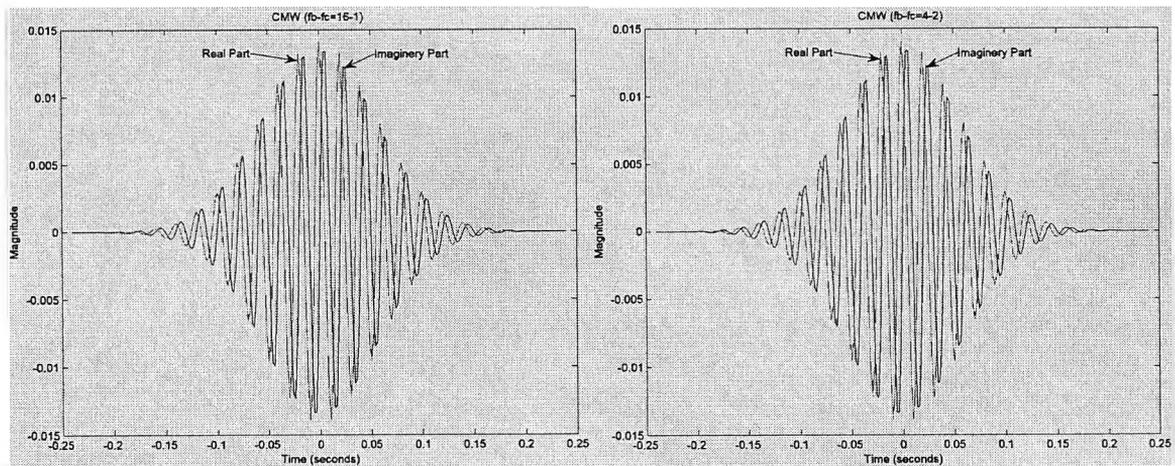
(a) f_b-f_c = 16-1   (b) f_b-f_c = 4-2

Fig. 6.2 Modified CMW with f_b-f_c = 16-1 & 4-2

Comparing Fig. 6.1 and 6.2, it can be seen that a larger $f_c\sqrt{f_b}$ would result in a wavelet of a longer duration. As estimated in Section 5.9, the time width is proportional to $f_c\sqrt{f_b}$.

6.3   Discrimination of Adjacent Frequencies

The MCMW is defined as (5.29),

$$\varphi(\frac{t}{a}) = \frac{1}{a}\frac{1}{\sqrt{\pi f_b}}e^{-(\frac{t}{a})^2/f_b}e^{j2\pi f_c(\frac{t}{a})}.$$

The FT of the MCMW function is (5.30)

$$\Phi(af) = e^{-\pi^2 f_b (af-f_c)^2}.$$

The wavelet filters produced by dilations all have the same lobe height of 1. The coefficients produced for high frequency signal will not be attenuated by the filter mainlobe height. Fig. 6.3 shows the plot of Fourier Transform of two modified CMWs with centre frequencies of f_c/a_1 and f_c/a_2 respectively in the frequency domain.

Assume that f_1 and f_2 represent the frequencies of two harmonics which are adjacent to each other. The f_1 and f_2 are represented in Fig. 6.3 as f_c/a_1 and f_c/a_2 respectively. In order to discriminate the two harmonic frequencies, the two peaks in Fig. 6.3 must be separated apart sufficiently [71,77].
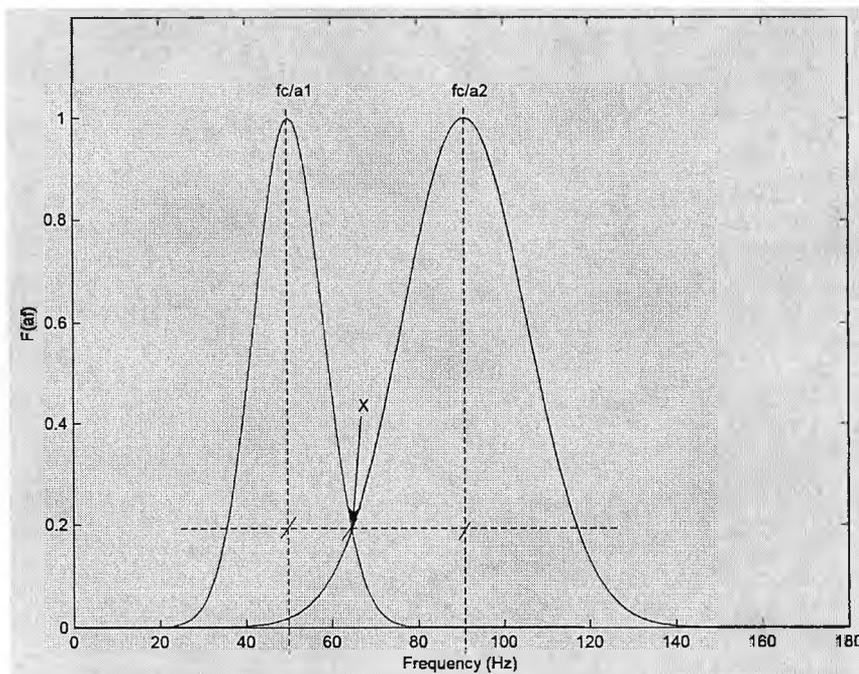
Fig. 6.3 Modified CMW filters with $f_c = f_1$ & f_2

Let x be the intersection of the two filters for the two frequencies f_1 and f_2 where $f_2 > f_1$,

Consider the frequency f_1 first by (5.30),

$$\Phi(a_1,f)=x=e^{-\pi^2 f_b(a_1 f - f_c)^2},$$

so that from (5.8),

$$f = \frac{f_c}{a_1} \pm \frac{1}{a_1}\frac{\sqrt{|ln(x)|}}{\pi}\frac{1}{\sqrt{f_b}}. \tag{6.1}$$

Similarly, for frequency f_2 by (5.30),

$$f = \frac{f_c}{a_2} \pm \frac{1}{a_2}\frac{\sqrt{|ln(x)|}}{\pi}\frac{1}{\sqrt{f_b}}. \tag{6.2}$$

Also from (5.8),

$$f_1 = \frac{f_c}{a_1}, \tag{6.3}$$

$$f_2 = \frac{f_c}{a_2}. \tag{6.4}$$

From (6.1), (6.2), (6.3) and (6.4),

$$f_2 - f_1 = \frac{f_c}{a_2} - \frac{f_c}{a_1} = \frac{1}{a_1}\frac{\sqrt{|ln(x)|}}{\pi}\frac{1}{\sqrt{f_b}} + \frac{1}{a_2}\frac{\sqrt{|ln(x)|}}{\pi}\frac{1}{\sqrt{f_b}}$$
$$= \frac{\sqrt{|ln(x)|}}{\pi}\frac{1}{\sqrt{f_b}}(\frac{1}{a_1}+\frac{1}{a_2}) \tag{6.5}$$

Substituting for a_1 and a_2,

$$f_2 - f_1 \geq \frac{\sqrt{|In(x)|}}{\pi} \frac{1}{\sqrt{f_b}} \left(\frac{f_1}{f_c} + \frac{f_2}{f_c} \right)$$

$$f_2 - f_1 \geq \frac{\sqrt{|In(x)|}}{\pi} \frac{f_1 + f_2}{f_c \sqrt{f_b}} \qquad (6.6)$$

$$f_c \sqrt{f_b} \geq \frac{\sqrt{|In(x)|}}{\pi} \left| \frac{f_1 + f_2}{f_1 - f_2} \right|$$

From (5.26), $Q = 2\pi f_c \sqrt{f_b}$.

Substituting (6.6) into (5.26) gives

$$Q = 2\pi f_c \sqrt{f_b} \geq 2\sqrt{|In(x)|} \left| \frac{f_1 + f_2}{f_1 - f_2} \right| . \qquad (6.7)$$

Therefore for the filter banks to be able to discriminate adjacent frequencies, the Q-factor of the modified CMW should satisfy the condition in (6.7). The x in (6.7) should be as small as possible for accurate harmonic frequency and amplitude estimation and would depend on

1)   the relative amplitudes of the harmonics;

2)   the accuracy required in the amplitude estimation.

A high Q-factor requires a long time signal for accurate amplitude estimation. The selection of the x value would therefore need to be compromised with the signal length to be used for analysis. It is found that x = 0.1 is sufficient for accurate frequency and amplitude detection if the amplitudes of adjacent frequencies are not differed very much from each other, which gives $\dfrac{\sqrt{|In(0.1)|}}{\pi} = 0.483 \approx 0.5$.

Consider a signal with frequency components of 40Hz and 60Hz respectively both of unit amplitude. From (6.6),

$$f_c \sqrt{f_b} \geq 0.483 \left| \frac{60 + 40}{60 - 40} \right| = 2.415 .$$

which requires that $f_b = 100$ and $f_c = 0.25$.

By using the wavelet ridges plot discussed in Section 5.11, Fig. 6.4 shows the wavelet ridges plot. The detected frequencies are exactly equal to 40Hz and 60Hz respectively. The amplitude estimated for 40Hz is exact; the amplitude estimated for 60Hz has an error of 0.1% which is negligibly small.
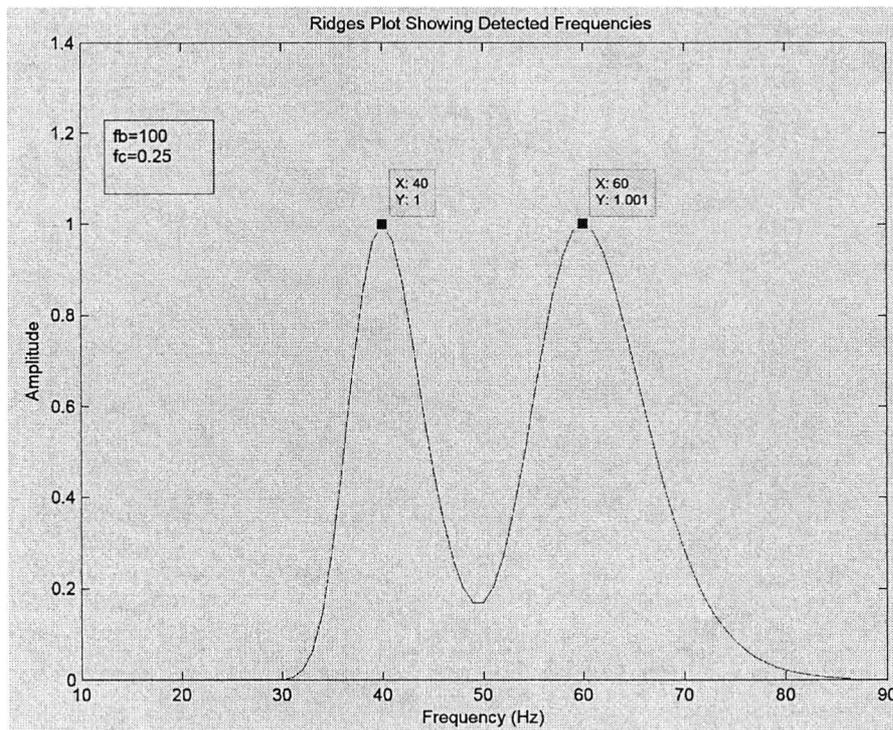
Fig. 6.4 Wavelet ridges plot for 40Hz and 60Hz ($f_c \sqrt{f_b} = 2.415$)

With x = 0.2, the $f_c \sqrt{f_b} = 2$ ($f_b = 100$, $f_c = 0.2$) which is smaller than 2.415, the wavelet ridges plot is shown in Fig. 6.5. The frequency estimation is correct but the error in the amplitude estimated for 60Hz increases to 1.2%.
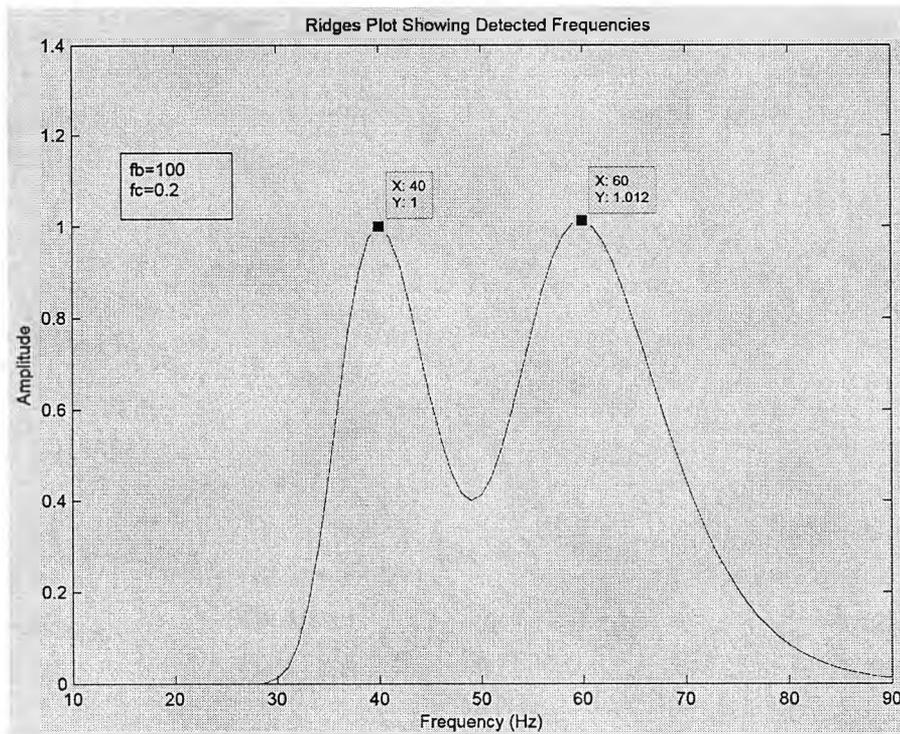
Fig. 6.5 Wavelet ridges plot for 40Hz and 60Hz ($f_c\sqrt{f_b} = 2$)

Fig. 6.6 and Fig. 6.7 show the wavelet ridges plot for $f_b = 100$, $f_c = 0.15$, ($f_c\sqrt{f_b} = 1.5$) and $f_b = 100$, $f_c = 0.05$, ($f_c\sqrt{f_b} = 0.5$) respectively. Both the frequency and amplitude estimated exhibit large errors. In Fig. 6.7, a single frequency is detected which is nearly equal to the average of the two harmonic frequencies in the signal.
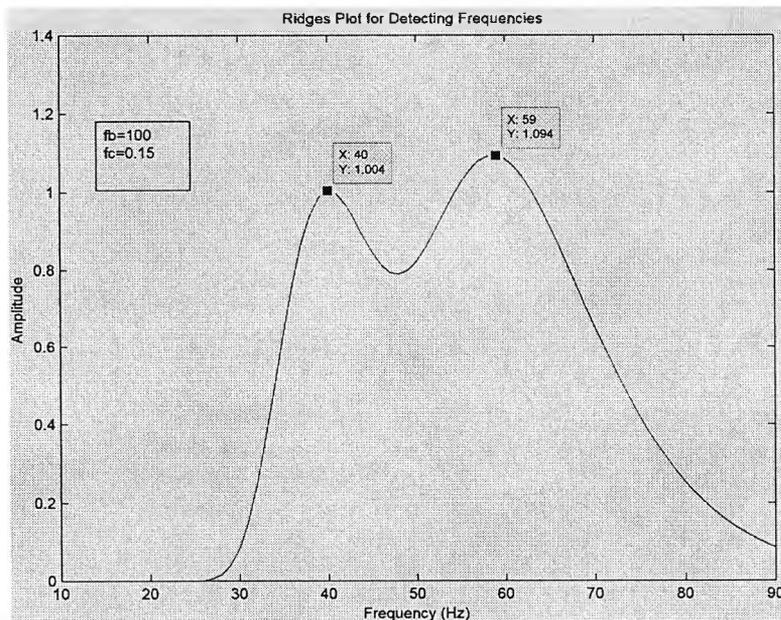
Fig. 6.6 Wavelet ridges plot for 40Hz and 60Hz ($f_c\sqrt{f_b} = 1.5$)
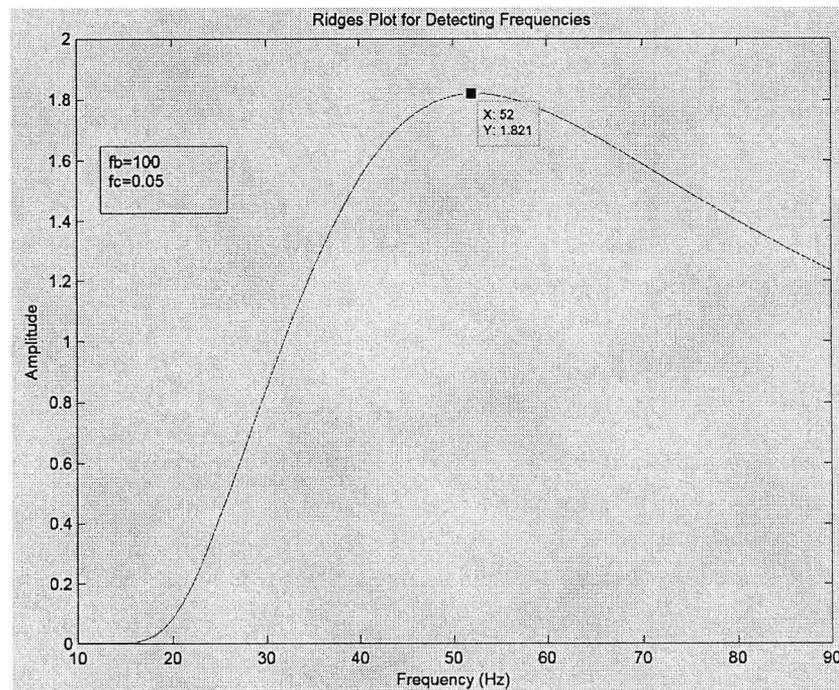
Fig. 6.7 Wavelet ridges plot for 40Hz and 60Hz ($f_c \sqrt{f_b} = 0.5$)

It can be seen that the value of x selected has significant effects on the accuracy in amplitude and frequency estimations.

6.4   The Sampling Frequency

In accordance with the classical signal processing theory, the sampling frequency must be twice the highest frequency component in the signal to avoid aliasing. Nyquist frequency is defined as equal to half of the sampling frequency.

As can be seen from Fig. 6.3, the filters produced by the MCMW have finite bandwidths, which may cause aliasing if the sampling frequency is close to the centre frequency of the dilated MCMW. From (6.2),

$$f = \frac{f_c}{a} \pm \frac{1}{a} \frac{\sqrt{|ln(x)|}}{\pi} \frac{1}{\sqrt{f_b}} .$$

Let the highest frequency, f_H, that the filter produced by a given MCMW would cover is given as

$$f_H = \frac{f_c}{a} + \frac{1}{a} \frac{\sqrt{|ln(x)|}}{\pi} \frac{1}{\sqrt{f_b}}.$$ (6.8)

With $\dfrac{1}{a} = \dfrac{f}{f_c}$ in (5.8), by setting f_H as the Nyquist frequency, i.e., $f_s/2$, then

$$\frac{f_s}{2} \geq f + \frac{f}{f_c} \frac{\sqrt{|ln(x)|}}{\pi} \frac{1}{\sqrt{f_b}}$$

$$f_s \geq 2f \left[1 + \frac{\sqrt{|ln(x)|}}{\pi} \frac{1}{f_c \sqrt{f_b}} \right].$$ (6.9)

$$f_s \geq 2f \left[1 + \frac{2\sqrt{|ln(x)|}}{Q} \right]$$

(6.9) provides an estimation of the minimum sampling frequency which is seen to be dependent on the Q-factor of the MCMW. The higher the Q-factor, the lower would be the minimum sampling frequency. As discussed in Section 5.8, to qualify as a wavelet, the term $f_c \sqrt{f_b}$ should not be smaller than 1.14. From Section 6.3, $\dfrac{\sqrt{|ln x|}}{\pi} = 0.483$ and with $f_c \sqrt{f_b} \geq 1.14$ as discussed in Section 5.8, from (6.9),

$$f_s \geq 2f \left[1 + \frac{0.483}{1.14} \right] = 2.85f \approx 2.9f.$$

Therefore, with complex CWT, the sampling frequency should be 2 to 2.9 times of the highest harmonic frequency in the harmonic signal. The higher the Q-factor or the factor $f_c \sqrt{f_b}$, the lower would be the minimum sampling frequency.

Consider $f = 1000Hz$, $x = 0.1$, f_b-f_c = 2-1, the minimum sampling frequency from (6.9) is

$$f_s \geq 2(1000) \left[1 + \frac{\sqrt{|ln(0.1)|}}{\pi} \frac{1}{1\sqrt{2}} \right] = 2683Hz.$$

When f_b-f_c = 100-1, the filter bandwidth is much narrower due to the high Q-factor, the minimum sampling frequency from (6.9) is

$$f_s \geq 2(1000)\left[1+\frac{\sqrt{|ln(0.1)|}}{\pi}\frac{1}{1\sqrt{100}}\right] = 2097Hz \,.$$

Therefore the filter has a much narrower frequency bandwidth.

Consider a signal containing 50Hz with amplitude equal to 1 and 800Hz with amplitude equal to 2, the minimum sampling frequency is determined as (6.9),

$$f_s \geq 2(800)\left[1+\frac{\sqrt{|ln(0.1)|}}{\pi}\frac{1}{1\sqrt{2}}\right] = 2146Hz \,, \text{ where } f_b\text{-}f_c = 2\text{-}1.$$

The actual sampling frequency used is 2000Hz. The frequency spectrum is from 0 to 1000Hz. The wavelet ridges plot is shown in Fig. 6.8. The detection of 50Hz signal component is accurate. The detection of the 800Hz signal component has an error of 5Hz.
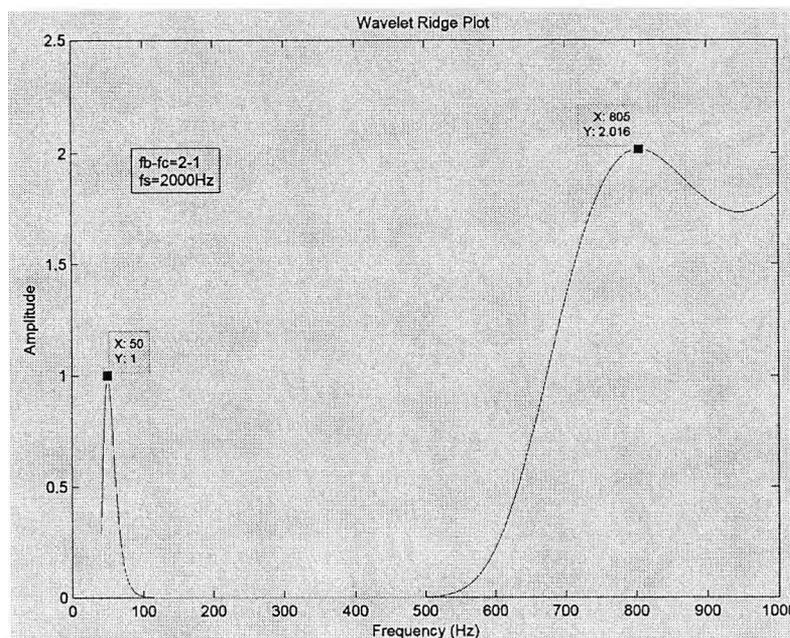
Fig. 6.8 Wavelet ridges plot for 50Hz and 800Hz (f_s = 2000Hz)

With the sampling frequency increased to 2200Hz, the frequency spectrum is from 0 to 1100Hz. The wavelet ridge plot is shown in Fig. 6.9. It can be seen that the frequencies and amplitudes of 50Hz and 800Hz estimated are very accurate.
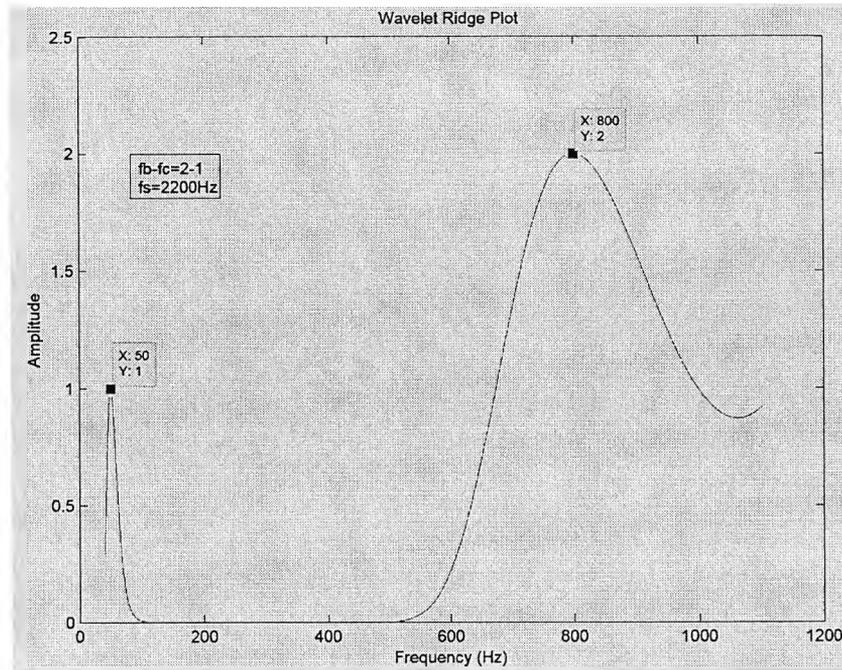
Fig. 6.9 Wavelet ridges plot for 50Hz and 800Hz (f$_s$ = 2200Hz)

6.5   Time Window

It is a common understanding that the larger the time window encompassing the signal under analysis, the better would be the estimation of the frequency and amplitude of the harmonics. On the other hand, for time event localization, the shorter the time window the better would be the localization of the time event.

The minimum time window length is controlled by the time width of the wavelet required to achieve a mean zero value. As estimated in Section 5.5, the factor f$_c$√f$_b$ should not be less than 1.14 in order that the MCMW should have practically zero mean value.

From (5.18), the spread in time of the MCMW is given as $\Delta t = \dfrac{a\sqrt{f_b}}{2}$.

Since from (5.8), $a = \dfrac{f_c}{f}$,

$$\Delta t = \frac{f_c}{f} \frac{\sqrt{f_b}}{2} = (\frac{f_c \sqrt{f_b}}{2}) \frac{1}{f}. \qquad (6.10)$$

Consider f_b-f_c = 2-1, f = 50Hz, which gives Δt = 0.0142 s. Fig. 6.10 shows the real part and imaginary part of the MCMW. It can be seen that within the time spread Δt, the sinusoids contained in the Gaussian function would not decline to zero.
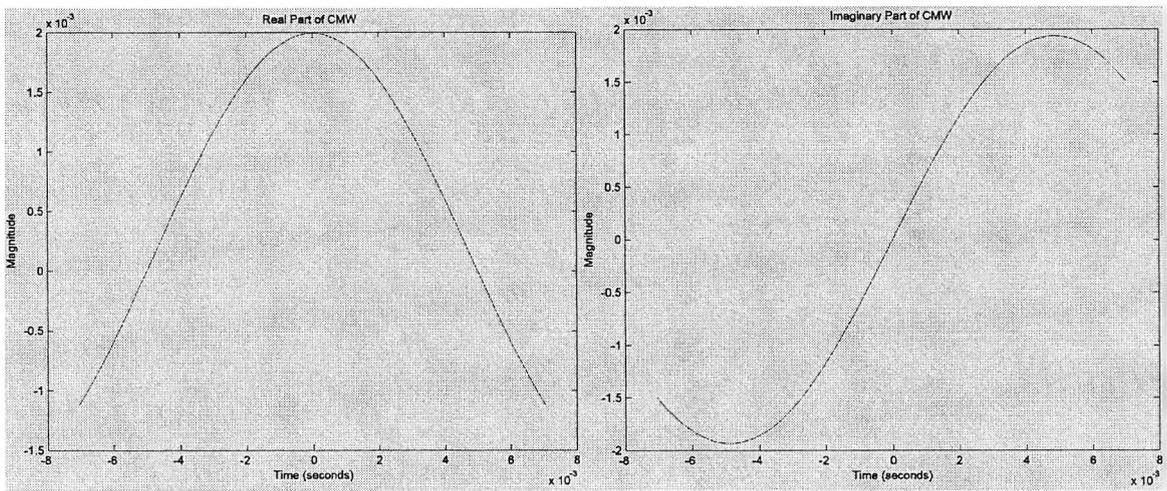
(a) real part   (b) imaginary part

Fig. 6.10 Modified CMW with Δt = 0.0142s

From (5.4), the mean value of the modified CMW in (5.29) is given by

$$\int_{-\infty}^{+\infty} \varphi(\frac{t}{a}) dt = \frac{1}{a} \frac{1}{\sqrt{\pi f_b}} \int_{-\infty}^{+\infty} e^{-(\frac{t}{a})^2 / f_b} e^{j2\pi f_c(\frac{t}{a})} dt = e^{-\pi^2 f_b f_c^2}. \qquad (6.11)$$

In (6.11), the integral is extending to negative and positive infinity. If the integral is taken for a period of Δt only, (6.11) shows that

$$\int_{-\frac{\Delta t}{2}}^{+\frac{\Delta t}{2}} \varphi(\frac{t}{a})dt = \frac{1}{a}\frac{1}{\sqrt{\pi f_b}} \int_{-\frac{\Delta t}{2}}^{+\frac{\Delta t}{2}} e^{-(\frac{t}{a})^2/f_b} e^{j2\pi f_c(\frac{t}{a})} dt$$

$$\frac{1}{a}\frac{1}{\sqrt{\pi f_b}} \int_{-\frac{\Delta t}{2}}^{+\frac{\Delta t}{2}} e^{-(\frac{t}{a})^2/f_b} [cos(2\pi f_c(\frac{t}{a})) + j\,sin(2\pi f_c(\frac{t}{a}))]dt \qquad (6.12)$$

$$= 7.108x10^{-4} - j4.39x10^{-6}$$

The mean value of the MCMW for the duration of Δt is approximately $7.108x10^{-4}$. It can be seen that the requirement of zero mean value is not fulfilled. A time width equal to the time spread of the MCMW is hence not sufficient, a longer time window is necessary so that the mean value of the MCMW is close to zero.

From (6.10), let

$$T = b(\frac{f_c\sqrt{f_b}}{2})\frac{1}{f} \qquad (6.13)$$

where b is a factor used to adjust the time spread of the MCMW.

Table 6.1 shows the time window width and the mean value of the MCMW for various b values.

Table 6.1 Time window length and mean value of modified CMW

b	Time Window Length (seconds)	Mean Value of MCMW
1	0.0142	$7.108x10^{-4}$
2	0.0284	$3.302x10^{-4}$
3	0.0426	$3.68x10^{-5}$
4	0.0568	$5.712x10^{-5}$
5	0.071	$3.631x10^{-5}$
6	0.0852	$6.309x10^{-6}$
7	0.0994	$2.957x10^{-6}$
8	0.1136	$1.887x10^{-6}$
9	0.1278	$3.491x10^{-7}$
10	0.142	$4.391x10^{-8}$
11	0.1562	$3.449x10^{-8}$
12	0.1704	$6.1x10^{-9}$
13	0.1846	$5.259x10^{-11}$
14	0.1988	$1.337x10^{-12}$
15	0.213	$3.432x10^{-11}$
16	0.2272	$8.45x10^{-14}$

It can be seen from Table 6.1 that at b = 10 the MCMW have a mean value close to zero. Therefore the time width, T, of the MCMW is determined as

$$T \geq \frac{5f_c\sqrt{f_b}}{f}.$$ (6.14)

It should be noted that when very accurate estimation in both frequency and amplitude is required, a larger value of b is to be used. A longer time width of the modified CMW is to be used which in turn requires a long time signal for estimation. The computation time is therefore longer.

With a shorter time length of the modified CMW, harmonic frequencies would still be estimated accurately. However the amplitudes estimated are erroneous.

Consider the harmonic signal shown in Fig. 6.11 having frequency components at 40Hz and 120Hz respectively, both are of unit amplitude.
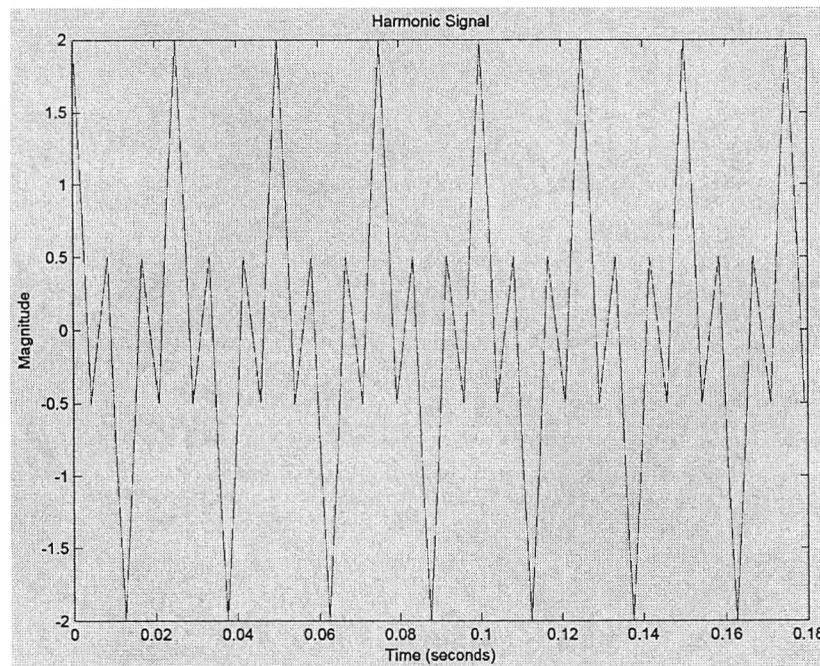
Fig. 6.11 Simulated signal (harmonics at 40Hz & 120Hz)

In order to discriminate the two harmonic frequencies, from (6.6),

$$f_c \sqrt{f_b} \geq 0.483 \left| \frac{120 + 40}{120 - 40} \right| = 0.996 \,.$$

The parameters of the MCMW are chosen as f_b-f_c = 2-1 so that the mean value of the MCMW is practically zero. The factor $f_c \sqrt{f_b}$ is equal to $\sqrt{2}$.

The sampling frequency is determined as from (6.9),

$$f_s \geq 2(120) \left[1 + \frac{\sqrt{|ln(0.1)|}}{\pi} \frac{1}{\sqrt{2}} \right] = 322 Hz \,.$$

A sampling frequency of 350Hz is chosen. The minimum time window length is estimated from (6.14),

$$T \geq \frac{5\sqrt{2}}{40} = 0.18 \,.$$

Fig. 6.12 shows the wavelet ridges plot of the signal. The harmonic frequencies and amplitudes estimated are exactly equal to the simulated harmonic signal.
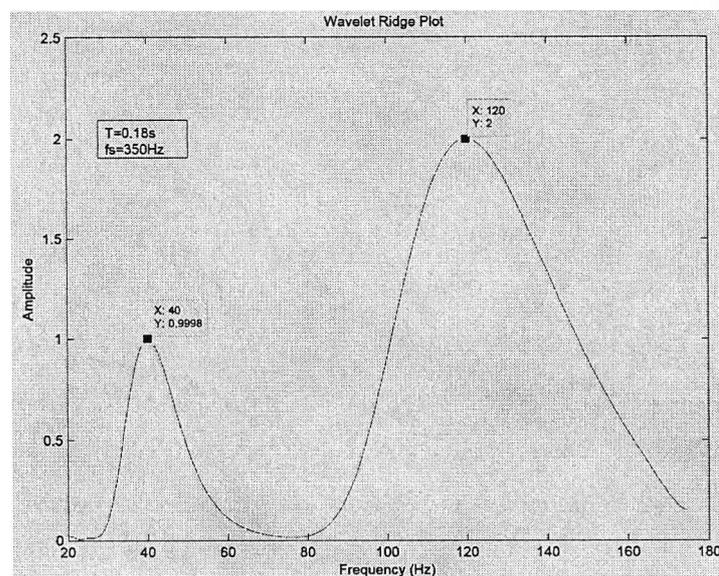
Fig. 6.12 Wavelet ridges plot for 40Hz and 120Hz (f_s = 350Hz, T = 0.18s)

Now the time window from (6.13) is reduced to

$$T \geq \frac{3\sqrt{2}}{40} = 0.11.$$

Fig. 6.13 shows the wavelet ridges plot. It can be seen that the detection of harmonic frequencies are accurate. However there are errors in amplitudes detection. The amplitude detection error is seen to be larger at low frequency.
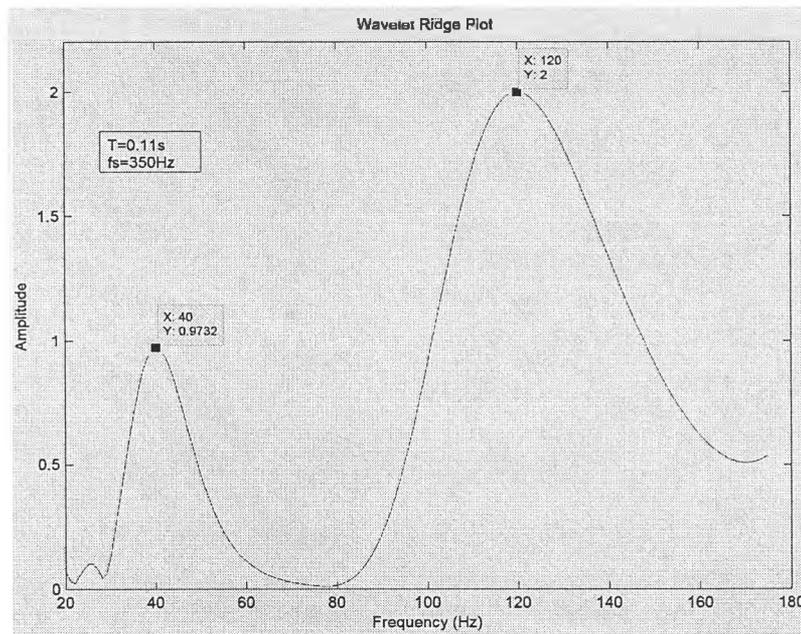
Fig. 6.13 Wavelet ridges plot for 40Hz and 120Hz (f_s = 350Hz, T = 0.11s)

Now the time window is further reduced to be equal to Δt of the MCMW,

$$T \geq \frac{\sqrt{2}}{40} = 0.036.$$

Fig. 6.14 shows the wavelet ridges plot. It can be seen that the detection of low harmonic frequency and amplitude are far from correct. There is also an error in the estimated amplitude of the higher harmonic frequency.
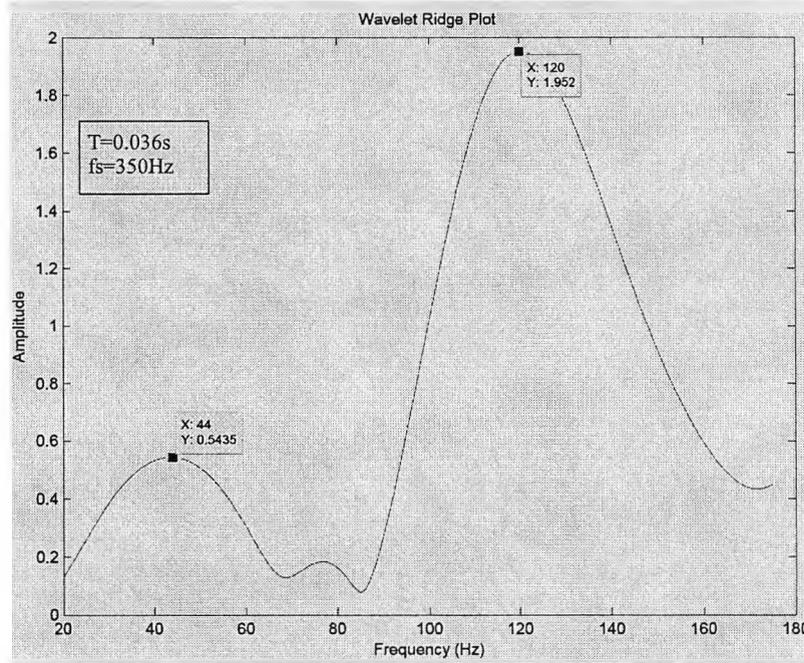
Fig. 6.14 Wavelet ridges plot for 40Hz and 120Hz (f_s = 350Hz, T = 0.036s)

6.6   Phase Estimation

The MCMW, given its analytic nature, can preserve signal phase information. Complex continuous wavelet transform would produce complex wavelet coefficients. When the complex wavelet coefficients are presented in polar form, each complex wavelet coefficient has a phase angle. The phase information contained in the wavelet coefficients is termed 'instantaneous phase'. Each sampled data point in the time signal has a wavelet coefficient related to it.

For a harmonic signal which contains harmonic frequencies, the relative phase difference between any two harmonics changes over time. Consider the two sinusoids defined as

$$v_1 = A_1 \cos(\omega_1 t + \theta_1)$$
$$v_2 = A_2 \cos(\omega_2 t + \theta_2)$$

(6.15)

Their phase difference at any time t is

$$\angle v_2 - \angle v_1 = \omega_2 t + \theta_2 - (\omega_1 t + \theta_1) = (\omega_2 - \omega_1)t + \theta_2 - \theta_1.$$

(6.16)

In (6.16), the phase difference has two terms. The first term depends on the frequency difference between the two sinusoids and is a function of time. The second term is the phase difference at time t = 0 and is a constant phase difference, which is termed as 'initial phase difference'.

The main purpose is to estimate the 'initial phase difference' by using the complex CWT based on MCMW. This is actually the phases of the harmonics at time zero, i.e. contained at the wavelet coefficient for the first data of the signal samples. Consider a harmonic signal of frequency ω and an initial phase angle θ. Let θ_w be the instantaneous phase obtained from the wavelet coefficient at time t. The instantaneous phase at time t is related to θ by

$$\theta_w = \omega t + \theta$$
$$\theta = \theta_w - \omega t \qquad . \tag{6.17}$$
$$\theta = \theta_w - 2\pi f t$$

Also the time t is related to the data sample n by

$$t = \frac{n-1}{f_s}. \tag{6.18}$$

Therefore from (6.17) and (6.18),

$$\theta = \theta_w - 2\pi f \left(\frac{n-1}{f_s} \right). \tag{6.19}$$

The initial phase angle θ, i.e., the phase angle of the harmonic signal at time t = 0 (n = 1), is

$$\theta = \theta_w - 2\pi f (0)$$
$$\theta = \theta_w \qquad . \tag{6.20}$$

The initial phase angle of the harmonic signal is hence equal to the phase angle of the

wavelet coefficient at n = 1 (t = 0). It is therefore seemed straightforward to use the first wavelet coefficient generated from the CWT to estimate the initial phase angles of all the harmonics in the signal.

However as will be discussed in Section 7.9, the edge effect would distort the wavelet coefficients at the boundaries of the sampled signal data, making those wavelet coefficients not representative of the harmonics contained in the harmonic signal. Wavelet coefficients which are sufficiently away from the edges of the sampled signal data should be used for phase estimation.

From (6.19), the initial phase difference between any two harmonics is given by

$$\theta_2 - \theta_1 = \left(\theta_{w2} - \theta_{w1}\right) - 2\pi(n-1)\frac{(f_2 - f_1)}{f_s}. \tag{6.21}$$

Therefore the initial phase difference can be estimated from (6.21) by using wavelet coefficients at any position n as long as n is sufficiently away for signal edges. It is suggested that the wavelet coefficient generated for the data at the centre position of the signal should be used for the phase estimation.

It should be noted that the initial phase difference estimated by (6.21) would depend on whether the harmonic signal is represented as a cosine or a sin function. They differ by 90°.

Consider the harmonic signals

$$f_1 = cos(\ 2\pi 249t + 10^o\ ), \tag{6.22a}$$

$$f_2 = sin(\ 2\pi 249t + 10^o\ ). \tag{6.22b}$$

(6.22a) represents a harmonic signal as a cosine function and (6.22b) represents a harmonic signal as a sine function.

For (6.22a), by using CWT based on the modified CMW, the initial phase estimated by using (6.19) is 10°. Similarly for (6.22b), the initial phase estimated by using (6.19) is -80°.

It can easily be seen that

$$\sin(\omega t + \theta) = \cos\left[90^\circ - (\omega t + \theta)\right]$$
$$\cos\left[\omega t + (\theta - 90^\circ)\right] \quad (6.23)$$

Therefore for $\theta = 10^\circ$,

$$\sin(\omega t + 10^\circ) = \cos\{\omega t + (10^\circ - 90^\circ)\} = \cos(\omega t - 80^\circ). \quad (6.24)$$

The CWT has a presumption that the harmonic signal is represented as a cosine function. This explains why the initial phase estimated by (6.19) for (6.22b) is -80°.

Now consider a signal that is represented as

$$f(t) = \cos(2\pi 50 t + 10^\circ) + 0.5\cos(2\pi 150 t - 25^\circ). \quad (6.25)$$

The signal is sampled at $f_s = 450$Hz, with a sampled signal length of 0.2s. The parameters of the MCMW is f_b-f_c = 2-1. Fig. 6.15 shows the wavelet ridges plot generated by the CWT based on MCMW.
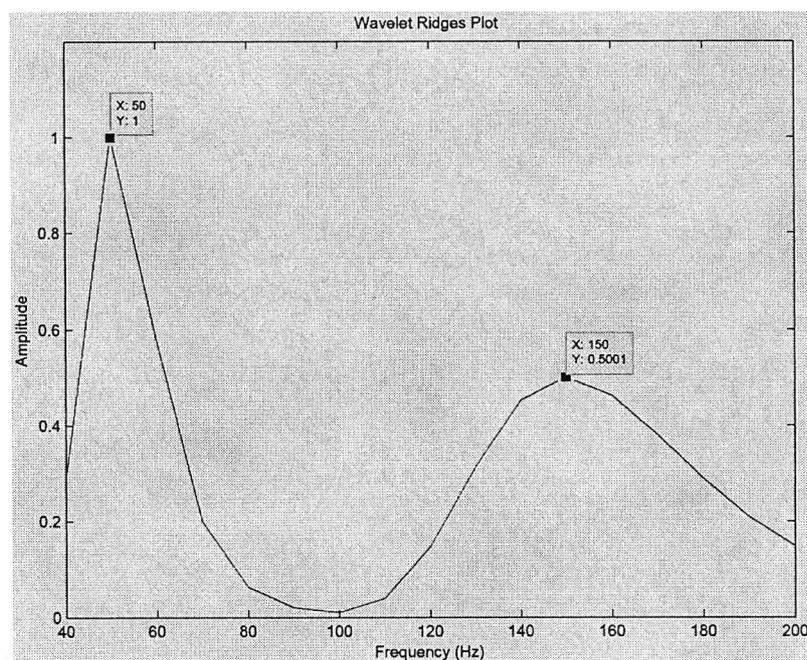
Fig. 6.15 Wavelet ridges plot for 50Hz and 150Hz ($f_s = 450$Hz, T = 0.2s)

The instantaneous phases estimated at 50Hz and 150Hz are shown in Fig. 6.16(a) and Fig. 6.16(b) respectively. The estimated phases obtained from the wavelet coefficients lie between $\pm\pi$. It can be seen in Fig. 6.16 that there are abrupt phase variations near the start and the end of the phase plots. This is due to the edge effect mentioned earlier and to be discussed in Section 7.9.
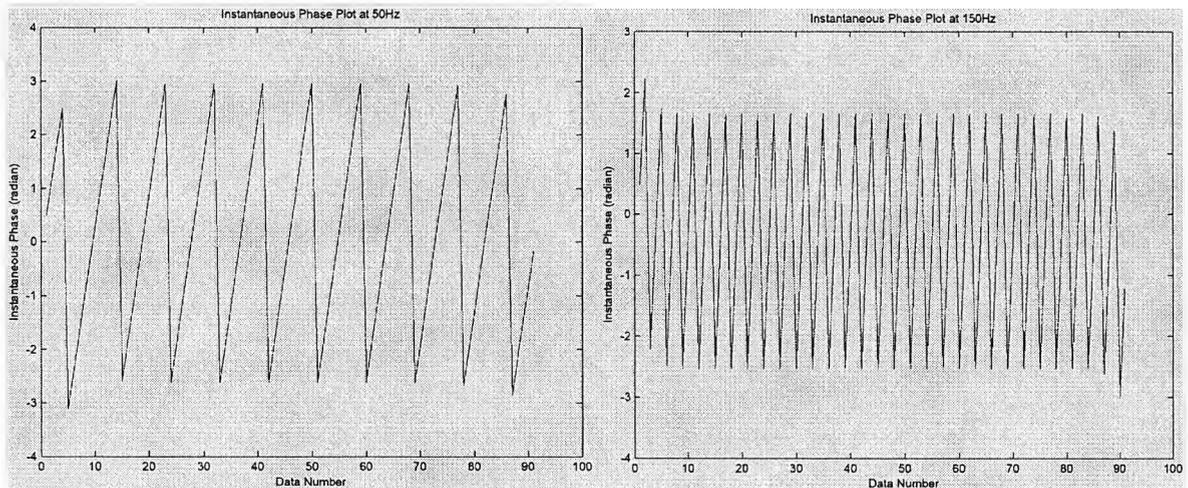
(a) 50Hz   (b) 150Hz

Fig. 6.16 Phase plots for 50Hz and 150Hz

Table 6.2 compares the estimated initial phases by (6.19) to the actual phases of the simulated signal. It can be seen that the initial phases estimated by the CWT based on MCMW are exactly equal to the initial phases of the simulated signal.

Table 6.2 Comparison of estimated phases and simulated phases

Frequency (Hz)	Set Initial Phase	Instantaneous Phase from Wavelet Coefficient at n=46	Estimated Initial Phase
50	0.1745 rad (10°)	31.5905 rad (1809.974°)	0.1746 rad (10°)
150	-0.4363 rad (-25°)	93.8116 rad (5375.03°)	-0.4362 rad (-24.99°)

Now consider a voltage waveform and a current waveform represented as v(t) and i(t) respectively.

$$v(t) = \cos(2\pi 50t + 10^o), \tag{6.26a}$$

$$i(t) = 0.2\cos(2\pi 50t - 22^o). \tag{6.26b}$$

Both waveforms have the same frequency. The signals are sampled at f_s = 450Hz, with a sampled signal length of 0.2s. The parameters of the MCMW is f_b-f_c = 2-1.

Fig. 6.17 shows the wavelet ridges plot for the two waveforms.
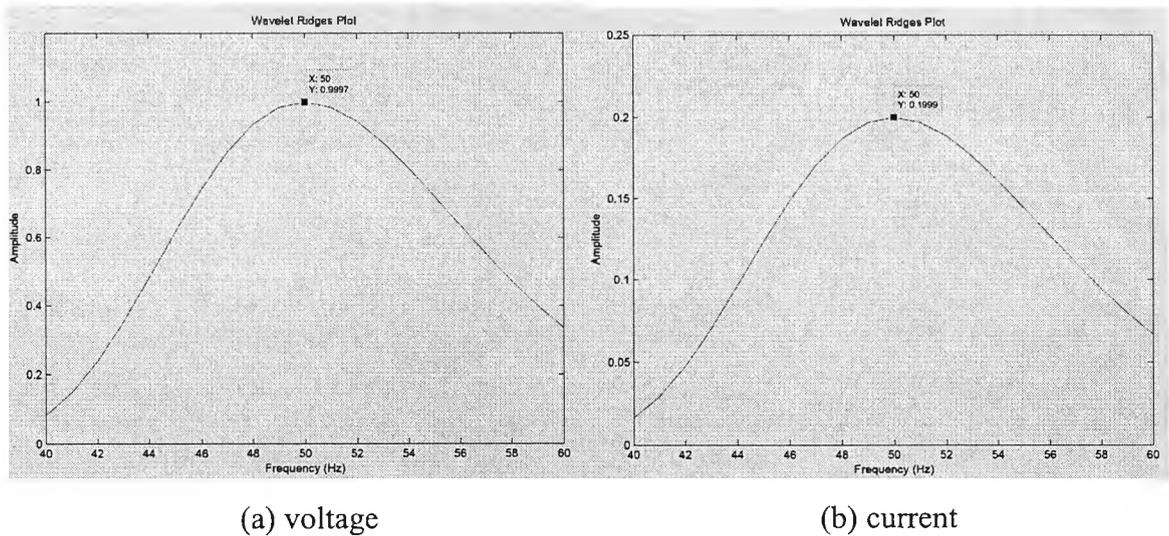
(a) voltage   (b) current

Fig. 6.17 Wavelet ridges plot of voltage and current waveforms

Table 6.3 compares the estimated phase difference to the set phase difference of the voltage and current signals. It can be seen that the phase difference estimated by the proposed algorithm is very accurate.

Table 6.3 Estimated phase difference between voltage and current waveform

	Voltage (50Hz)	Current (50Hz)	Phase Difference
Set Initial Phase (deg.)	10°	-22°	32°
Estimated Instantaneous Phase (deg.)	9.9992^o	-21.9984^o	31.9976^o

For harmonic analysis, it is not particularly useful to know the 'initial phases' of harmonics

in a harmonic signal. Rather it would be more useful to know the phase differences between two harmonics of the same frequency, for example, the phase difference between the harmonic voltage and the corresponding harmonic current. In this case the phase difference is preserved by every wavelet coefficients as long as they are far from the signal edges. From (6.21),

$$\theta_2 - \theta_1 = \left(\theta_{w2} - \theta_{w1}\right) - 2\pi(n-1)\frac{(f_2 - f_1)}{f_s}.$$

Since $f_2 = f_1$,

$$\theta_2 - \theta_1 = \left(\theta_{w2} - \theta_{w1}\right) - 2\pi(n-1)\frac{(f_2 - f_2)}{f_s}$$

$$\theta_2 - \theta_1 = \left(\theta_{w2} - \theta_{w1}\right) - 2\pi(n-1)(0) \qquad . \qquad (6.27)$$

$$\theta_2 - \theta_1 = \theta_{w2} - \theta_{w1}$$

6.7 Conclusion

The shape, oscillating frequency, and duration of the MCMW are determined by the Q-factor or the factor $f_c\sqrt{f_b}$ of the MCMW. The factor $f_c\sqrt{f_b}$ is determined from the frequency separation of adjacent frequencies. In order to avoid aliasing, the minimum sampling frequency should be estimated from the Q-factor. It is found that the minimum sampling frequency lies between 2 to 2.9 times of the highest harmonic frequency in the signal.

The time duration of the signal should be at least equal to the time duration of the MCMW. The time duration of the MCMW is dependent on the factor $f_c\sqrt{f_b}$ and the period of the lowest harmonic frequency in the signal. It should be chosen such that the mean value of the MCMW should be close to zero.

The complex wavelet coefficients obtained from complex CWT based on MCMW contains the instantaneous phase information. Theoretically the initial phases of the harmonics in the harmonic signal are equal to the instantaneous phases obtained from the first wavelet coefficients at the corresponding scales. Because of the edge effect, wavelet coefficients

sufficiently far away from the signal edges should be used to estimate the initial phases of harmonics. The phase difference between any two harmonics of the same frequency can be calculated easily from any wavelet coefficients as far as they are not distorted by the edge effect.

From the underlying principles of the complex CWT and the characteristics of the MCMW, it can be seen that the suggested harmonic analysis method can be used to detect any frequency components in a signal, including sub-harmonics, harmonics, inter-harmonics.

Chapter 7

Wavelet-Based Algorithm for Harmonics Analysis

7.1 Introduction

As with mathematical tools used to investigate physical phenomena, a number of practical issues must be taken into consideration when implementing the harmonic analysis algorithm. There is no exception with the case of using the complex continuous wavelet transform. The results obtained must be viewed in terms of the limitations in the data analysis method used. These limitations stem from a number of sources, including the discrete nature of the data, the finite resolution of the data, the finite extent of the data, the wavelet used, the discretization and numerical computation of the transform, and so on.

7.2 Complex CWT Implementation by FFT

The computation of the CWT can simply be performed by a naive discretization of the transform integral. Because of the shifting property of the transform, the WT of a function at a given scale is a convolution integral between the function of interest and the wavelet function at the given scale. Therefore the basic algorithm for computing the WT is a set of convolution integrals parametrised by the scale a. The standard convolution algorithm is slow because of large number of multiplications and additions that must be calculated. When the convolution algorithm is conducted by a computer, the computation speed is very slow. As convolution in time domain becomes multiplication in frequency domain, it is computationally economical to replace one convolution with two DFTs, a multiplication, and an IDFT, by using the FFT. The proposed WT-based harmonic analysis algorithm is therefore implemented by FFT with in the Matlab software.

Fig. 7.1 shows the flow chart of the computational algorithm for computing wavelet coefficients by FFT [78].
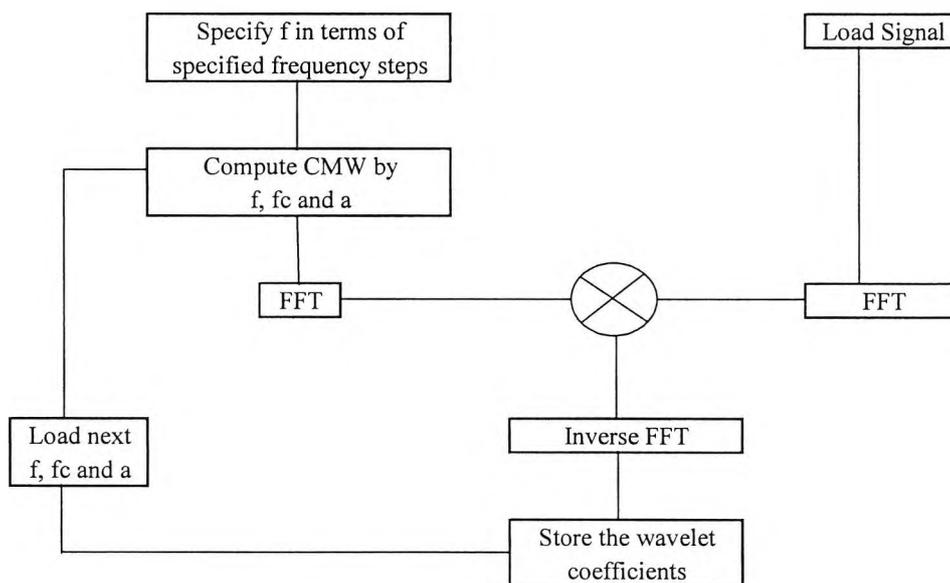
Fig. 7.1 Flow chart for the computation of wavelet coefficients by FFT

7.3 Adaptive Settings of Modified CMW

As discussed in Section 5.3, the detection of harmonic frequencies in a harmonic signal can be effected by dilating a MCMW of a given centre frequency f_c and bandwidth parameter f_b. The disadvantages with this approach are firstly that a very large scale a should be used for low harmonic frequency, which requires a very long signal length, and the computation time is also very long. Secondly, the wavelet coefficients obtained at a large scale a are also subject to computation errors. Thirdly, the frequency resolution at small scale a (i.e. at high harmonic frequency) is poor. For harmonic analysis, it would be more desirable to maintain approximately constant frequency resolution and time spread at all harmonic frequencies. This is achieved by adapting the centre frequency f_c of the MCMW to the harmonic frequency to be analyzed, with the bandwidth parameter f_b kept constant. The value of the centre frequency f_c is governed by the required separation frequency between adjacent frequencies and the harmonic frequency in the harmonic signal, as discussed below.

7.4 Computational Settings

As discussed in Section 6.3, the settings of the modified CMW is determined by the separation frequency between adjacent frequencies, determined by (6.6) as

$$f_c\sqrt{f_b} \geq \frac{\sqrt{|In(x)|}}{\pi}\left(\frac{f_1+f_2}{f_1-f_2}\right),$$

where f_1 and f_2 are the frequencies of two adjacent harmonics components, with $f_1 > f_2$.

The parameters f_b and f_c of the MCMW would depend on the likely separation of adjacent frequencies in the harmonic signal. Let the separation frequency between adjacent frequencies is represented as f_{sep}, and the highest harmonic frequency in the harmonic signal is represented as f_H. Let $f_1 = f_H$, then $f_2 = f_H - f_{sep}$ in (6.6),

$$f_c\sqrt{f_b} \geq y\left(\frac{f_H + f_H - f_{sep}}{f_{sep}}\right)$$

$$f_c\sqrt{f_b} \geq y\left(\frac{2f_H - f_{sep}}{f_{sep}}\right) \qquad (7.1)$$

$$f_c\sqrt{f_b} \geq 2y\left(\frac{f_H}{f_{sep}} - \frac{1}{2}\right)$$

where $y = \dfrac{\sqrt{|In(x)|}}{\pi}$. $\qquad (7.2)$

By putting $x = 0.1$ in (7.2), then $y = 0.483 \approx 0.5$ and (7.1) becomes

$$f_c\sqrt{f_b} \geq \left(\frac{f_H}{f_{sep}} - \frac{1}{2}\right). \qquad (7.3)$$

(7.3) is valid only when $f_H \geq f_{sep}$. This requirement is easily fulfilled in integer harmonic frequency detection where the harmonic frequencies are multiples of the fundamental frequency. The fundamental frequency is either 50Hz or 60Hz. The estimation of

inter-harmonic requires a smaller f_{sep} so that the requirement in (7.3) is fulfilled. For sub-harmonics detection, the expected separation of adjacent frequencies is smaller, and so the requirement in (7.3) is also fulfilled.

Using $f_b = 10000$, then (7.3) becomes

$$f_c \geq \frac{1}{100}\left(\frac{f_H}{f_{sep}} - \frac{1}{2} \right).$$
(7.4)

From (6.9), the minimum sampling frequency to avoid aliasing is estimated as

$$f_s \geq 2f_H\left[1 + \frac{y}{f_c\sqrt{f_b}} \right].$$

Substituting (7.4) into (6.9),

$$f_s \geq 2f_H\left(\frac{2f_H}{2f_H - f_{sep}} \right)$$
$$f_s \geq \frac{4f_H^2}{2f_H - f_{sep}}$$
(7.5)

At high harmonic frequencies, $2f_H \gg f_{sep}$, (7.5) becomes

$$f_s \geq 2f_H,$$
(7.6)

which agrees with the classical sampling theorem.

From (6.14), the minimum time window length of the MCMW for accurate frequency and amplitude detection is estimated by

$$T = \frac{5f_c\sqrt{f_b}}{f_L};$$

where f_L is the lowest harmonic frequency in the harmonic signal.

From (6.6), $\qquad f_c\sqrt{f_b} \geq \dfrac{\sqrt{|In(x)|}}{\pi}\left(\dfrac{f_1 + f_2}{f_1 - f_2}\right)$, where $f_1 > f_2$.

Let $f_1 = f_L$ and $f_2 = f_L + f_{sep}$, and $y = 0.5$ in (7.2) , then (6.6) becomes

$$f_c\sqrt{f_b} \geq \frac{1}{2}\left(\frac{f_L + f_L + f_{sep}}{f_{sep}}\right)$$

$$f_c\sqrt{f_b} \geq \frac{1}{2}\left(\frac{2f_L + f_{sep}}{f_{sep}}\right) \qquad (7.7)$$

$$f_c\sqrt{f_b} \geq \left(\frac{f_L}{f_{sep}} + \frac{1}{2}\right)$$

Substituting (7.7) into (6.14),

$$T \geq \frac{5f_c\sqrt{f_b}}{f_L}$$

$$T \geq \frac{5}{f_L}\left(\frac{f_L}{f_{sep}} + \frac{1}{2}\right) \qquad (7.8)$$

$$T \geq 5\left(\frac{1}{f_{sep}} + \frac{1}{2f_L}\right)$$

It is logical that the minimum signal time length is dependent on the lowest harmonic frequency in the harmonic signal. From (7.8), the minimum time length of the signal is also dependent on the separation frequency between adjacent frequencies. This also confirms with the common understanding [26] that the closer the frequency of two harmonic frequencies, the longer the signal length is required to distinguish them.

Furthermore consider if fsep $\ll$ f_L or $f_L \rightarrow \infty$ in (7.8),

$$T \rightarrow 5\left(\frac{1}{f_{sep}}\right), \text{ or } T \rightarrow 10y\left(\frac{1}{f_{sep}}\right), \text{ with } y = 0.5. \qquad (7.9)$$

(7.9) tells that when the separation frequency between two harmonics is very small or

when the harmonic frequencies are very high, the time window length is dependent on f_{sep} only.

Consider two adjacent harmonic frequencies of 40 and 40.5 Hz respectively, which are separated apart by 0.5Hz, (7.8) gives

$$T \geq 5\left(\frac{1}{0.5} + \frac{1}{2x40}\right)$$
$$= 10.025s$$

There time window length is practically dependent on the separation frequency only.

Consider a harmonic signal containing harmonics from 2nd to 51st, with the fundamental frequency set as 50Hz. Fig. 7.2 shows the minimum time signal length for harmonic frequencies at a separation frequencies f_{sep} of 10Hz, 20Hz, 30Hz, 40Hz and 50Hz respectively. In (7.2), y is set as 0.5. It is evident that at high harmonic frequencies, the minimum time signal length is mainly determined by the separation frequency only.
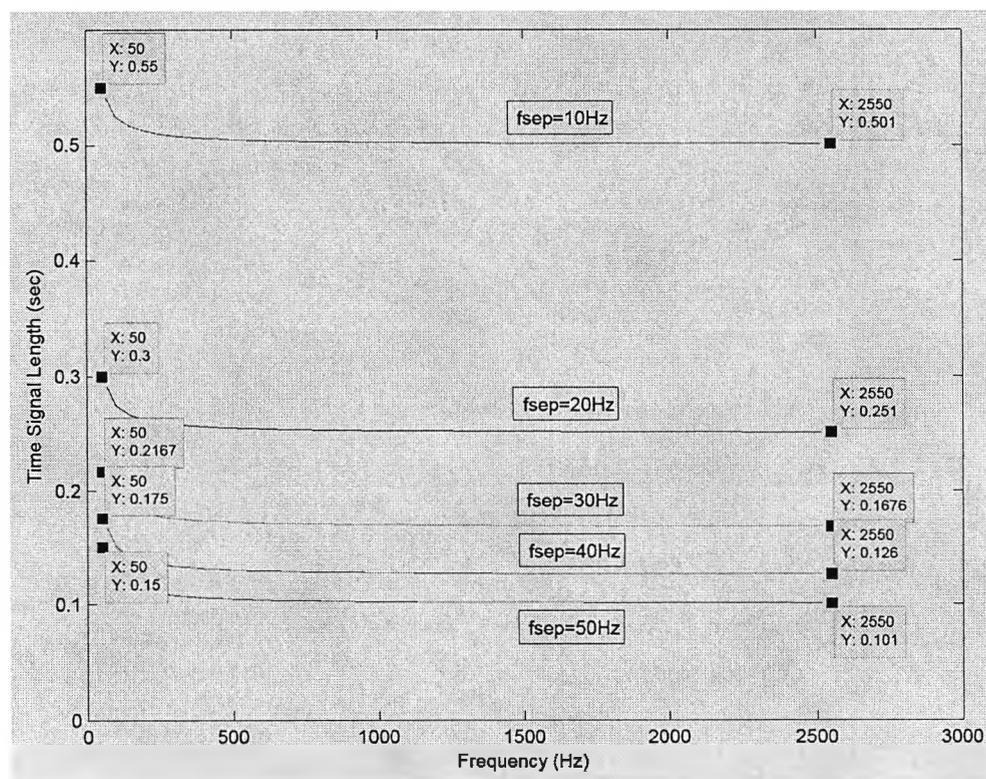
Fig. 7.2 Relationship between signal length and frequency separation

For harmonic signals containing only integer harmonics, the separation between adjacent frequencies would be set as 50Hz. A time signal length of 0.15 seconds would be used. For detecting harmonic frequencies higher than 1000Hz, a time signal length of 0.1 seconds is sufficient. From (7.9) with y = 0.5 in (7.2),

$$T \approx \left(\frac{5}{f_{sep}} \right) \quad \text{for } f_L \geq 1000\text{Hz.}$$

If a harmonic signal contains inter-harmonics, it would be desirable to set the separation frequency to 25Hz. For sub-harmonics detection, it would be necessary to use a smaller f_{sep}.

A further consideration for the setting of the minimum sampling frequency and time signal length is that for accurate initial phase estimation of the harmonics and to maintain the symmetry of the MCMW, the number of data used in the estimation should be an odd number. In other words, the product of the time period and the sampling frequency should be an even number, and including the data at t = 0, the number of data used would become an odd number.

7.5 Scale Population

Mathematically, the CWT includes all scales over the range [0+,∞]. From a signal analysis point of view, the computed scales should include those of physical interest in the signal. However there is also a practical upper and lower limit of scale which depends on the highest frequency that can be analyzed and the number of points in the signal time series to be analyzed [78].

7.5.1   Minimum Scale

Following the proof in (6.2),

$$f = \frac{f_c}{a} + \frac{1}{a} \frac{\sqrt{|ln(x)|}}{\pi} \frac{1}{\sqrt{f_b}} .$$

From (7.2),
$$y = \frac{\sqrt{|ln(x)|}}{\pi},$$

and take the sampling frequency into account, (6.2) becomes,

$$f = \frac{f_s f_c}{a} + y \frac{f_s}{a} \frac{1}{\sqrt{f_b}}. \tag{7.10}$$

The minimum scale appears when the signal frequency is equal to Nyquist frequency,

$$\frac{f_s}{2} = \frac{f_s f_c}{a_{min}} + y \frac{f_s}{a_{min}} \frac{1}{\sqrt{f_b}}. \tag{7.11}$$

Therefore

$$a_{min} \geq 2f_c \left(1 + \frac{y}{f_c \sqrt{f_b}} \right)$$

$$a_{min} \geq 2f_c + \frac{2f_c y}{f_c \sqrt{f_b}} \tag{7.12}$$

$$a_{min} \geq 2f_c + \frac{2y}{\sqrt{f_b}}$$

This is the smallest scale that can be used without aliasing.

Using $f_b = 10000$, and $y = 0.5$, (7.12) becomes

$$a_{min} \geq 2f_c + \frac{2 \times 0.5}{\sqrt{10000}}$$

$$a_{min} \geq 2f_c + \frac{1}{100} \tag{7.13}$$

Since from (5.8) with sampling frequency taken into account,

$$a = \frac{f_c}{f} f_s.$$
(7.14)

Substituting (7.14) into (7.10),

$$\frac{f_s f_c}{f} \geq 2f_c + \frac{1}{100}$$

$$f_s \geq 2f\left(1 + \frac{1}{200 f_c}\right).$$
(7.15)

Therefore, as long as the requirement for minimum sampling frequency is fulfilled, the minimum scale for avoiding aliasing could be satisfied.

7.5.2   Maximum Scale

Consider the process of discrete convolution when the signal time series has a finite number of points. When a convolution at a sample point is calculated, the shift function is centered at that sample and the value of the convolution depends upon contributions from points before and after the sample point. It is clear that points near the end cannot represent the true discrete convolution between the signal time series and function. In fact when using the FFT to perform convolution, the convolved points near the end include contributions that are located at the opposite end of the signal time series, so called 'wrap-around' points. Furthermore, as the scale increases, the number of wavelet samples to each side of the wavelet centre also increases so that the number of wrap-around points increases with the scale. These points do not represent the true wavelet coefficients and should not be used in subsequent analysis. With large enough scale, all of the computed wavelet coefficients are wrap-around points.

A sufficient long time window length of the wavelet should be used so that a sufficient central portion of wavelet coefficients not contaminated by the edge effect would contain useful information. The minimum time window length for the MCMW is calculated in (6.14) as

$$T \geq \frac{5f_c\sqrt{f_b}}{f_L}.$$

From (5.8), $a = \dfrac{f_c}{f_L}$ and from (6.14),

$$T \geq 5a_{max}\sqrt{f_b}$$
$$a_{max} \leq \frac{T}{5\sqrt{f_b}} . \tag{7.16}$$

(7.16) determines the maximum scale that can be used without being affected by the edge effects.

7.6 Dilation Steps

As discussed in Section 5.3, the CWT is the process of conducting convolution integrals of the harmonic signal with wavelets produced by translation and dilation of the mother wavelet. As the computation process is conducted by computers, both the dilated wavelets and the harmonic signals are digitized, and the convolution is in fact a discretised integral. The CWT should be termed 'Discretised CWT', abbreviated as D-CWT. In decomposition by scale dilation, once the minimum scale and maximum scale are determined by the Nyquist frequency and the time window length respectively, the decomposition would be conducted in accordance with the dilation step size.

The dilation step size of the scales for the D-CWT affects the accuracy in harmonic frequency detection. The smaller the dilation step size, the better the accuracy in harmonic frequency detection. However with a very fine dilation step size, the computation time would be very long and the wavelet coefficients generated would be highly redundant. Since the relationship between the scale and the frequency is given as in (7.14),

$$a = \frac{f_s f_c}{f} ;$$

given $f_s = 1000Hz$, $f = 49.5Hz$ and $f_c = 1$, then a = 20.2.

In other words, the scale dilation should have a maximum step of 0.2 for the estimation of 49.5Hz. If the actual dilation size is 1, the harmonic frequency will be misinterpreted as at a=20, and the harmonic frequency is estimated as 50Hz.

To overcome this problem for harmonic frequency analysis, it is suggested to firstly determine the required frequency resolution; the corresponding scales are determined accordingly by (7.14) for the required f_c.

By this dilation approach, the frequency resolution can be altered easily for different frequency ranges. It is desirable to have a fine frequency resolution at low frequencies and a comparatively more coarse frequency resolution for high frequencies.

7.7   Assignment of Frequency Bands

As it is desirable to have a fine frequency resolution at low frequencies and a comparatively more coarse frequency resolution for high frequencies, the decomposition can be divided into frequency bands. For each frequency band, f_c is calculated by (7.4) for the frequencies contained in the frequency band, in steps of the required frequency resolution. The f_b is fixed and set as 10000. The corresponding scales can be calculated readily for each f_c generated from each frequency in the frequency band by (7.4) and (7.14) respectively.

$$a = \frac{f_c}{f} = \frac{1}{100f}\left(\frac{f}{f_{sep}} - \frac{1}{2}\right) = 0.01\left(\frac{1}{f_{sep}} - \frac{1}{2f}\right)$$

This approach also allows a particular frequency separation between adjacent frequencies be used for each frequency band. However the frequency bands should be carefully chosen to avoid having harmonic frequencies fall between two frequency bands. If the same frequency resolution and frequency separation between adjacent frequencies are to be applied to all harmonic frequencies, assignment of frequency bands are not necessary. Fig. 7.3 shows the flowchart of the decomposition according to frequency bands. Table 7.1 shows the suggested assignment of frequency bands.

Specify frequency
separation of adjacent
frequencies

Specify the lowest
& highest frequencies
in the signal

Determine the minimum
sampling frequency

Determine the minimum
time period of CMW

Specify the frequency
bands according to
frequency resolution
requirements

Set fb=10000

For each frequency
band, compute fc & a

Next frequency
band

Compute wavelet
coefficients for the
frequency band

Fig. 7.3 Flow chart showing WT decomposition settings

Table 7.1 Assignment of frequency bands

Band 1	12Hz – 45Hz
Band 2	46Hz – 75Hz
Band 3	76Hz – 275Hz
Band 4	276Hz – 525Hz
Band 5	526 – 775Hz
Band 6	776Hz – 2550Hz

7.8   Extraction of Frequency Information by Wavelet Ridges

As discussed in Section 5.11, the frequency information of the signal would be estimated by wavelet ridges plot calculated from the complex wavelet coefficients generated from complex WT. Once the harmonic frequencies of the signal are identified, the corresponding amplitudes and initial phase angles would be computed easily. Fig. 7.4 shows the flowchart of the estimation of harmonic frequencies, amplitudes and initial phase angles.

```
┌─────────────────────┐
│   Extract frequency  │
│    information by    │
│  Wavelet Ridges Plot │
└─────────────────────┘
           │
┌─────────────────────┐
│   For each maximum   │
│ wavelet ridge, compute│
│  the amplitudes plot │
└─────────────────────┘
           │
┌─────────────────────────┐
│For each maximum wavelet ridge,│
│  estimate the initial phase  │
│ angles from complex wavelet  │
│        coefficients          │
└─────────────────────────┘
```
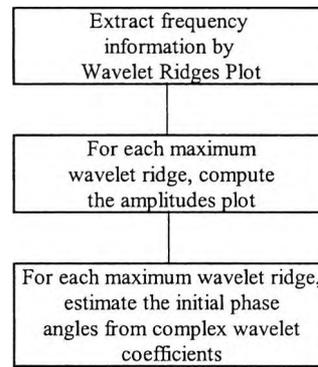
Fig. 7.4 Flow chart for estimating frequency, amplitude and initial phase

7.9   Edge (Boundary) Effect

Theoretically, the WT integral extends from negative infinity to positive infinity as shown in (3.5). In practice, experimental data sets are finite in extent. An obvious consequence of wavelet analysis of a finite data set is that, as the wavelet gets closer to the edge of the data, parts of it begin 'spill over' the edge. This creates an edge effect, where transform values close to the boundary of the signal are tainted by the discontinuous nature of the signal edge. The affected region increases in extent as the dilation of the analyzing wavelet increases. Large wavelet coefficients are realized close to the edge of the transform plot, which increases in extent as the scale a increases. This region affected by a discontinuity is known as the 'Cone of Influence' [61,78]. The extent of the cone increases linearly with the scale a, i.e. it is proportional to the temporal support (or width) of the wavelet. The cone boundaries at either ends of the signal define the region which is significantly influenced by the signal edges. If the signal length is long enough such that the cone of influence would not affect all the wavelet coefficients, then useful information can still be found at the centre portion of the wavelet coefficients.

Consider a harmonic signal containing a fundamental frequency at 50Hz of amplitude equal to 1 and a harmonic frequency at 150Hz and of amplitude equal to 2. The wavelet parameter is chosen as f_b-f_c = 2-1. The sampling frequency of 2000Hz is used. Fig. 7.5 shows the wavelet ridges plot and Fig. 7.6 shows the amplitudes plot of the two harmonic frequencies.
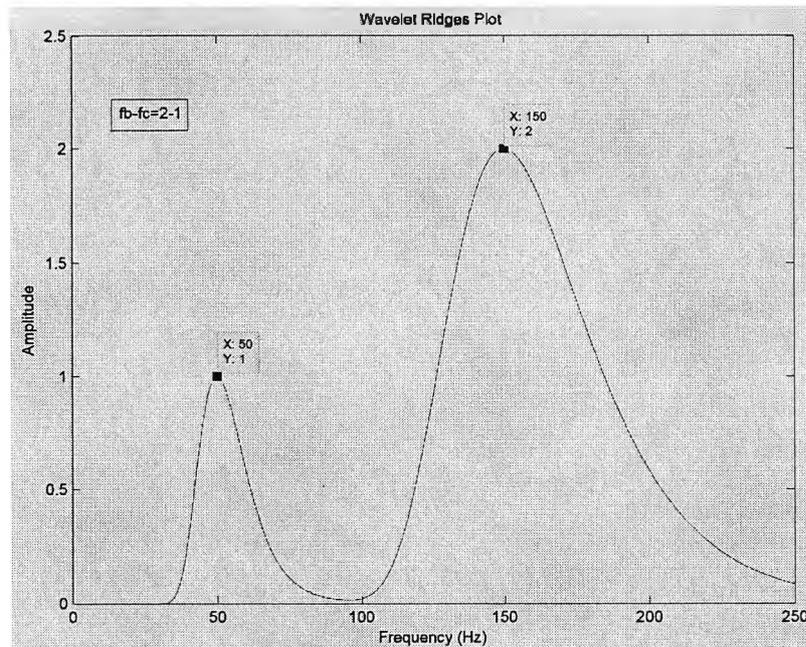
Fig. 7.5 Wavelet ridges plot for 50Hz and 150Hz
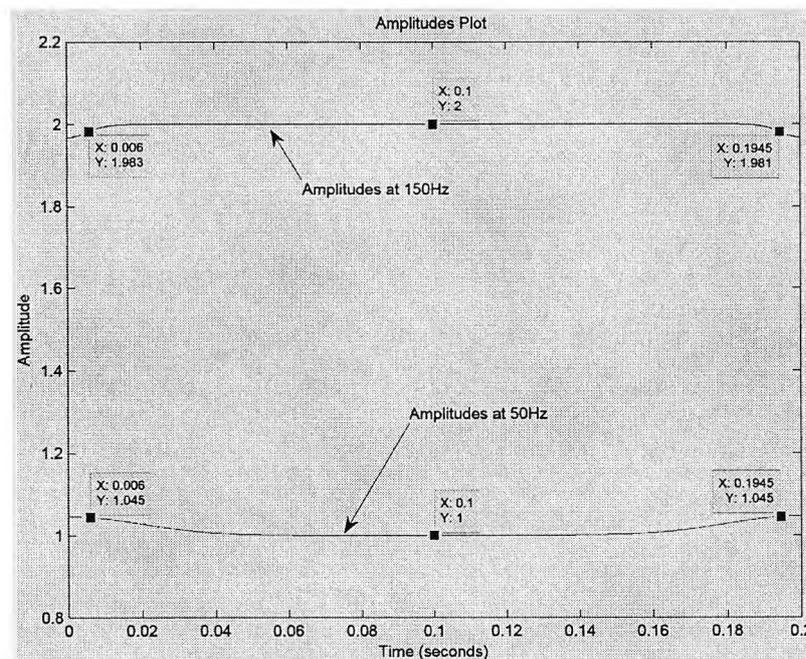
Fig. 7.6 Amplitudes plot for 50Hz and 150Hz

It can be seen that at 50Hz where the scale a used is comparatively larger, the boundary effects are more evident. This is understandable as at large scales, the wavelet spans a longer time width outside the signal window. It is therefore recommended that when computing the scalogram, only wavelet coefficients at the centre portion be used so that

large wavelet coefficients at the edges would not distort the wavelet ridges plot.

Even with the boundary effect, the amplitude estimation error as seen in Fig. 7.6 is not very significant. If the time signal used is not sufficiently long, it is always preferable to use the estimated amplitude at the centre portion of the amplitudes plot.

7.10 Conclusion

In this Chapter, a practical computation algorithm is developed for harmonic analysis based on complex CWT. The proposed range of harmonic frequencies is suggested to be divided into frequency bands. The advantages are that for different separation frequency between adjacent frequencies, different dilation steps would be assigned for each frequency band so that computation time would be saved.

It is proved that both the harmonic frequencies and the required separation frequency between adjacent harmonic frequencies would affect the signal time signal and the sampling frequency. A computation formula for the estimation of the minimum sampling frequency without aliasing is proposed. The signal time signal is determined mathematically by considering the lowest harmonic frequencies and the separation frequency between adjacent harmonic frequencies in the harmonic signal. For harmonic frequencies higher than 1000Hz, the minimum signal time signal is practically determined by the separation frequency between adjacent frequencies only.

Furthermore, the accuracy in harmonics amplitudes estimation is dependent on the time signal length used in the harmonic analysis. A longer time signal length would require longer computer time; a compromise should be reached between the accuracy required in the harmonics amplitudes estimation and the computation time. The setting of the f_b-f_c parameters of the MCMW should also be based on the harmonic frequencies in the signal and the required frequency separation between adjacent harmonic frequencies.

The detection of the initial phases of harmonics requires that the number of data points used in the WT-based estimation algorithm should be an odd number. In other words, the product of the time period and the sampling frequency should be an even number.

On the setting of dilation scales, the minimum scale to be used is related to the minimum sampling frequency. The maximum scale to be set is related to the signal time length. It is suggested that instead of dilating the MCMW by incrementing the scale, it would be more convenient and accurate for harmonics analysis to determine the corresponding scales of dilation from the required frequency resolution.

To avoid the edge effect from blurring the useful information in the wavelet coefficients, it is suggested, in both frequency information extraction and amplitude estimation, to use the data at the centre portion of the wavelet coefficients.

Chapter 8

Application Studies

8.1 Introduction

The developments in Chapter 5 and 6 are integrated into a WT-based algorithm for harmonic analysis in Chapter 7. In this Chapter, the proposed algorithm is first applied for analysis of synthesized harmonic signals for validation purpose. It is then applied for analysis of field harmonic signals. The first two field harmonic signal are the phase input currents to a three-phase variable speed drive (VSD), with the output frequency set to 20Hz and 30Hz respectively. The third field harmonic signal is the single-phase current of a single-phase circuit, which is supplying power to an electronic dimmer-controlled lamp bulb, fluorescent luminaries complete with electronic ballast, a hairdryer and an air compressor motor. DFT-based algorithm implemented with FFT is being used in all the tests for synthesized harmonic signals and field harmonic signals for comparison purpose.

In all the tests to be presented below, the decompositions are not divided into frequency bands, and the same frequency resolution is being used for all frequencies.

8.2 Synthesized Harmonic Signal Analysis

Three tests for synthesized harmonic signal analysis are conducted. In the first test, the WT-based algorithm is being tested with a synthesized harmonic signal containing sub-harmonics. In the second test, the WT-based algorithm is being tested with a synthesized harmonic signal containing inter-harmonics. The third test is for testing the WT-based algorithm with a synthesized harmonic signal containing even harmonics of very small amplitude. The results obtained from WT-based algorithm are compared with

the results from DFT-based algorithm.

8.2.1   Stationary Harmonic signal with Sub-harmonics

The harmonic signal contains the sub-harmonic components as shown in Table 8.1.

Table 8.1 Sub-harmonics in synthesized signal

Harmonic Frequency (Hz)	Amplitude	Phase Angle (deg.)
13	0.01	8
20.5	0.32	12
25.6	0.87	-15
36.6	0.75	-20
46.2	0.33	-10
49.8	1	0

The waveform of the synthesized harmonic signal is shown in Fig. 8.1.
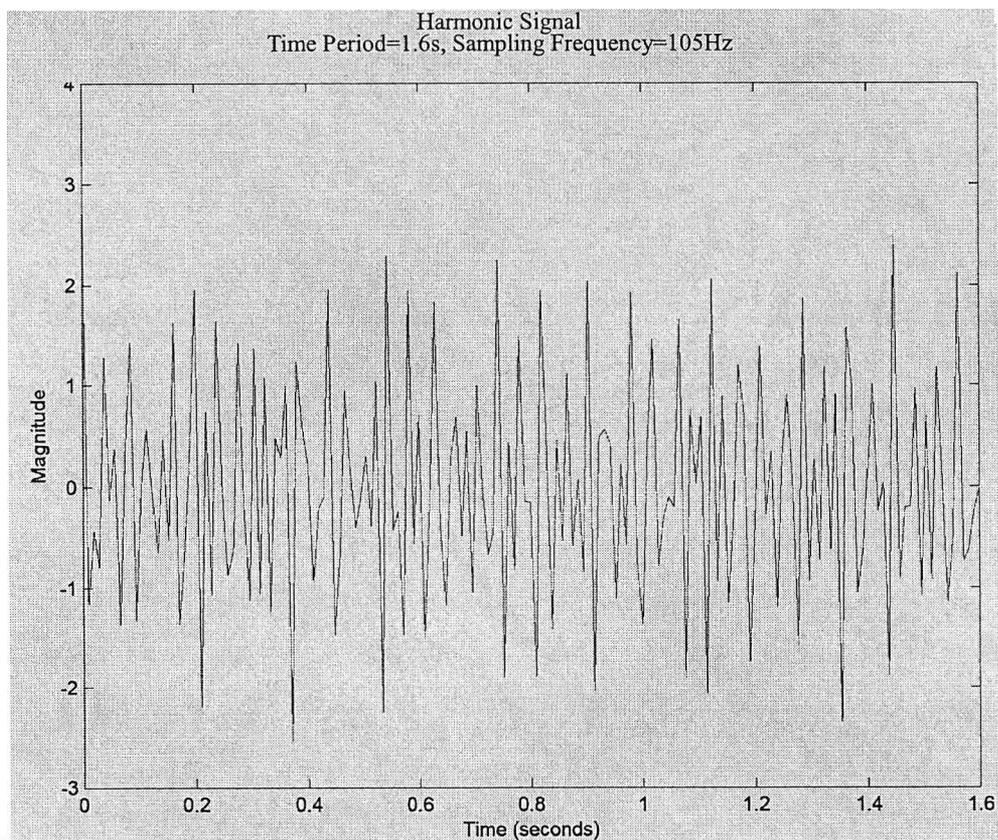
Fig. 8.1 Waveform of synthesized sub-harmonics signal

From Table 8.1, the highest harmonic frequency is 50Hz, the minimum separation frequency f_{sep} is set as 3.8Hz. The minimum sampling frequency and the minimum signal length are determined as follows. From (7.4), the minimum sampling frequency is estimated as

$$f_s \geq \frac{4f_H^2}{2f_H - f_{sep}} = \frac{4 \times 49.8^2}{2 \times 49.8 - 3.6} = 103.34Hz \ .$$

The sampling frequency is selected as 105Hz. From (7.8), the minimum signal time length is estimated as:

$$T \geq 5\left(\frac{1}{f_{sep}} + \frac{1}{2f_L}\right) = 5\left(\frac{1}{3.6} + \frac{1}{2 \times 13}\right) = 1.581s \ .$$

The minimum signal time length is selected as 1.6 seconds. The number of data N used to represent the harmonic signal, including the data at t=0, is calculated by (4.5),

$$N = f_s \times T + 1 = 1.6s \times 105Hz + 1 = 169.$$

Fig. 8.2 shows the wavelet ridges plot of the harmonic analysis. Fig. 8.3 shows the amplitudes plot, and Fig. 8.4 shows the phase plots.

Fig. 8.2 Wavelet ridges plot of synthesized sub-harmonics signal
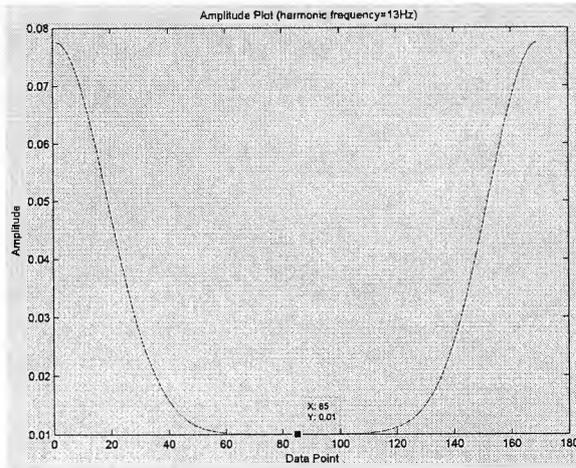
(a) 13Hz
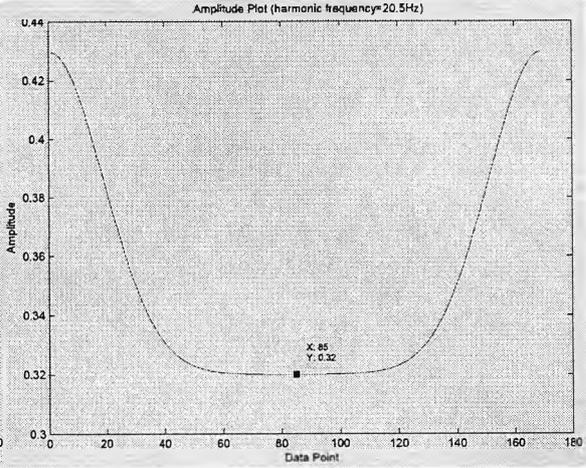
(b) 20.5Hz
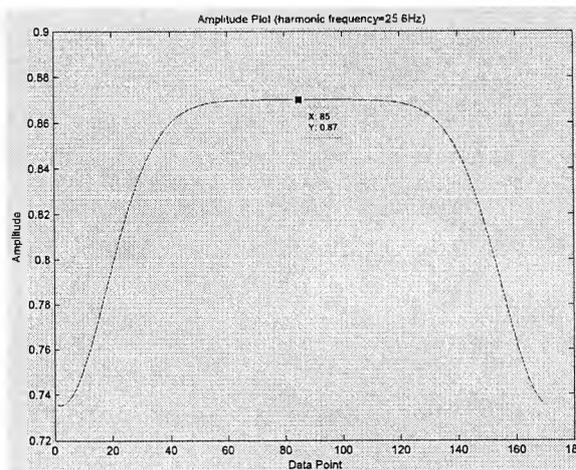
(c) 25.6Hz
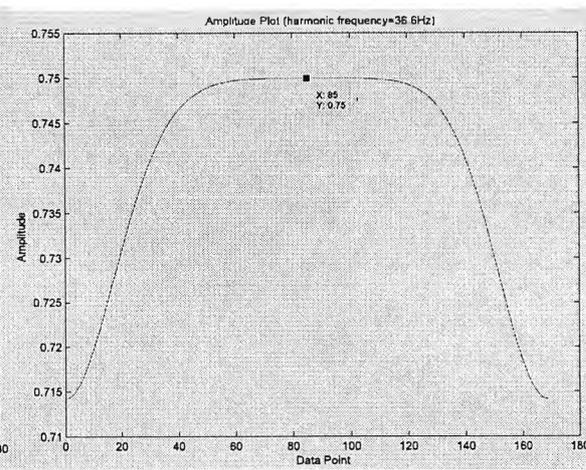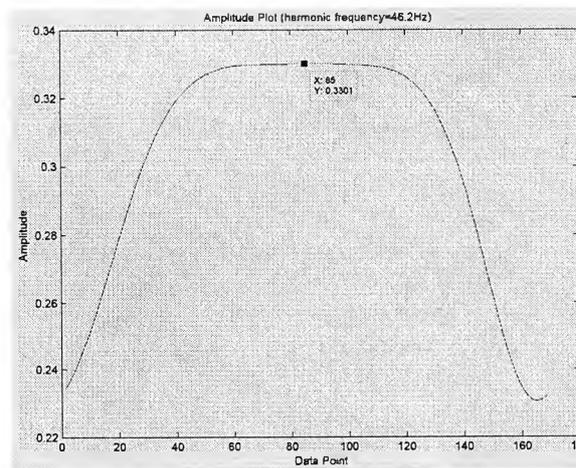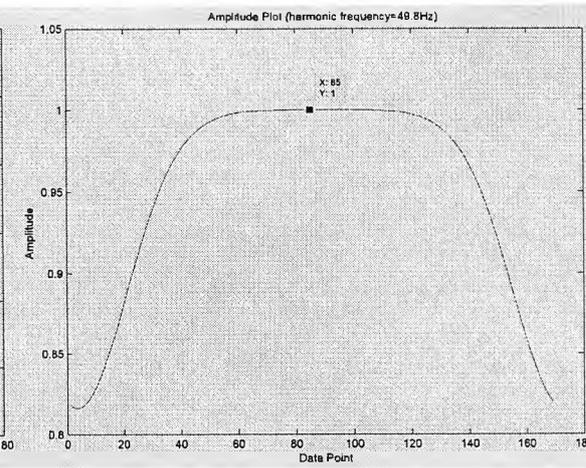
(d) 36.6Hz

(e) 46.2Hz

(f) 49.8Hz

Fig. 8.3 Amplitudes plot of sub-harmonic components
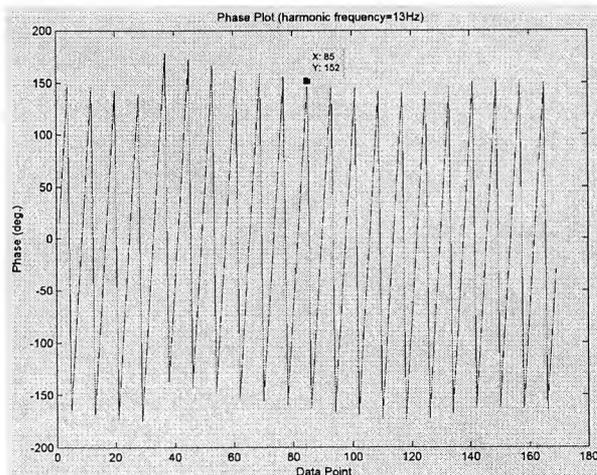
(a) 13Hz
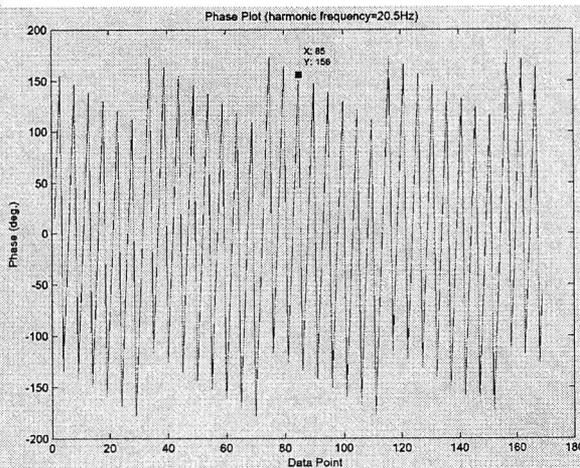
(b) 20.5Hz
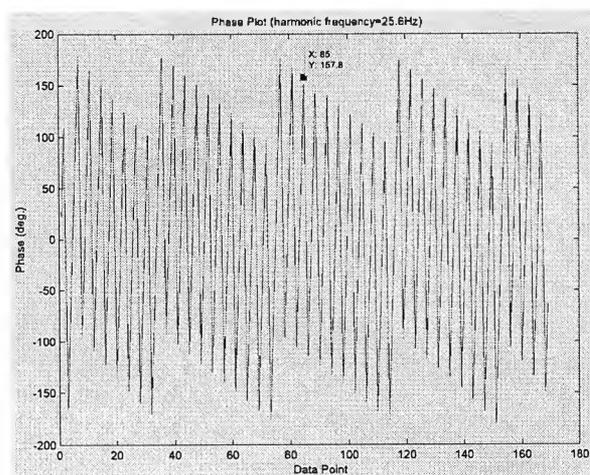
(c) 25.6Hz
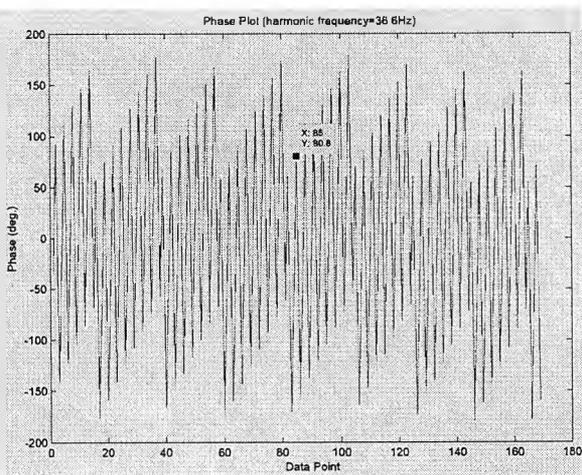
(d) 36.6Hz
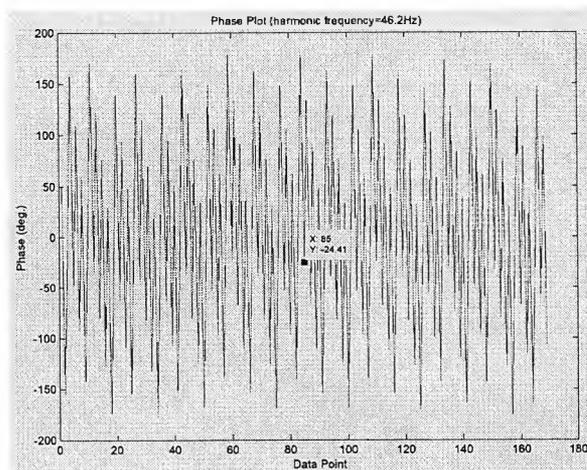
(e) 46.2Hz
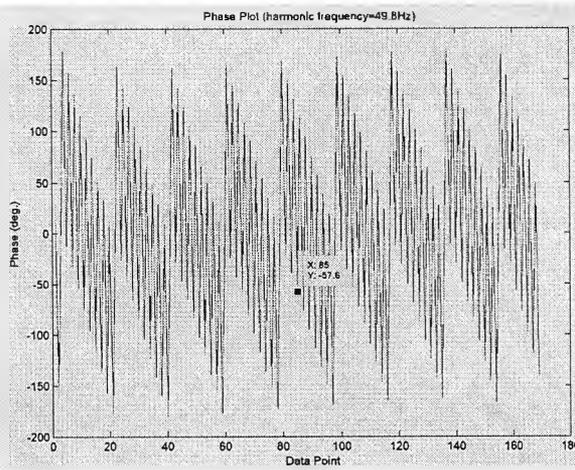
(f) 49.8Hz

Fig. 8.4 Phase plots of sub-harmonic components

As seen in Fig. 8.3, the edge effects are very obvious in the amplitudes plots. The data points at location 85 which is the middle point of the signal data are used to estimate the initial phases of the harmonic frequencies by (6.19).

DFT-based algorithm implemented with FFT is also used to estimate the harmonics of the same harmonic signal. The fft no. used is 1050, which is necessary for achieving a frequency resolution of 0.1 Hz.

In order to reduce the effect of discontinuities at the window edges and leakages, a hamming window is applied. The Hamming window is calculated as in (4.10),

$$W_H(t) = 0.54 - 0.46\cos(\frac{2\pi t}{T}).$$

Since the fft no. being used is different from the number of data of the harmonic signal and because hamming window is applied, the amplitudes estimated by FFT should be scaled by 0.54 for the hamming window, and by the ratio of fft no. to data number. Fig. 8.5 shows the frequency spectrum produced by FFT and Fig. 8.6 shows the phases plot.
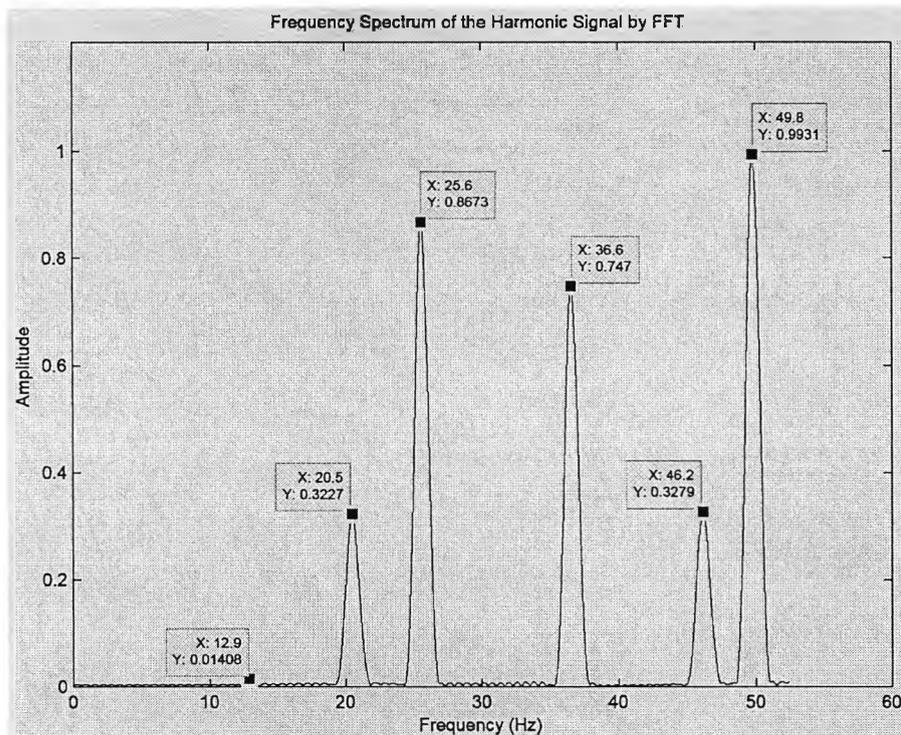
Fig. 8.5 Frequency spectrum by FFT of synthesized sub-harmonics signal
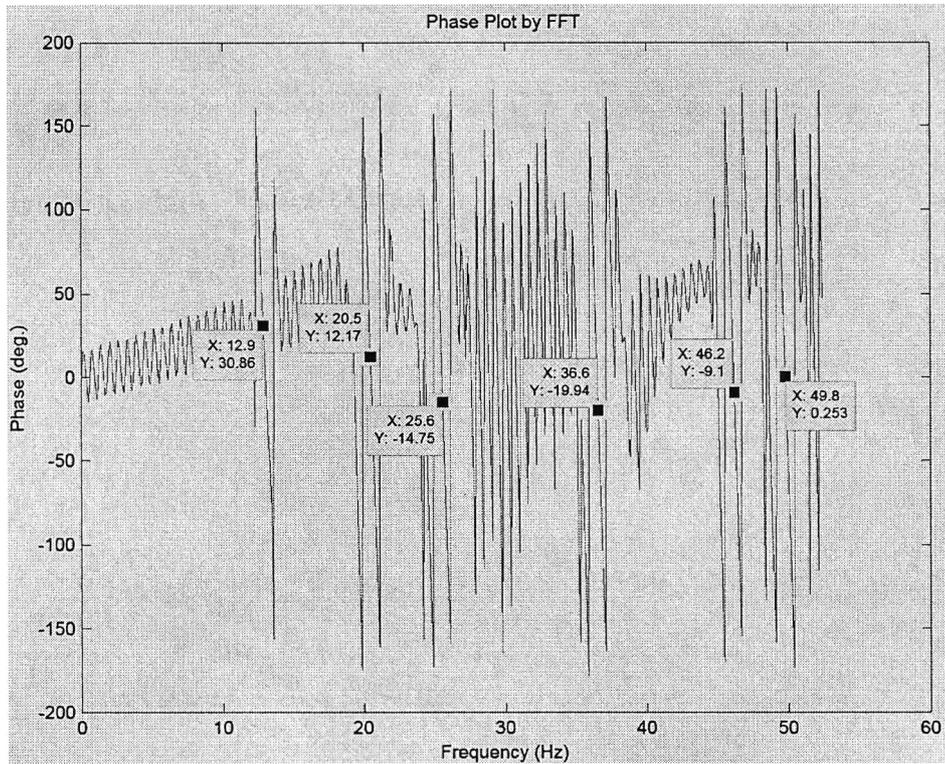
Fig. 8.6 Phase plots by FFT of synthesized sub-harmonics signal

The sub-harmonics in the synthesized signal estimated by both the WT-based algorithm and the DFT-based algorithm are tabulated in Table 8.2. On frequency estimation, both DFT-based algorithm and WT-based algorithm are very accurate. DFT-based algorithm would have small frequency detection error when the amplitude of the harmonic is comparatively small. On amplitudes and initial phase detection, WT-based algorithm is accurate than DFT-based algorithm.

Table 8.2 Sub-harmonics estimated by WT-based algorithm & DFT-based algorithm

Synthesized Waveform Information			WT-based algorithm			DFT-based algorithm		
Frequency (Hz)	Amplitude	Initial Phase (deg.)	Frequency (Hz)	Amplitude	Initial Phase (deg.)	Frequency (Hz)	Amplitude	Initial Phase (deg.)
13	0.01	8	13	0.01	8	12.9	0.014	30.86
20.5	0.32	12	20.5	0.32	12	20.5	0.323	12.17
25.6	0.87	-15	25.6	0.87	-15	25.6	0.867	-14.75
36.6	0.75	-20	36.6	0.75	-20	36.6	0.747	-19.94
46.2	0.33	-10	46.2	0.3301	-10.01	46.2	0.328	-9.1
49.8	1	0	49.8	1	0	49.8	0.993	0.253

8.2.2   Stationary Harmonic Signal with Inter-harmonics

The harmonic signal contains integer harmonics and inter-harmonic components as shown in Table 8.3. The waveform of the synthesized harmonic signal is shown in Fig. 8.7.

Table 8.3 Inter-harmonics in synthesized signal

Frequency (Hz)	Amplitude	Initial Phase (deg.)	Frequency (Hz)	Amplitude	Initial Phase (deg.)
49.5	311	0	1336.5	20	8
102	288	10	1435.5	18	-8
148.5	280	-15	1534.5	15	20
247.5	225	-12	1633.5	13	-30
346.5	180	-20	1732.5	11	12
445.5	155	-14	1831.5	9	-8
544.5	130	30	1930.5	7	9
643.5	102	36	2029.5	5.5	9
742.5	80	42	2128.5	3	35
811	76	11	2160	2.2	-4
841.5	62	-28	2227.5	3	-32
940.5	53	5	2326.5	2	7
1039.5	32	7	2425.5	1	2
1138.5	30	15	2524.5	0.5	1
1237.5	26	-15			
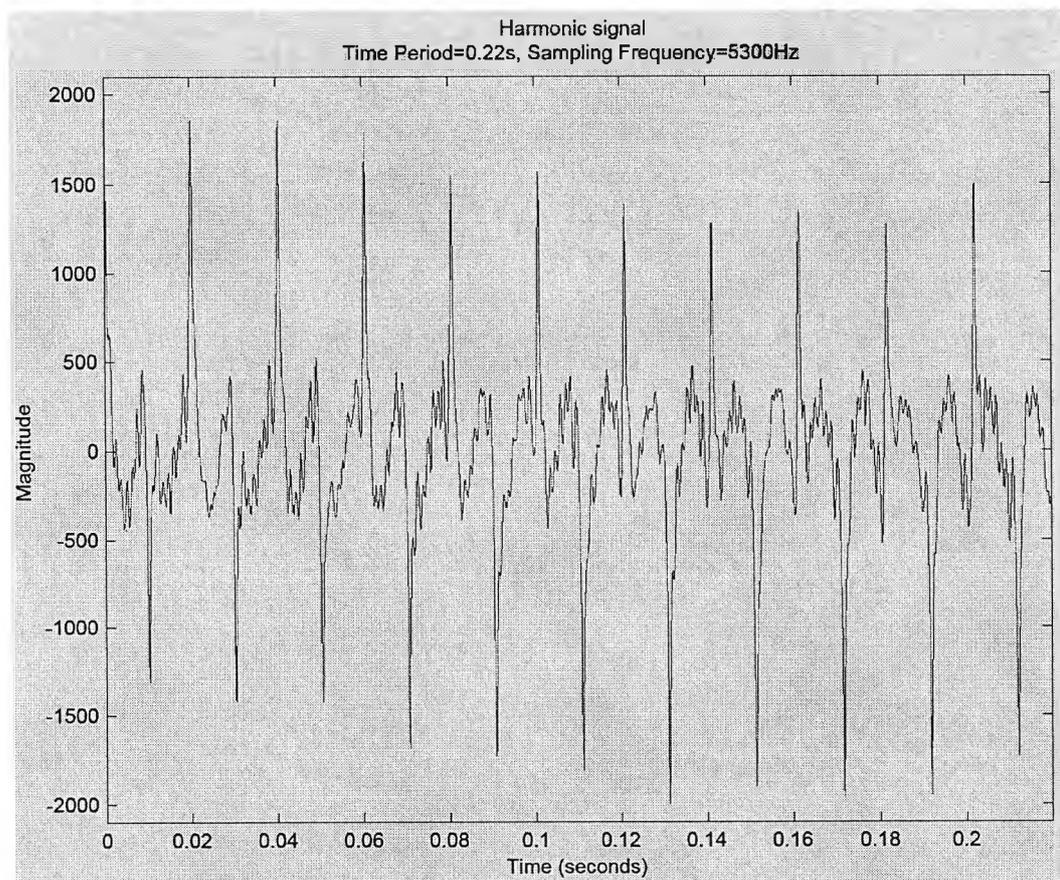
Fig. 8.7 Waveform of synthesized inter-harmonics signal

Generally the power supply authority specifies that the supply frequency of 50Hz has a variation of ±2%, i.e. ±1Hz. The lowest harmonic frequency that would be found in the harmonic signal is therefore 49Hz. The WT-based algorithm is set to detect up to the 51st harmonics. The 51st harmonic may have the highest frequency of 2601Hz when the fundamental frequency is 51Hz. The minimum frequency range being specified for the WT-based algorithm is therefore from 49Hz to 2601Hz.

The minimum separation frequency f$_{sep}$ is set as 30Hz. The minimum sampling frequency and the minimum signal length are determined by (7.4) and (7.8) as follows.

$$f_s \geq \frac{4f_H^2}{2f_H - f_{sep}} = \frac{4 \times 2601^2}{2 \times 2601 - 30} = 5232.2Hz \approx 5233Hz.$$

The sampling frequency used should not be less than 5233Hz.

$$T \geq 5\left(\frac{1}{f_{sep}} + \frac{1}{2f_L}\right) = 5\left(\frac{1}{30} + \frac{1}{2 \times 49}\right) = 0.218s \approx 0.22s.$$

The minimum signal time length is chosen as 0.22s.

In order that the number of data representing the harmonic signal is an odd number, the sampling frequency is chosen as 5300Hz. The number of data used to represent the harmonic signal, including the data at t=0, is equal to 1167.

For harmonic frequencies higher than 1275Hz, the signal length is reduced to 0.18s to save computation time. The number of data used is 955.

Fig. 8.8 shows the wavelet ridges plot of the signal containing inter-harmonics. The detection results of harmonic frequencies and their respective amplitudes and initial phase angles are presented in Table 8.4.
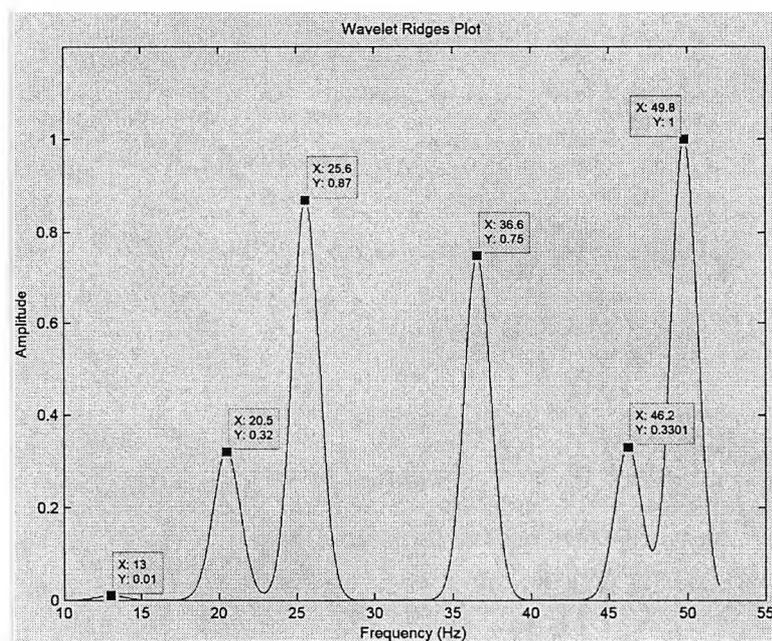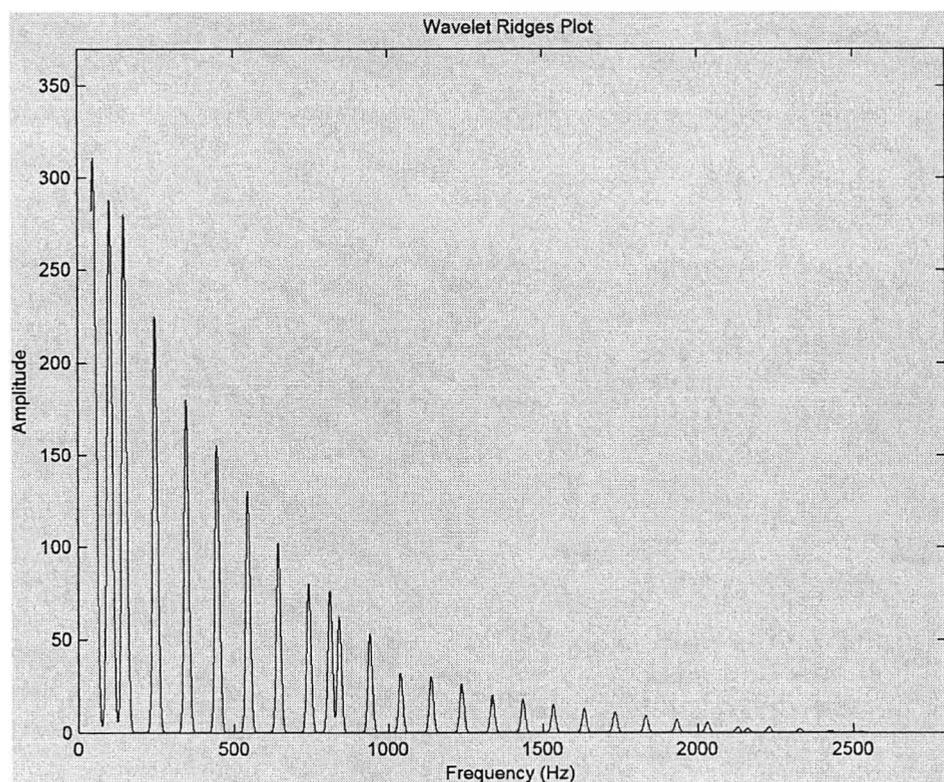
Fig. 8.8 Wavelet ridges plot of synthesized inter-harmonics signal

DFT-based algorithm implemented with FFT is also used to estimate the harmonics of the synthesized signal represented in Table 8.3 and Fig. 8.7. The fft no. used is 10600, which is necessary for achieving a frequency resolution of 0.5 Hz. The Hamming window is being used to reduce edge effects and leakages. The amplitudes estimated by FFT are scaled by 0.54 for the hamming window, and by the ratio of fft no. to data number.

Fig. 8.9 shows the frequency spectrum of the harmonic signal produced by FFT. The harmonic frequencies, their respective amplitudes and initial phase angles are presented in Table 8.4.
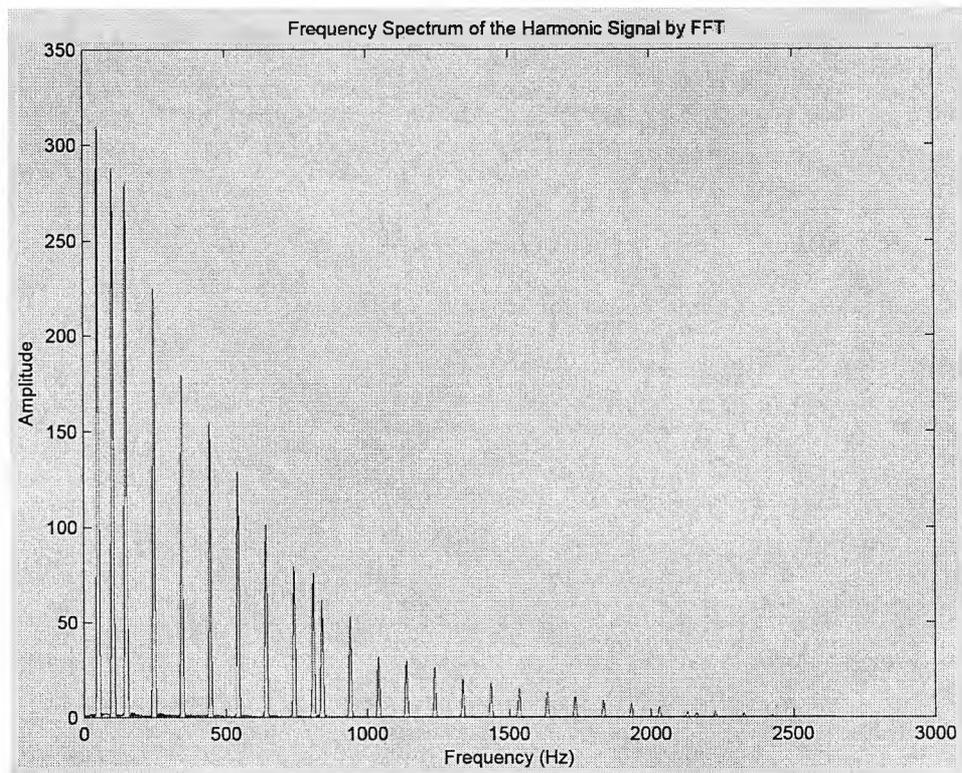
Fig. 8.9 Frequency spectrum by FFT of synthesized inter-harmonics signal

Table 8.4 Inter-harmonics estimated by WT-based algorithm & DFT-based algorithm

Synthesized Waveform Information			WT-based algorithm			DFT-based algorithm		
Frequency (Hz)	Amplitude	Initial Phase (deg.)	Frequency (Hz)	Amplitude	Initial Phase (deg.)	Frequency (Hz)	Amplitude	Initial Phase (deg.)
49.5	311	0	49.5	311	0	49.5	*310.3*	*0.12*
102	288	10	102	288	10	102	*288.5*	*9.75*
148.5	280	-15	148.5	280	-15	148.5	*280.6*	*-15.12*
247.5	225	-12	247.5	225	-12	247.5	*224.7*	*-12.1*
346.5	180	-20	346.5	180	-20	346.5	*179.6*	*-20.2*
445.5	155	-14	445.5	155	-14	445.5	*154.8*	*-14.3*
544.5	130	30	544.5	130	30	544.5	*129.5*	*29.76*
643.5	102	36	643.5	102	36	643.5	*101.6*	*35.69*
742.5	80	42	742.5	80	42	742.5	*79.8*	*41.64*
811	76	11	811	76	11	811	*76.16*	*10.93*
841.5	62	-28	841.5	62	-28	841.5	*62.38*	*-28.66*
940.5	53	5	940.5	53	5	940.5	*53.15*	*4.4*
1039.5	32	7	1039.5	32	7	1039.5	*32.18*	*6.22*
1138.5	30	15	1138.5	30	15	1138.5	*30.12*	*14.33*
1237.5	26	-15	1237.5	26	-15	1237.5	*26.25*	*-15.55*
1336.5	20	8	1336.5	20	8	1336.5	*20.15*	*7.05*
1435.5	18	-8	1435.5	18	-8	1435.5	*18.28*	*-8.78*
1534.5	15	20	1534.5	15	20	1534.5	*15.17*	*18.89*
1633.5	13	-30	1633.5	13	-30	1633.5	*13.29*	*-30.17*
1732.5	11	12	1732.5	11	12	1732.5	*11.17*	*10.92*
1831.5	9	-8	1831.5	9	-8	1831.5	*9.249*	*-8.93*
1930.5	7	9	1930.5	7	9	1930.5	*7.233*	*7.42*
2029.5	5.5	9	2029.5	5.5	9	2029.5	*5.75*	*7.46*
2128.5	3	35	2128.5	3	35	*2129*	*3.207*	*12.71*
2160	2.2	-4	2160	2.2	-4	2160	*2.447*	*-5.46*
2227.5	3	-32	2227.5	3	-32	2227.5	*3.243*	*-31.1*
2326.5	2	7	2326.5	2	*6.95*	2326.5	*2.243*	*4.07*
2425.5	1	2	2425.5	1	*1.95*	2425.5	*1.278*	*-0.95*
2524.5	0.5	1	2524.5	0.5	*0.96*	2524.5	*0.7768*	*-0.17*

*Errors are shown bold and italic

The harmonic frequencies estimated by WT-based algorithm are practically 100% correct. The highest amplitude detection error found is only 0.2% and the highest initial phase detection error is 2.5%.

The harmonic frequencies estimated by DFT-based algorithm are practically 100% correct. However, the amplitudes and initial phase angles estimated by DFT-based algorithm are erroneous. For amplitudes detection, the highest error is 27.8%, while the highest initial phase detection error is as high as 148%. The errors in amplitudes and initial phases at harmonics with small amplitudes are very significant. It can be observed from the results in Table 8.4 that DFT-based algorithm is quite good at frequency estimation. This is expected as DFT is a frequency domain analysis tool. As WT is regarded as a time-frequency domain analysis tool, it can be used to estimate frequency, amplitude and phase with high accuracy.

8.2.3   Stationary Harmonic Signal with Even Harmonics of Small Amplitudes

The purpose of the test is to investigate whether the WT-based algorithm is able to estimate the harmonics of very small amplitude compared to adjacent harmonics. The harmonic signal contains a sum of harmonic components as shown in Table 8.5.

Table 8.5 Harmonics in synthesized signal

Frequency (Hz)	Amplitude	Initial Phase (deg.)
49.95	1.524	0
99.9	0.059	-10
149.85	0.288	4
199.8	0.054	-12
249.75	1.254	-5
349.65	0.925	11
399.6	0.03	7
449.55	0.133	-16
549.45	0.54	15
649.35	0.301	-6
749.25	0.044	-9
849.15	0.126	13
949.05	0.045	-20

The waveform of the synthesized harmonic signal is shown in Fig. 8.10.
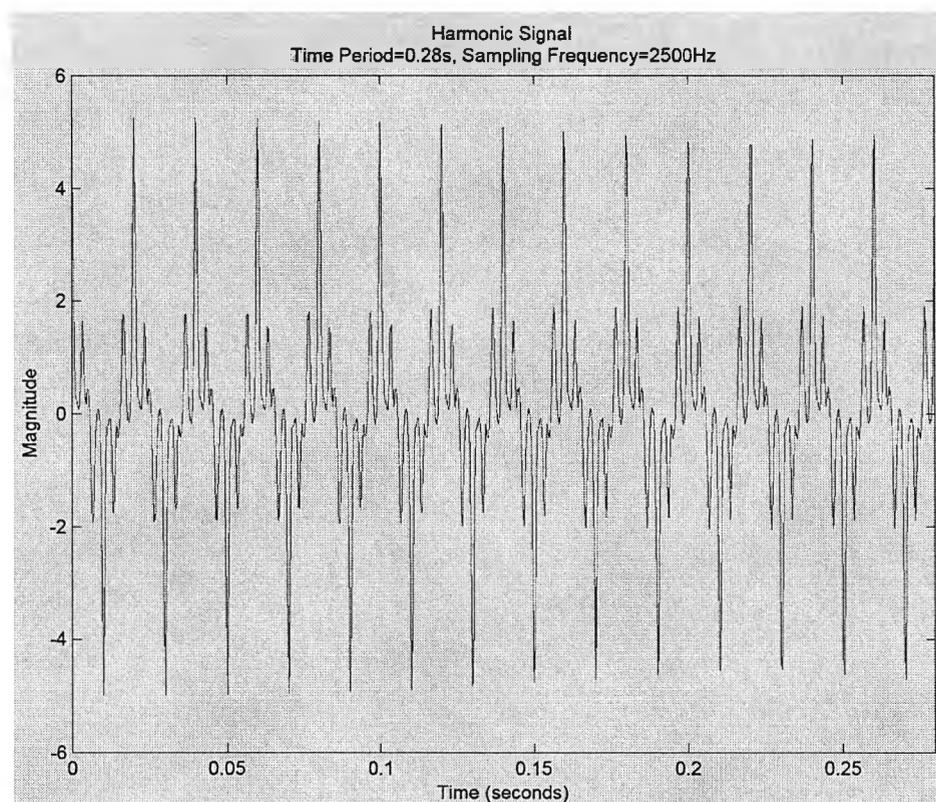
Fig. 8.10 Waveform of synthesized harmonics signal

The minimum separation frequency f_{sep} is set as 30Hz. The minimum sampling frequency is determined by (7.4) as follows.

$$f_s \geq \frac{4f_H^2}{2f_H - f_{sep}} = \frac{4 \times 1000^2}{2 \times 1000 - 40} = 2040.82Hz \approx 2041Hz.$$

The minimum sampling frequency is chosen as 2500Hz.

From (7.2), $y = \frac{\sqrt{|\ln x|}}{\pi} = \frac{\sqrt{|\ln(0.1)|}}{\pi} = 0.483 \approx 0.5.$

For detection of adjacent frequencies with large difference in amplitude, $x = 0.002$ is required. The value of y would then be calculated by (7.2) as 0.8. The value of y would affect the time length required of the harmonic signal for analysis.

The minimum signal time length for x=0.1 by (7.2) and (7.8) is

$$T \geq 5\left(\frac{1}{f_{sep}} + \frac{1}{2f_L}\right) = 5\left(\frac{1}{40} + \frac{1}{2x50}\right) = 0.175s \approx 0.18s.$$

The minimum signal time length for x=0.002 by (7.2) and (7.8) is

$$T \geq 8\left(\frac{1}{f_{sep}} + \frac{1}{2f_L}\right) = 8\left(\frac{1}{40} + \frac{1}{2x50}\right) = 0.28s.$$

The proposed WT-based algorithm is used to analyze the harmonic signal with signal lengths of T = 0.18s and 0.28s respectively.

The detection results of harmonic frequencies, their respective amplitudes and initial phase angles by the WT-based algorithm are presented in Table 8.6.

DFT-based algorithm implemented with FFT is also used to estimate the harmonics. In order to achieve a frequency resolution of 0.05Hz, the fft no. used is 2500/0.05=50000. A hamming window represented by (4.10) is applied to reduce the effect of discontinuities at the window edges and the leakages.

The amplitudes estimated by FFT are scaled by 0.54 for the hamming window, and by the ratio of fft no. to data number for correction to the amplitudes.

The harmonic frequencies, their respective amplitudes and initial phase angles estimated by the FFT are presented in Table 8.6.

Table 8.6 Even-harmonics estimated by WT-based algorithm & DFT-based algorithm

Time Period = 0.28s

DFT-based algorithm						WT-based algorithm					
Freq (Hz)	Amp	Phase (deg.)	%freq Er	%Amp Er	%Phase Er	Freq (Hz)	Amp	Phase (deg.)	%freq Er	%Amp Er	%Phase Er
49.95	1.523	0	*0*	*0*	*0*	49.95	1.524	0	*0*	*0*	*0*
100.35	0.06	-31.7	*-0.45*	*-1.69*	*-217*	99.9	0.059	-10	*0*	*0*	*0*
149.9	0.288	1.5	*0*	*0*	*62.5*	149.85	0.288	4	*0*	*0*	*0*
199.65	0.055	-4.4	*0*	*-1.85*	*63.3*	199.8	0.054	-12	*0*	*0*	*0*
249.75	1.253	-5	*0*	*0*	*0*	249.75	1.254	-5	*0*	*0*	*0*
349.7	0.925	8.5	*0*	*0*	*22.7*	349.65	0.925	11	*0*	*0*	*0*
400.45	0.033	-34	*-0.213*	*-10*	*585.7*	399.6	0.03	7	*0*	*0*	*0*
449.7	0.134	-23.2	*0*	*-0.75*	*-45*	449.55	0.133	-16	*0*	*0*	*0*
549.5	0.54	12.5	*0*	*0*	*16.7*	549.45	0.54	15	*0*	*0*	*0*
649.4	0.301	-8.4	*0*	*0*	*-40*	649.35	0.301	-6	*0*	*0*	*0*
749.6	0.045	-25.1	*0*	*-2.27*	*-178.9*	749.25	0.044	-9	*0*	*0*	*0*
849.3	0.127	5.7	*0*	*-0.79*	*56.2*	849.15	0.126	13	*0*	*0*	*0*
949.25	0.045	-28.5	*0*	*0*	*-42.5*	949.05	0.045	-20	*0*	*0*	*0*

Time Period = 0.18s

DFT-based algorithm						WT-based algorithm					
Freq (Hz)	Amp	Phase (deg.)	%freq Er	%Amp Er	%Phase Er	Freq (Hz)	Amp	Phase (deg.)	%freq Er	%Amp Er	%Phase Er
49.95	1.523	0	*0*	*0*	*0*	49.95	1.524	0	*0*	*0*	*0*
100.8	0.063	-37.7	*-0.901*	*-6.78*	*-277*	99.95	0.059	-11.64	*0*	*0*	*-16.4*
149.95	0.289	0.78	*0*	*-0.35*	*80.5*	149.85	0.288	4	*0*	*0*	*0*
199.6	0.056	-5	*0.1*	*-3.7*	*58.3*	199.8	0.054	-12	*0*	*0*	*0*
249.75	1.253	-5	*0*	*0*	*0*	249.75	1.254	-5	*0*	*0*	*0*
349.7	0.925	9.38	*0*	*0*	*14.7*	349.65	0.925	11	*0*	*0*	*0*
401.1	0.036	-40	*-0.375*	*-20*	*671.4*	399.6	0.03	7	*0*	*0*	*0*
449.9	0.135	-26.7	*0*	*-1.5*	*-66.9*	449.55	0.133	-16	*0*	*0*	*0*
549.55	0.541	11.8	*0*	*-0.19*	*21.3*	549.45	0.54	15	*0*	*0*	*0*
649.5	0.302	-10.6	*0*	*-0.33*	*-76.7*	649.35	0.301	-6	*0*	*0*	*0*
750	0.047	-30.8	*-0.1*	*-6.82*	*-242.2*	749.25	0.044	-9	*0*	*0*	*0*
849.45	0.128	3.6	*0*	*-1.59*	*72.3*	849.15	0.126	13	*0*	*0*	*0*
949.55	0.047	-33.1	*0*	*-4.44*	*-65.5*	949.05	0.045	-20	*0*	*0*	*0*

It can be seen that the estimation results by DFT-based algorithm are largely affected by the signal length. The DFT-based algorithm requires a longer signal length for more accurate estimations. In both cases of T=0.18s and T=0.28s, the percentage errors in frequency detection by DFT-based algorithm are smaller than 1%, the percentage errors in amplitude detection are quite significant at signal length of 0.18s. In both signal time lengths, the phase angles estimated by DFT-based algorithm are not reliable. It is understandable as phase angle detection is dependent on the accuracy in frequency detection and amplitude detection.

On the other hand, the estimation results in frequencies, amplitudes and initial phase angles produced by the proposed WT-based harmonic detection algorithm are exactly equal to the synthesized signal for both T=0.18s and T=0.28s. A frequency detection error of 0.05% is found at a harmonic frequency of 99.9Hz with signal length of 0.18s. The corresponding initial phase detection error is 16.4%.

As the amplitude of the 99.9Hz harmonic is 0.059 which is very small compared to the amplitude of the adjacent 49.95Hz harmonic (amplitude=1.524, the ratio is 0.04:1) and 149.85Hz harmonic (amplitude=0.288, the ratio is 0.2), the wavelet filter constructed for the 99.9Hz harmonic would be distorted slightly by the amplitudes of adjacent harmonics.

Based on the above analysis, it can be seen that the proposed WT-based algorithm requires a shorter signal for harmonic analysis with more accurate results, as compared to DFT-based algorithm. The WT-based algorithm is also able to estimate harmonic frequencies of very small amplitudes.

8.3   Field Harmonic Signal Analysis

Three tests are conducted. The first two tests dealt with the analysis of field waveforms obtained from the red-phase input current to a three-phase variable speed drive supplying a submersible water pump. The waveform of the input current to the VSD with its output frequency at 20Hz and 30Hz respectively are being analyzed. The third test is conducted to the current of a single-phase final circuit supplying power to a number of single loads including an electronic dimmer-controlled lamp bulb, fluorescent luminaries complete with electronic ballasts, a hairdryer and an air compressor motor.

8.3.1   Input Current to a Three-Phase Six-Pulse Variable Speed Drive

The field harmonic signal used is obtained from the red-phase input current to a three-phase variable speed drive supplying a submersible water pump. The frequency of the output voltage of the variable speed drive is set at 20Hz. Given the nature of a six-pulse three-phase VSD, the input current would contain 5th, 7th, 11th, 13th, 17th and 19th ... harmonics. The input current waveform is sampled at 10kHz. A low pass filter with a cutoff frequency of 4kHz is applied. By checking zero crossing, the average fundamental frequency of the harmonic signal for a time period of 0.6s, i.e. 30 cycles of the fundamental frequency, is 49.958Hz. The whole time period of the field harmonic signal is shown in Fig. 8.11. Fig. 8.12 shows two cycles of the field harmonic signal.
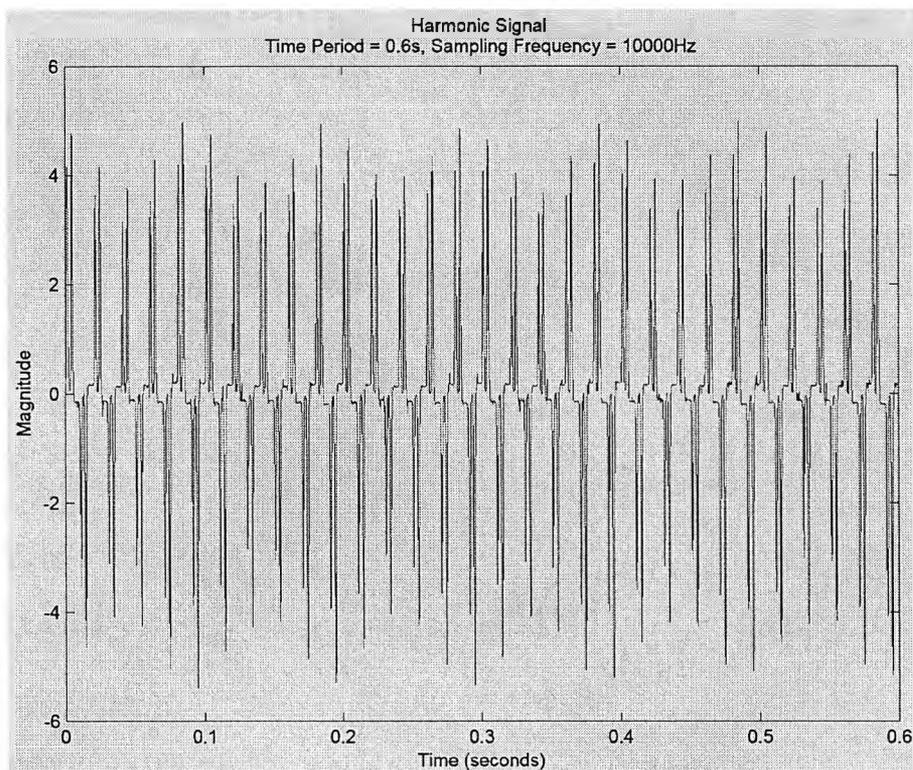
Fig. 8.11 Waveform of VSD input current (T = 0.6s)
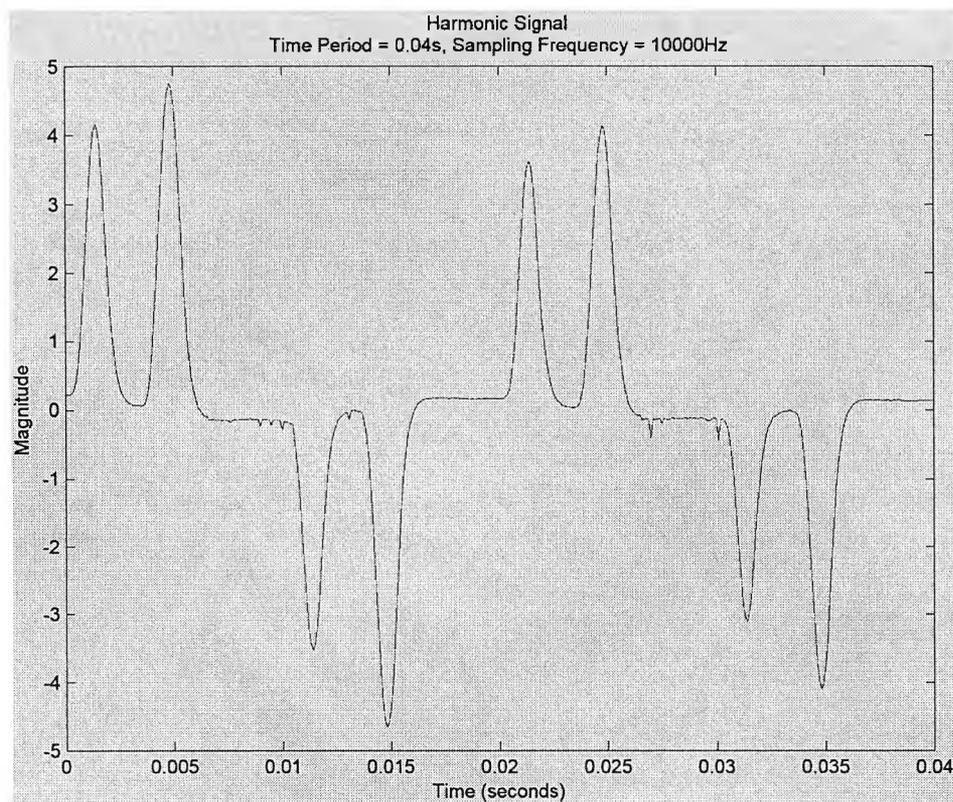
Fig. 8.12 Waveform of two cycles of VSD input current

Due to waveform variations, even harmonics of small magnitudes may exist in the harmonic signal, therefore the separation between adjacent frequencies, f_{sep}, should be set to 25Hz. The minimum signal time length is calculated as in (7.8),

$$T \geq 12\left(\frac{1}{f_{sep}} + \frac{1}{2f_L}\right) = 12\left(\frac{1}{25} + \frac{1}{2x50}\right) = 0.6s .$$

A field signal with the time length T = 0.6s is used for analysis by both the WT-based algorithm and DFT-based algorithm. The frequency resolution is selected as 0.02Hz.

The harmonics estimation results of the input current to VSD by the WT-based algorithm and the DFT-based algorithm are tabulated in Table 8.7.

Table 8.7 Harmonics estimated by WT-based algorithm & DFT-based algorithm for VSD input current (output frequency = 20Hz)

Harmonic No.	Expected Frequency (Hz)*	WT-based algorithm				DFT-based algorithm			
		Frequency (Hz)	% Error	Amplitude	Initial Phase (deg.)	Frequency (Hz)	% Error	Amplitude	Initial Phase (deg.)
1	49.958	49.96	-0.004	1.526	-56.31	49.96	-0.004	1.522	-56.37
2	99.916	100.16	-0.244	0.066	-40.77	100.08	-0.164	0.062	-34.85
3	149.874	149.86	0.009	0.276	92.67	149.86	0.009	0.278	92.65
4	199.832	199.54	0.146	0.057	-117.52	199.62	0.106	0.055	-124.68
5	249.79	249.78	0.004	1.257	-95.58	249.78	0.004	1.255	-95.53
7	349.706	349.7	0.002	0.928	141.91	349.7	0.002	0.927	141.85
8	399.664	399.82	-0.039	0.032	157.51	399.76	-0.024	0.032	160.84
9	449.622	449.62	0	0.128	-93.31	449.6	0.005	0.129	-91.24
10	499.58	499.38	0.04	0.02	70.28	499.32	0.052	0.02	77.11
11	549.538	549.52	0.003	0.542	110.99	549.52	0.003	0.542	110.96
13	649.454	649.46	-0.001	0.303	-3.87	649.44	0.002	0.3031	-1.74
15	749.37	749.34	0.004	0.0432	68.57	749.36	0.001	0.0435	66.72
17	849.235	849.28	0.001	0.1266	-37.87	849.28	0.001	0.1271	-37.98
19	949.145	949.2	0	0.0455	-128.44	949.18	0.002	0.0455	-126.26

*note: based on a fundamental frequency of 49.958Hz.

Besides the characteristic harmonics of a six-pulse three-phase VSD, the harmonic signal contains triplen harmonics and even harmonics. The triplen harmonics may be produced by the single-phase control circuit. The even harmonics are of very small amplitudes which may be due to waveform asymmetry produced by load changes and the thyristor switching, or errors introduced during measurements.

Comparing the odd harmonics, both the DFT-based algorithm and the WT-based algorithm give nearly identical estimated harmonic frequencies. The estimated amplitudes and initial

phase angles by both DFT-based algorithm and WT-based algorithm are also comparable.

The above test is repeated with the VSD output frequency changed to 30Hz. By checking zero crossing, the average fundamental frequency of the harmonic signal for a time period of 0.6s, i.e. 30 cycles of the fundamental frequency is 49.983Hz.

The results are shown in Table 8.8. It can be seen that the accuracy in the estimations by both WT-based algorithm and DFT-based algorithm are comparable to that shown in Table 8.7.

Table 8.8 Harmonics estimated by WT-based algorithm & DFT-based algorithm for VSD input current (output frequency = 30Hz)

Harmonic No.	Expected Frequency (Hz)*	WT-based algorithm				DFT-based algorithm			
		Frequency (Hz)	% Error	Amplitude	Initial Phase (deg.)	Frequency (Hz)	% Error	Amplitude	Initial Phase (deg.)
1	49.983	49.98	*0.006*	3.7372	-77.61	49.98	*0.006*	3.7348	-77.64
2	99.966	100.02	*-0.054*	0.1094	-68.73	100.14	*-0.174*	0.1111	-81.82
3	149.949	149.96	*-0.007*	0.5336	26.11	149.96	*-0.007*	0.536	26.26
4	199.932	199.9	*0.016*	0.0901	130.08	199.76	*0.086*	0.09	147.33
5	249.915	249.92	*-0.002*	2.7426	153.95	249.92	*-0.002*	2.742	154.01
7	349.881	349.88	*0*	1.8322	-8.39	349.88	*0*	1.8323	-8.33
9	449.847	449.9	*-0.012*	0.1506	56.01	449.9	*-0.012*	0.1508	56.07
11	549.813	549.82	*-0.001*	0.6762	-133.37	549.82	*-0.001*	0.6761	-133.27
13	649.779	649.78	*0*	0.2324	74.99	649.78	*0*	0.2322	75.1
15	749.745	749.8	*-0.007*	0.0507	50.02	749.78	*-0.005*	0.0514	52.29
17	849.711	849.76	*-0.006*	0.046	163.05	849.74	*-0.003*	0.0459	165.34
19	949.677	949.68	*0*	0.065	-23.73	949.68	*0*	0.0648	-23.91

*note: based on a fundamental frequency of 49.983Hz.

8.3.2   Single-Phase Non-linear Loads

Fig. 8.13 and Fig. 8.14 show respectively the complete waveform and the waveform of four cycles of the current taken from a single-phase final circuit rated at 220volt ± 6%, 50Hz ± 2% and is supplying power to an electronic dimmer controlled lamp bulb, fluorescent luminaries complete with electronic ballasts, a hairdryer and an air compressor motor.
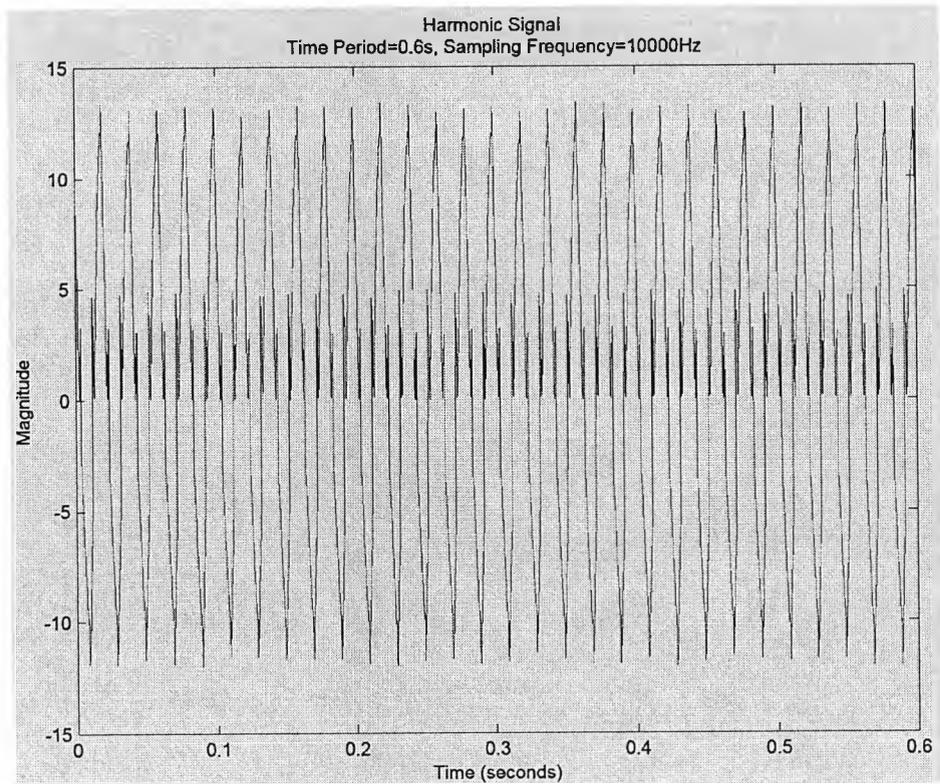
Fig. 8.13 Waveform of single-phase input current (T = 0.6s)
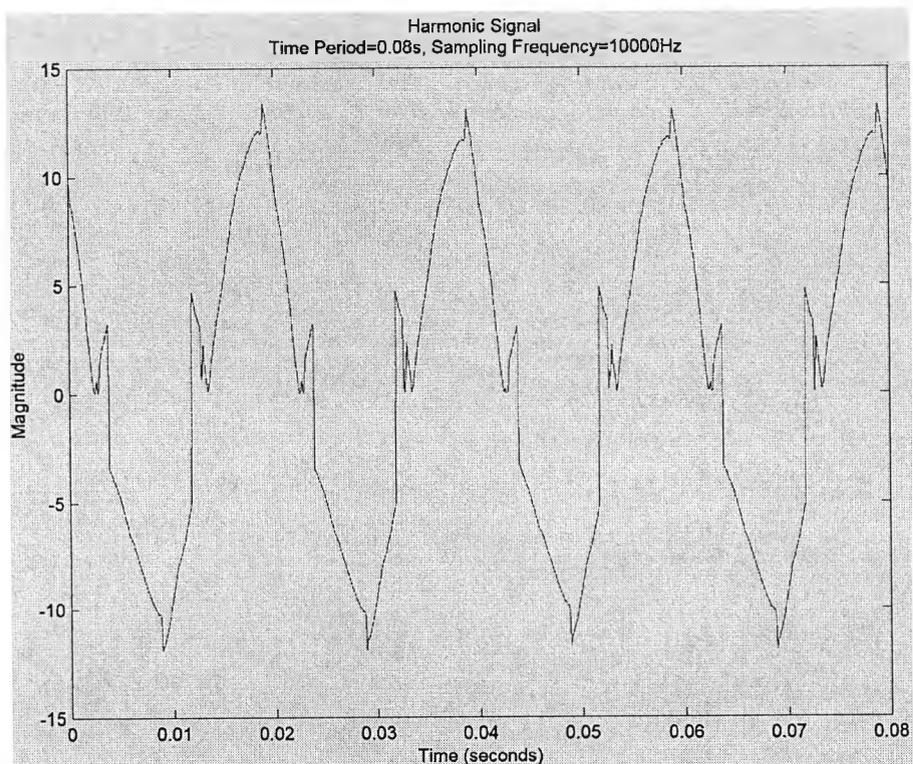
Fig. 8.14 Waveform of four cycles of single-phase input current

The f_{sep} used and the signal time length are set to 25Hz and 0.6s respectively, which are the same as in Section 8.3.1. By checking zero crossing, the average fundamental frequency of the harmonic signal for a time period of 0.6s, i.e. 30 cycles of the fundamental frequency is 50.026Hz. The estimation results by both WT-based algorithm and DFT-based algorithm are tabulated in Table 8.9.

Table 8.9 Harmonics estimated by WT-based algorithm & DFT-based algorithm
for single-phase input current

Harmonic No.	Expected Frequency (Hz)*	WT-based algorithm				DFT-based algorithm			
		Frequency (Hz)	% Error	Amplitude	Initial Phase (deg.)	Frequency (Hz)	% Error	Amplitude	Initial Phase (deg.)
1	50.026	50.02	*0.012*	10.3274	34.52	50.02	*0.012*	10.3269	34.49
3	150.078	150.08	*-0.001*	1.4587	56.71	150.1	*-0.015*	1.4595	54.54
4	200.104	200.08	*0.012*	0.7041	173.66	200.08	*0.012*	0.702	173.45
5	250.13	250.14	*-0.004*	0.9474	6.68	250.16	*-0.012*	0.9497	4.49
6	300.156	300.14	*0.005*	0.5211	72.4	300.18	*-0.008*	0.5207	67.62
7	350.182	350.18	*0.001*	0.6644	-105.87	350.18	*0.001*	0.6658	-105.69
8	400.208	400.16	*0.012*	0.2018	-6.56	400.3	*-0.023*	0.2026	-21.96
9	450.234	450.24	*-0.001*	0.8836	161.28	450.24	*-0.001*	0.8824	161.2
11	550.286	550.28	*0.001*	0.6169	85.6	550.3	*-0.003*	0.6154	83.16
13	650.338	650.3	*0.006*	0.1681	-25.5	650.4	*-0.01*	0.1687	-36.81
14	700.364	700.36	*0.001*	0.373	-168.56	700.38	*-0.002*	0.3718	-170.73
15	750.39	750.28	*0.015*	0.0408	-85.81	750.48	*-0.012*	0.0408	-105.58
16	800.416	800.4	*0.002*	0.3209	105.95	800.44	*-0.003*	0.3184	101.25
17	850.442	850.44	*0*	0.2543	-69.93	850.48	*-0.004*	0.2562	-74.19
18	900.468	900.44	*0.003*	0.1654	21.48	900.52	*-0.006*	0.1645	12.24

*note: based on a fundamental frequency of 50.026Hz.

It can be seen that the harmonic signal contains odd harmonics and even harmonics. The even harmonics are of small amplitudes which may be due to waveform asymmetry produced by load changes and switched mode power supply switching, or errors introduced during measurements.

Both WT-based algorithm and DFT-based algorithm are able to estimate the harmonic frequencies accurately as compared to the expected harmonic frequencies of the field harmonic signal with an average fundamental frequency of 50.026Hz. In a strict sense, the WT-based algorithm is slightly better but the difference is very small. The amplitudes of the harmonics estimated by both WT-based algorithm and DFT-based algorithm are comparable. However there are large deviations in initial phase estimations.

8.4 Conclusion

The proposed WT-based algorithm is tested vigorously by both synthesized harmonic signals and field harmonic signals. It is observed from the test results that the proposed WT-based algorithm is better than DFT-based algorithm in frequency estimation when the harmonic signal contains harmonic frequencies which are not integer multiples of the fundamental frequency. On amplitude and initial phase estimations, the WT-based algorithm is obviously better than DFT-based algorithm. In addition, the proposed WT-based algorithm requires a shorter signal length as compared to DFT-based algorithm for harmonic analysis with reasonable accuracy.

Chapter 9

The Wavelet-Based Dynamic Waveform Reconstruction Algorithm

9.1 Introduction

In Chapter 8, the proposed WT-based algorithm is tested with synthesized harmonic signals and field harmonic signals. The results showed that the proposed WT-based algorithm is able to estimate the amplitudes, frequencies and initial phase angles of the harmonics accurately. The proposed WT-based algorithm requires a finite length of the harmonic signal for the estimation, and this is inevitable as in any harmonic estimation tools such as DFT. The variation in amplitudes of any harmonic frequency components within the analysis period will be averaged in the estimation process. If the time length of the harmonic signal required for the analysis is very short and if the signal amplitude is only varying very slightly, the amplitudes estimated can be regarded as truly reflecting the amplitudes of the harmonics. Otherwise, the amplitudes estimated are only approximates [79]. This Chapter will go on developing a WT-based dynamic waveform reconstruction algorithm to reconstruct the harmonic waveforms from the complex CWT coefficients. This is useful for identifying the amplitude variations of the harmonics over the estimation period [80,81].

9.2 Basic Theory

The WT of a continuous signal, f(t), is defined in (3.5) as

$$Wf(u,a) = \langle f, \varphi_{u,a} \rangle = \int_{-\infty}^{+\infty} f(t) \frac{1}{\sqrt{a}} \varphi^* (\frac{t-u}{a}) dt.$$

From (5.29), the modified CMW is represented as

$$\varphi(\frac{t}{a}) = \frac{1}{a}\frac{1}{\sqrt{\pi f_b}}e^{-(\frac{t}{a})^2/f_b}e^{j2\pi f_c(\frac{t}{a})}.$$

The complex continuous wavelet transform by using the modified CWM is given as

$$Wf(u,a) = \langle f, \varphi_{u,a} \rangle = \int_{-\infty}^{+\infty} f(t)\frac{1}{a}\frac{1}{\sqrt{\pi f_b}}e^{-\left(\frac{t-u}{a}\right)^2/f_b}e^{-j\omega_c\left(\frac{t-u}{a}\right)}dt. \tag{9.1}$$

The real part and imaginary part of the complex wavelet coefficients generated by (9.1) are represented as

$$\text{Re}[Wf(u,a)] = \int_{-\infty}^{+\infty} f(t)\frac{1}{a}\frac{1}{\sqrt{\pi f_b}}e^{-\left(\frac{t-u}{a}\right)^2/f_b}\cos[\frac{\omega_c}{a}(t-u)]dt; \tag{9.2}$$

$$\text{Im}[Wf(u,a)] = -\int_{-\infty}^{+\infty} f(t)\frac{1}{a}\frac{1}{\sqrt{\pi f_b}}e^{-\left(\frac{t-u}{a}\right)^2/f_b}\sin[\frac{\omega_c}{a}(t-u)]dt. \tag{9.3}$$

Given a harmonic signal represented as

$$f(t) = A\cos(\omega t), \tag{9.4}$$

the real part of the complex CWT coefficient for (9.4) is given as

$$Re[Wf(u,a)] = \int_{-\infty}^{+\infty} [A\cos(\omega t)]\frac{1}{a}\frac{1}{\sqrt{\pi f_b}}e^{-\left(\frac{t-u}{a}\right)^2/f_b}\cos[\frac{\omega_c}{a}(t-u)]dt$$
$$= \frac{A}{a\sqrt{\pi f_b}}\int_{-\infty}^{+\infty} e^{-\left(\frac{t-u}{a}\right)^2/f_b}\cos(\omega t)\cos[\frac{\omega_c}{a}(t-u)]dt \tag{9.5}$$

Let x = t-u, then t = x+u and dt = dx. Substituting this into (9.5)

$$Re[\,Wf\,(u,a\,)] = \frac{A}{a\sqrt{\pi f_b}} \int_{-\infty}^{+\infty} e^{-\left(\frac{x}{a}\right)^2 / f_b} \cos[\,\omega(x+u)]\cos(\frac{\omega_c}{a}x)dx \,. \tag{9.6}$$

Replace x by t again in (9.6) becomes

$$Re[\,Wf\,(u,a\,)] = \frac{A}{a\sqrt{\pi f_b}} \int_{-\infty}^{+\infty} e^{-\left(\frac{t}{a}\right)^2 / f_b} \cos[\,\omega(t+u)]\cos(\frac{\omega_c}{a}t)dt \,. \tag{9.7}$$

The wavelet coefficient will be the largest when the frequency of a harmonic signal is equal to the wavelet centre frequency at a given dilation. Therefore substitute $\omega = \dfrac{\omega_c}{a}$ from (5.8) into (9.7),

$$\begin{aligned} Re[\,Wf\,(u,a\,)] &= \frac{A}{a\sqrt{\pi f_b}} \int_{-\infty}^{+\infty} e^{-\left(\frac{t}{a}\right)^2 / f_b} \cos[\,\omega(t+u)]\cos(\,\omega t\,)dt \\ &= \frac{A}{a\sqrt{\pi f_b}} \int_{-\infty}^{+\infty} e^{-\left(\frac{t}{a}\right)^2 / f_b} [\cos(\,\omega u\,)\cos^2(\,\omega t\,) - \sin(\,\omega u\,)\sin(\,\omega t\,)\cos(\,\omega t\,)]\,dt \end{aligned} \tag{9.8}$$

From (9.3), the imaginary part of the complex CWT coefficient for (9.4) is given as

$$\begin{aligned} Im[\,Wf\,(u,a\,)] &= -\int_{-\infty}^{+\infty} A\cos(\,\omega t\,)\frac{1}{a}\frac{1}{\sqrt{\pi f_b}} e^{-\left(\frac{t-u}{a}\right)^2 / f_b} \sin[\frac{\omega_c}{a}(t-u)]\,dt \\ &= -\frac{A}{a\sqrt{\pi f_b}} \int_{-\infty}^{+\infty} e^{-\left(\frac{t-u}{a}\right)^2 / f_b} \cos(\,\omega t\,)\sin[\frac{\omega_c}{a}(t-u)]\,dt \end{aligned} \tag{9.9}$$

By change of variable in (9.9), as in (9.6) and (9.7) for the real part of the complex CWT coefficient, and substituting $\omega = \dfrac{\omega_c}{a}$ gives

$$Im[\,Wf\,(u,a\,)] = -\frac{A}{a\sqrt{\pi f_b}} \int_{-\infty}^{+\infty} e^{-\left(\frac{t}{a}\right)^2 / f_b} \cos[\,\omega(t+u)]\sin(\,\omega t\,)dt \,. \tag{9.10}$$

Shifting the imaginary part of the complex CWT coefficient by 90° backward in time, (9.10) becomes

$$Im[Wf(u+\frac{\pi}{2\omega},a)] = -\frac{A}{a\sqrt{\pi f_b}}\int_{-\infty}^{+\infty}e^{-\left(\frac{t}{a}\right)^2/f_b}\cos[\omega(t+u+\frac{\pi}{2\omega})]\sin(\omega t)dt$$

$$\frac{A}{a\sqrt{\pi f_b}}\int_{-\infty}^{+\infty}e^{-\left(\frac{t}{a}\right)^2/f_b}[\cos(\omega u)\sin^2(\omega t)+\sin(\omega u)\sin(\omega t)\cos(\omega t)]dt$$

(9.11)

Adding (9.8) and (9.11) produces,

$$Re[Wf(u,a)]+Im[Wf(u+\frac{\pi}{2\omega},a)] = \frac{A}{a\sqrt{\pi f_b}}\cos(\omega u)\int_{-\infty}^{+\infty}e^{-\left(\frac{t}{a}\right)^2/f_b}dt$$

$$=\frac{A}{a\sqrt{\pi f_b}}\cos(\omega u)(a\sqrt{\pi f_b})$$

$$= A\cos(\omega u)$$

(9.12)

(9.12) verifies mathematically that for any sinusoidal waveform of sufficient length and by using the modified CMW for the complex CWT, the waveform can be fully reconstructed by adding the real part of the corresponding complex CWT coefficients to the imaginary part of the corresponding complex CWT coefficients being shifted backward in time by 90°. (9.12) also verifies that the reconstruction is time-invariant. The instantaneous phase of the harmonic component is preserved in the reconstructed waveform.

9.3 Waveform Reconstruction Algorithm

From the proof in Section 9.2, it can be seen that once the harmonic frequency of a harmonics component in a harmonic signal can be determined, the waveform variations of the harmonics would be reconstructed easily from the complex wavelet coefficients. Fig. 9.1 shows the flowchart of the WT-based dynamic waveform reconstruction algorithm.

```
┌─────────────────────────┐
│  Determine the Harmonic │
│        Frequency        │
└─────────────────────────┘
            │
┌─────────────────────────┐
│      Set fb = 10000     │
└─────────────────────────┘
            │
┌─────────────────────────┐
│   Compute fc and a for the │
│     harmonic frequency  │
└─────────────────────────┘
            │
┌─────────────────────────┐
│  Compute the complex wavelet │
│        coefficients     │
└─────────────────────────┘
            │
┌─────────────────────────┐
│  Extract the real part and the │
│ imaginary part of the complex │
│     wavelet coefficients │
└─────────────────────────┘
            │
┌─────────────────────────┐
│   Shift the imaginary part │
│    backward by 90 degree │
└─────────────────────────┘
            │
┌─────────────────────────┐
│  Add the real part and the │
│ shifted imaginary part  of the │
│  complex wavelet coefficients │
└─────────────────────────┘
```
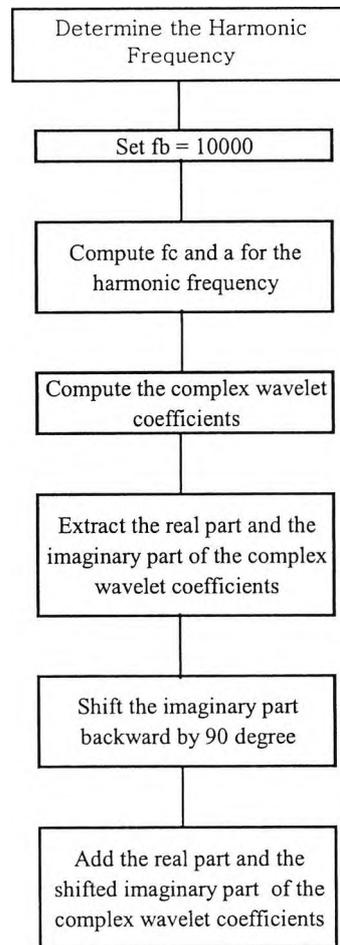
Fig. 9.1   Flow chart of the WT-based dynamic waveform reconstruction algorithm

9.4   Waveform Reconstruction of Synthesized Waveforms

Three tests are conducted to verify the effectiveness of the wavelet-based waveform reconstruction algorithm. In the first test, the WT-based waveform reconstruction algorithm is being tested with a synthesized waveform of ten cycles at 50Hz, with an amplitude of 1. One of the cycles is a sag [82] with an amplitude of 0.5. In the second test, the algorithm is being tested with a synthesized waveform containing ten cycles of waveform at 50Hz with slowly-varying amplitudes. The third test is conducted to a harmonic waveform consisting of the waveform in the second test together with some harmonics.

9.4.1   Synthesized Waveform with One Cycle of Sag

Consider a synthesized waveform of unity amplitude and a frequency of 50Hz, represented as

$$f(t)=\cos(2\pi 50t-90^\circ). \tag{9.13}$$

The waveform has 10 cycles (i.e. time period = 0.2s). The 5th cycle of the synthesized waveform in (9.13) is replaced by a sag with an amplitude of 0.5, as shown in Fig. 9.2. It is sampled at 2000Hz.
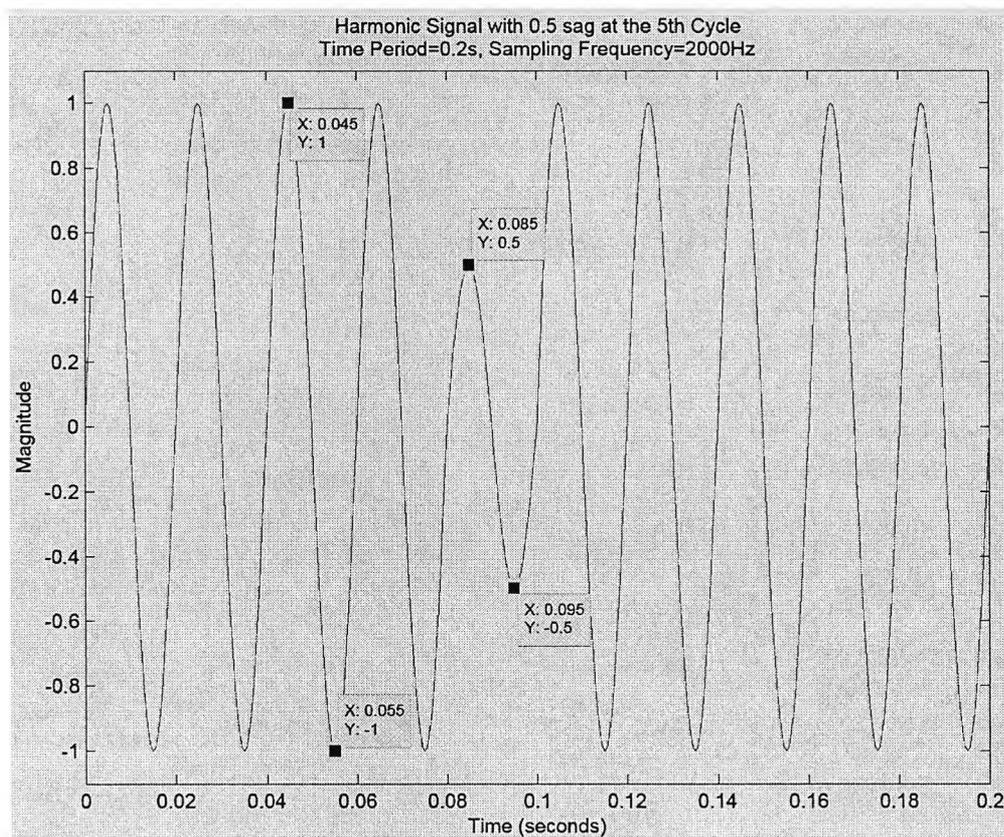
Fig. 9.2 Waveform of synthesized signal with one cycle of sag

By using the WT-based reconstruction algorithm developed in Section 9.2 the synthesized waveform is reconstructed from the complex wavelet coefficients. Fig. 9.3 shows the comparison between the synthesized waveform and the reconstructed waveform.

Fig. 9.3 Synthesized waveform vs. reconstructed waveform (sag)

Most part of the reconstructed waveform coincides with the synthesized waveform. Due to the finite support of the modified CMW and the abrupt change in the amplitude of the waveform in a short duration, the reconstructed waveform unavoidably has a small error at the negative peak of the sag. From this test, it can be seen that the proposed waveform reconstruction algorithm is able to reproduce a sudden variation in a waveform, with the variation as short as one cycle.

9.4.2   Synthesized Waveform with Slowly-Varying Amplitudes

Consider again the waveform simulated by (9.13). The synthesized waveform is modified such that the amplitudes of the cycles of the waveform are slowly varying, as shown in Fig. 9.4.
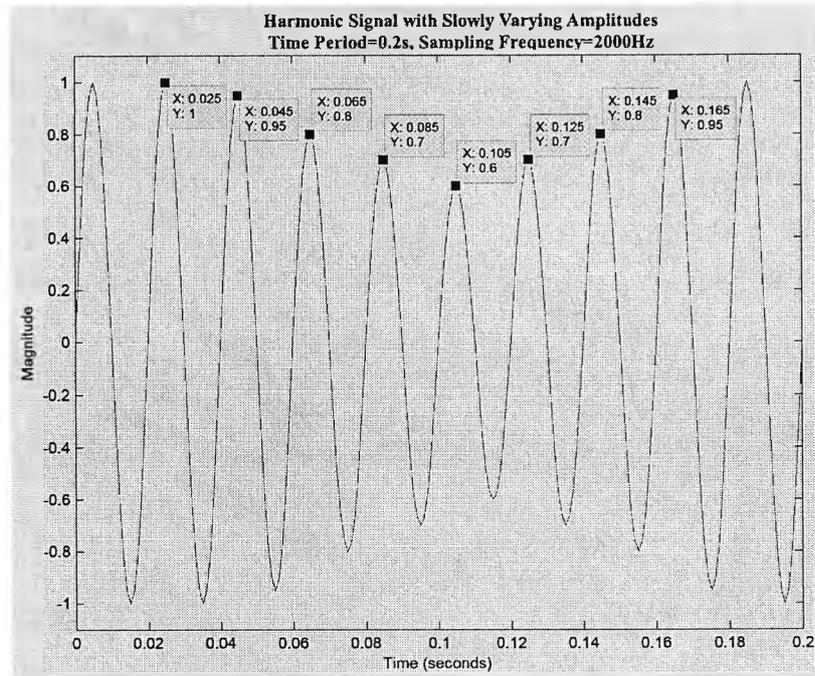
Fig. 9.4 Waveform of synthesized signal with slowly-varying amplitudes

By using the WT-based reconstruction algorithm shown in Fig. 9.1, the synthesized waveform is reconstructed from the complex wavelet coefficients. Fig. 9.5 shows the comparison between the synthesized waveform and the reconstructed waveform.
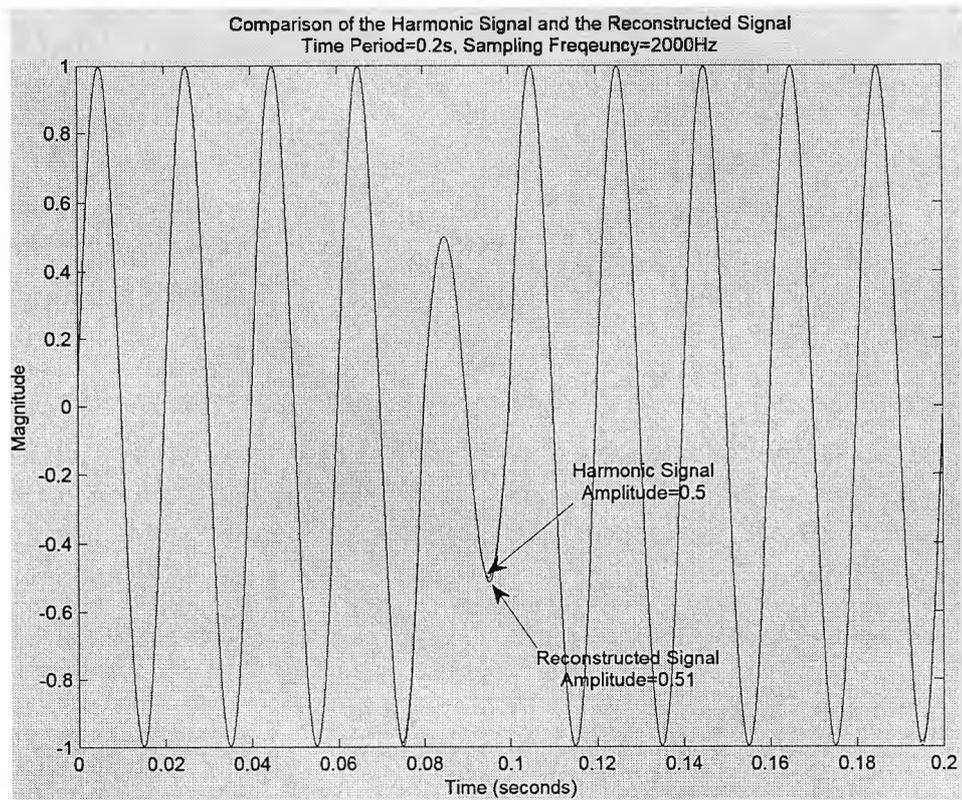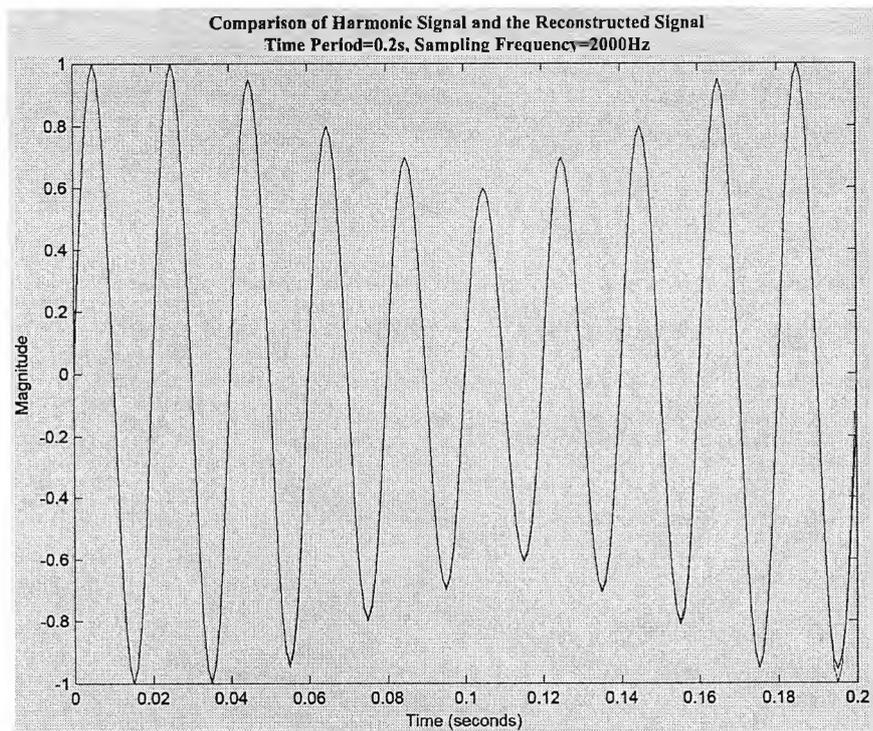

Fig. 9.5 Synthesized waveform vs. reconstructed waveform

(slowly-varying amplitudes)

It can be seen that with a waveform of slowly-varying amplitudes, the proposed waveform reconstruction algorithm is able to reproduce the waveform exactly. The proposed algorithm can estimate and reproduce variations as short as one cycle.

9.4.3   Synthesized Harmonic Waveform

The synthesized waveform with slowly-varying amplitudes in Fig. 9.4 is now mixed with harmonics synthesized as

$$0.5\cos(2\pi 150t) + 0.3\cos(2\pi 250t + 45°) + 0.2\cos(2\pi 350t). \tag{9.14}$$

The synthesized harmonic waveform is sampled at 2000Hz and the signal length is 0.2s. Fig. 9.6 shows the synthesized harmonic waveform.
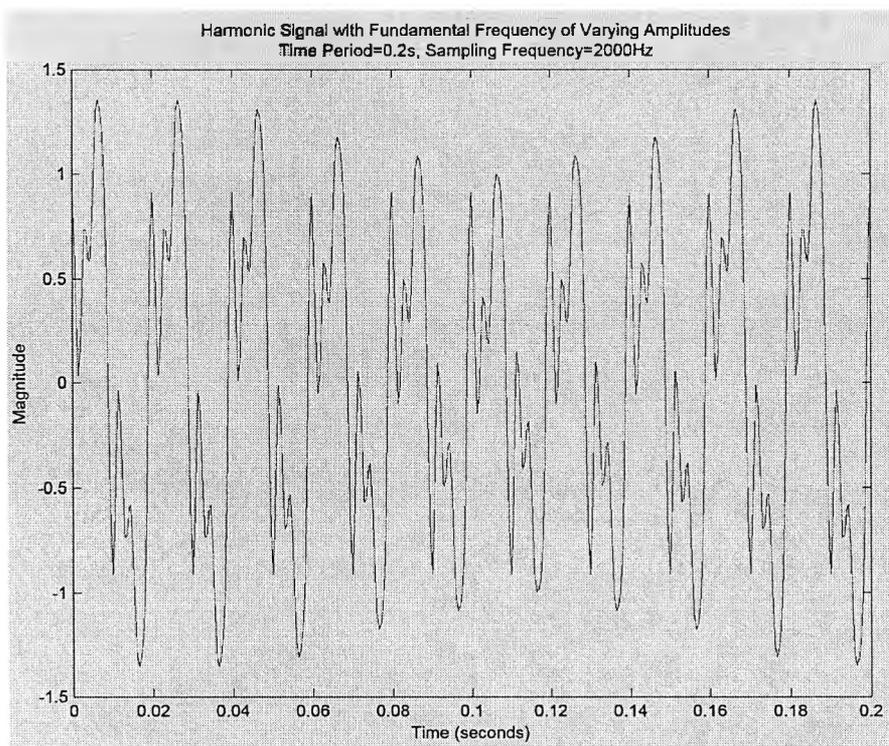
Fig. 9.6 Synthesized harmonics with slowly-varying amplitudes

Fig. 9.7 shows the comparison of the reconstructed waveform at fundamental frequency and the synthesized fundamental frequency waveform with slowly-varying amplitudes.
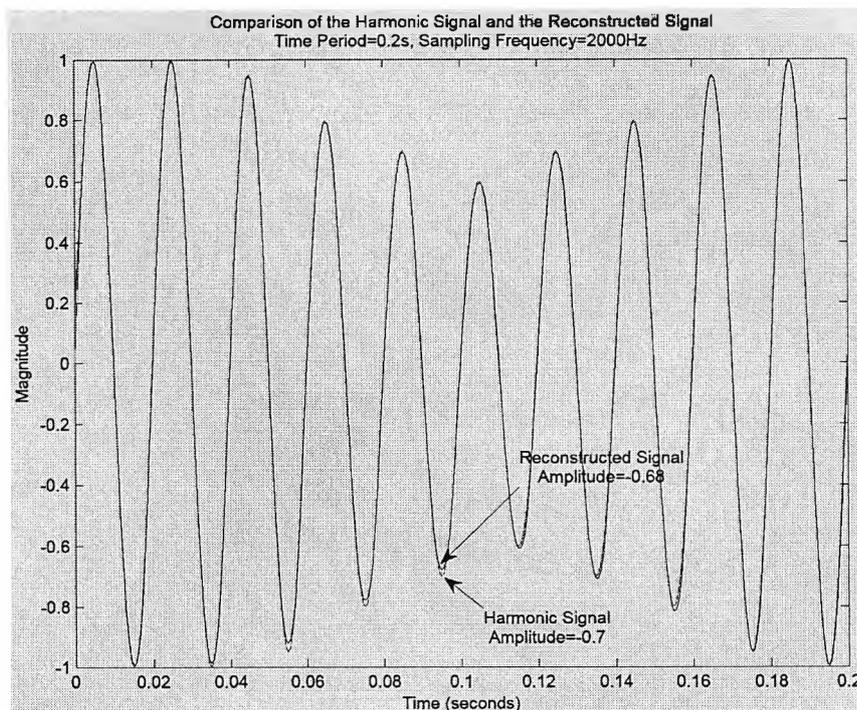
Fig. 9.7 Synthesized waveform vs. reconstructed fundamental waveform

(slowly-varying amplitudes)

The reconstruction algorithm is not affected by the presence of other harmonic frequencies and is nearly exact for most part of the waveform.

Table 9.1 summarizes the waveforms reconstruction results for the three synthesized waveforms.

9.5   DWT-Based Waveform Reconstruction

Discrete wavelet transform (DWT) has been using for detection of waveform variations by many researchers and has very prominent applications in power transients detection [83]. The three synthesized waveforms in Section 9.4 are also reconstructed by DWT to serve as a comparison to the proposed WT-based dynamic waveform reconstruction algorithm. Table 9.1 shows the comparison of reconstructions by DWT and the proposed WT-based dynamic waveform reconstruction algorithm.

Table 9.1
Comparison of waveform reconstruction
by DWT and the proposed algorithm

	Synthesized Signal		DWT-Based Reconstruction				CWT-Based Reconstruction			
	Set Amplitude		Estimated Amplitude		%Error		Estimated Amplitude		%Error	
	+ peak	- peak	+ peak	- peak	+ peak	- peak	+ peak	- peak	+ peak	- peak
(A) Synthesized waveform with a sag at 5th cycle										
5th cycle	0.5	-0.5	0.5241	-0.4909	*4.82%*	*1.82%*	0.5	-0.5117	*0%*	*2.34%*
(B) Synthesized waveform of slowly-varying amplitudes										
3rd cycle	0.95	-0.95	0.9552	-0.9503	*0.55%*	*0.03%*	0.95	-0.9465	*0%*	*0.37%*
4th cycle	0.8	-0.8	0.8088	-0.8007	*1.1%*	*0.09%*	0.8	-0.7977	*0%*	*0.29%*
5th cycle	0.7	-0.7	0.7064	-0.7006	*0.91%*	*0.09%*	0.7	-0.6977	*0%*	*0.33%*
6th cycle	0.6	-0.6	0.6069	-0.5961	*1.15%*	*0.65%*	0.6	-0.6023	*0%*	*0.38%*
7th cycle	0.7	-0.7	0.6993	-0.6936	*0.1%*	*0.91%*	0.7	-0.7023	*0%*	*0.33%*
8th cyle	0.8	-0.8	0.8	-0.7919	*0%*	*1.01%*	0.8	-0.8035	*0%*	*0.44%*
9th cycle	0.95	-0.95	0.9482	-0.9433	*0.19%*	*0.71%*	0.95	-0.9512	*0%*	*0.13%*
(C) Synthesized waveform of slowly-varying amplitudes and mixed with harmonics										
3rd cycle	0.95	-0.95	1.022	-0.9696	*7.58%*	*2.06%*	0.944	-0.9217	*0.63%*	*2.98%*
4th cycle	0.8	-0.8	0.8764	-0.8215	*9.55%*	*2.69%*	0.794	-0.7791	*0.75%*	*2.61%*
5th cycle	0.7	-0.7	0.788	-0.7228	*12.57%*	*3.26%*	0.694	-0.6791	*0.86%*	*2.99%*
6th cycle	0.6	-0.6	0.7003	-0.6177	*16.72%*	*2.95%*	0.594	-0.6087	*1%*	*1.45%*
7th cycle	0.7	-0.7	0.7892	-0.714	*12.74%*	*2%*	0.6939	-0.7087	*0.87%*	*1.24%*
8th cyle	0.8	-0.8	0.8779	-0.8105	*9.74%*	*1.31%*	0.7939	-0.8161	*0.76%*	*2.01%*
9th cycle	0.95	-0.95	1.02	-0.9607	*7.37%*	*1.13%*	0.9438	-0.9513	*0.65%*	*0.14%*

The sampling frequency of the synthesized signal, as mentioned in Section 9.4 is 2000Hz, with a signal length of 0.2s. The Daubechies Db-8 type wavelet was chosen as the mother wavelet. The synthesized signals were decomposed up to the fourth-scale. The frequency bands at each scale are shown in Table 9.2. The signal, three detail coefficients, and the third approximation coefficients are shown in each case.

Table 9.2
Frequency bands at each scale

Scale	Frequency Band
d1	500 - 1000Hz
d2	250 - 500Hz
d3	125 - 250Hz
a3	0 - 125Hz

9.5.1   Synthesized Waveform with One Cycle of Sag

Fig. 9.8 shows the detailed wavelet analysis results of the waveform. The reconstructed waveform is shown at the third approximation.
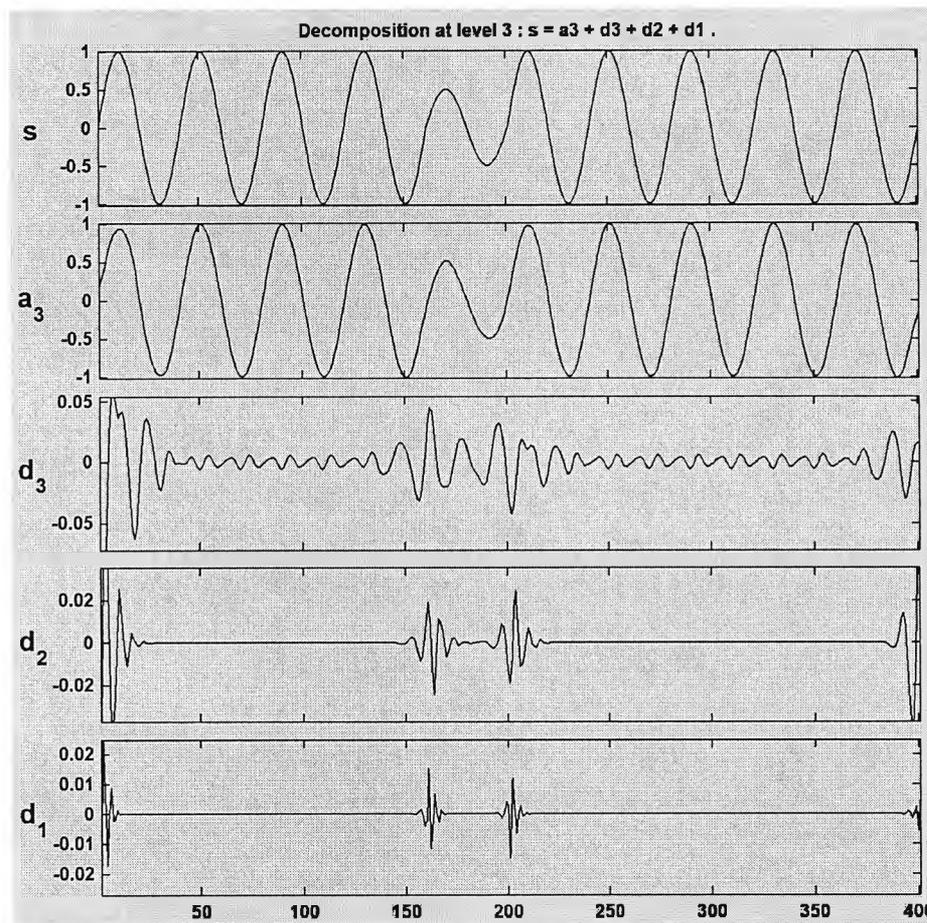
Fig. 9.8 Reconstructed waveform at the approximation (sag at the 5th cycle)

9.5.2   Synthesized Waveform with Slowly-Varying Amplitudes

Fig. 9.9 shows the detailed wavelet analysis results of the waveform. The reconstructed waveform is shown at the third approximation.
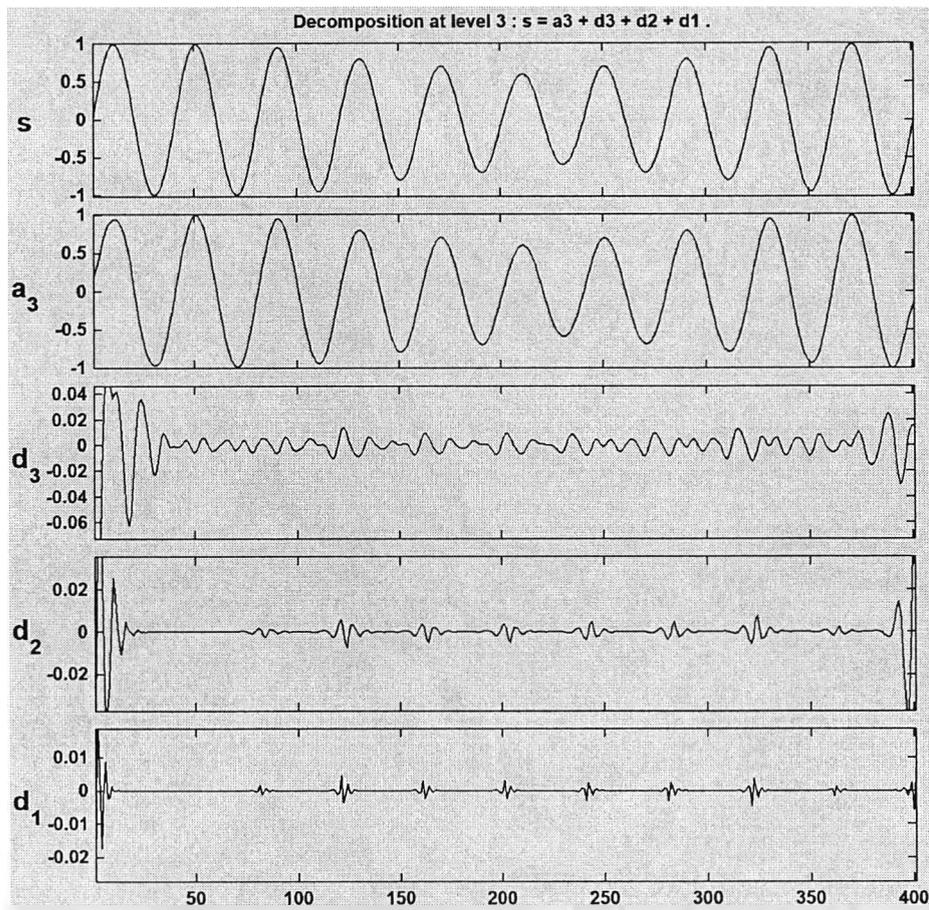
Fig. 9.9 Reconstructed waveform at the approximation (slowly-varying amplitudes)

9.5.3   Synthesized Harmonics Waveform

Fig. 9.10 shows the detailed wavelet analysis results of the waveform. The reconstructed waveform of the fundamental component is shown at the third approximation. The reconstructed waveform is seen to be distorted.
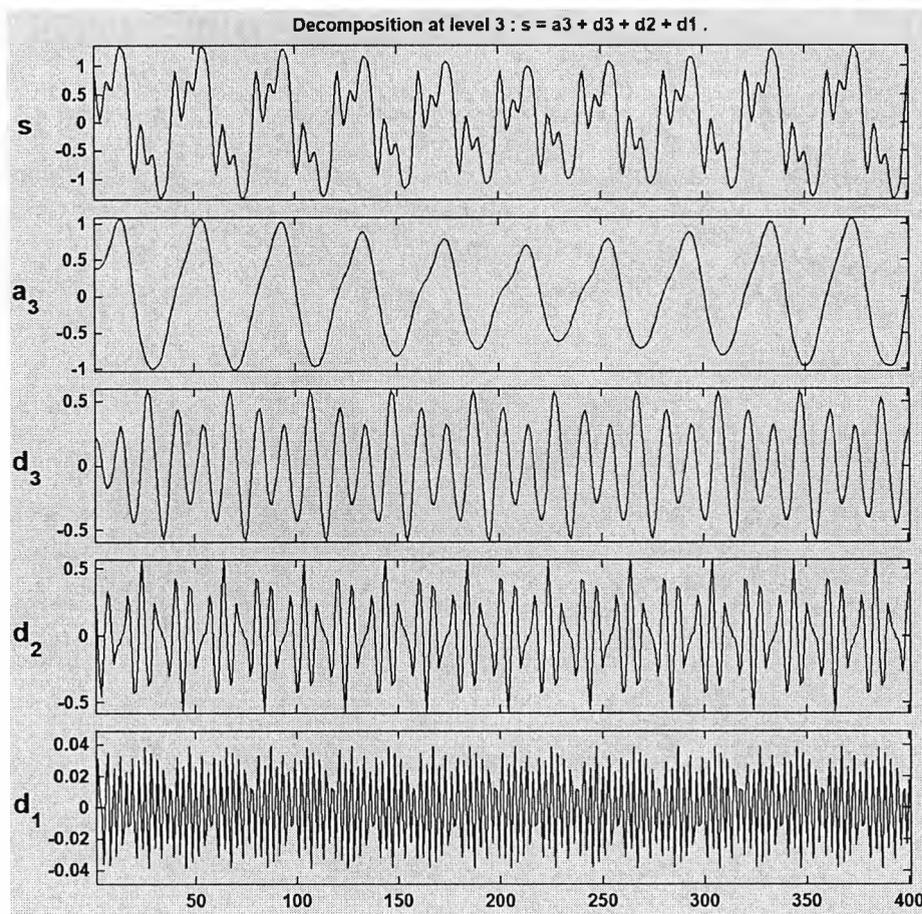
Fig. 9.10 Reconstructed fundamental waveform at the approximation
(slowly-varying amplitudes)

It can be seen from Table 9.1 that when the waveform contains a single frequency component only, DWT is able to reconstruct the variation in waveform amplitudes quite accurately. The proposed WT-based waveform reconstruction algorithm performs better over the DWT on positive peaks estimation, but is comparable with DWT on negative peaks reconstruction.

When the waveform contains fundamental component with slowly-varying-amplitudes and some harmonic frequencies, the waveform of the fundamental frequency component reconstructed by DWT is erroneous, while the proposed WT-based waveform reconstruction algorithm is able to reconstruct the waveform accurately. Another disadvantage of the DWT is that it would be difficult to reconstruct the waveforms of harmonics by DWT, but the proposed WT-based waveform reconstruction algorithm is able to reconstruct any harmonic components easily and efficiently.

9.6 Waveform Reconstruction of Field Harmonic Waveforms

Two tests are conducted. The first test dealt with the analysis of the field harmonic waveform discussed in Section 8.3.1. The second test is conducted to the field harmonic waveform discussed in Section 8.3.2.

9.6.1   Input Current to a Three-Phase Six-Pulse Variable Speed Drive

From Table 8.7 of Section 8.3.1, the field harmonic signal obtained from the red phase input current to a three-phase VSD drive with output frequency set at 20Hz has a fundamental component with the characteristics reproduced in Table 9.3.

Table 9.3 Estimated fundamental component of field harmonic waveform
(Section 8.3.1)

Sampling Frequency	10000 Hz
Time Period	0.6 s
Frequency	49.96 Hz
Amplitude	1.526 A
Initial Phase	-56.309°

By using the WT-based reconstruction algorithm in Fig. 9.1, the current at fundamental frequency is reconstructed to show the variation of the fundamental current within the time period of 0.6s. The reconstruction waveform is shown in Fig. 9.11 together with the field harmonic waveform for comparison.
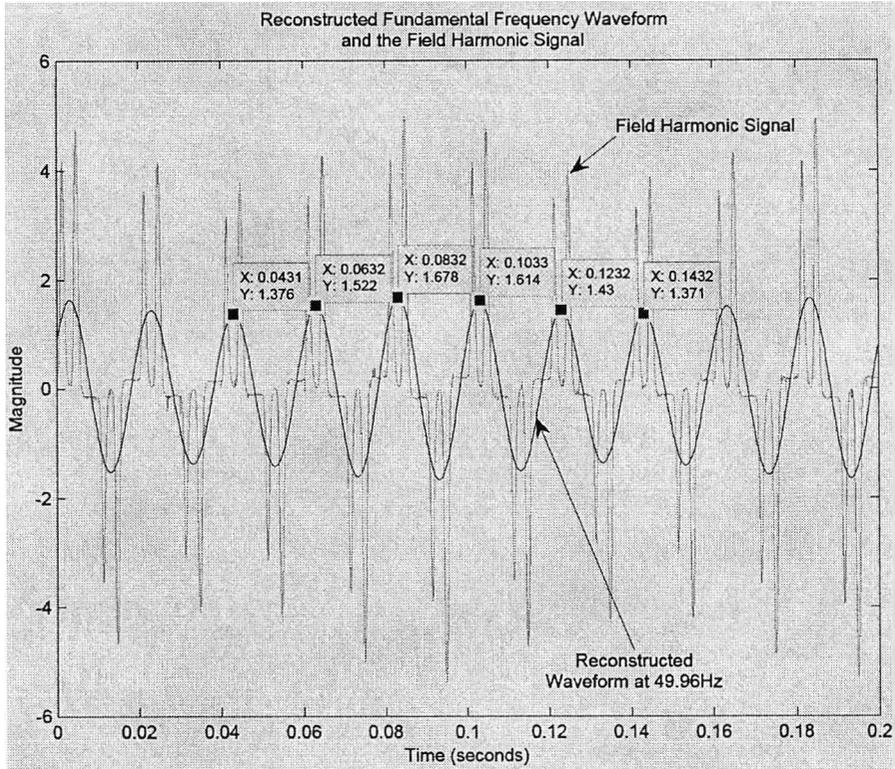
Fig. 9.11 Field harmonic signal vs. reconstructed waveform

It can be seen from Fig. 9.11 that the reconstructed current waveform at fundamental frequency coincides exactly with the field harmonic signal in terms of time location and frequency of oscillation. The reconstruction algorithm is also able to represent the variations in amplitude of the current waveform at fundamental frequency. The same reconstruction algorithm can also be used to represent the amplitude variations of other harmonic frequencies.

From Table 8.7 of Section 8.3.1, the major harmonics of the input current to the VSD (output frequency = 20Hz) is the 5th harmonics with the characteristics reproduced in Table 9.4 below.

Table 9.4 Estimated 5th harmonics of field harmonic signal
(Section 8.3.1)

Sampling Frequency	10000 Hz
Time Period	0.6 s
5th Harmonics	249.78 Hz
Amplitude	1.257 A
Initial Phase	-95.58°

Fig. 9.12 shows the reconstructed fundamental component and the 5th harmonics waveform

together with the field harmonic waveform.
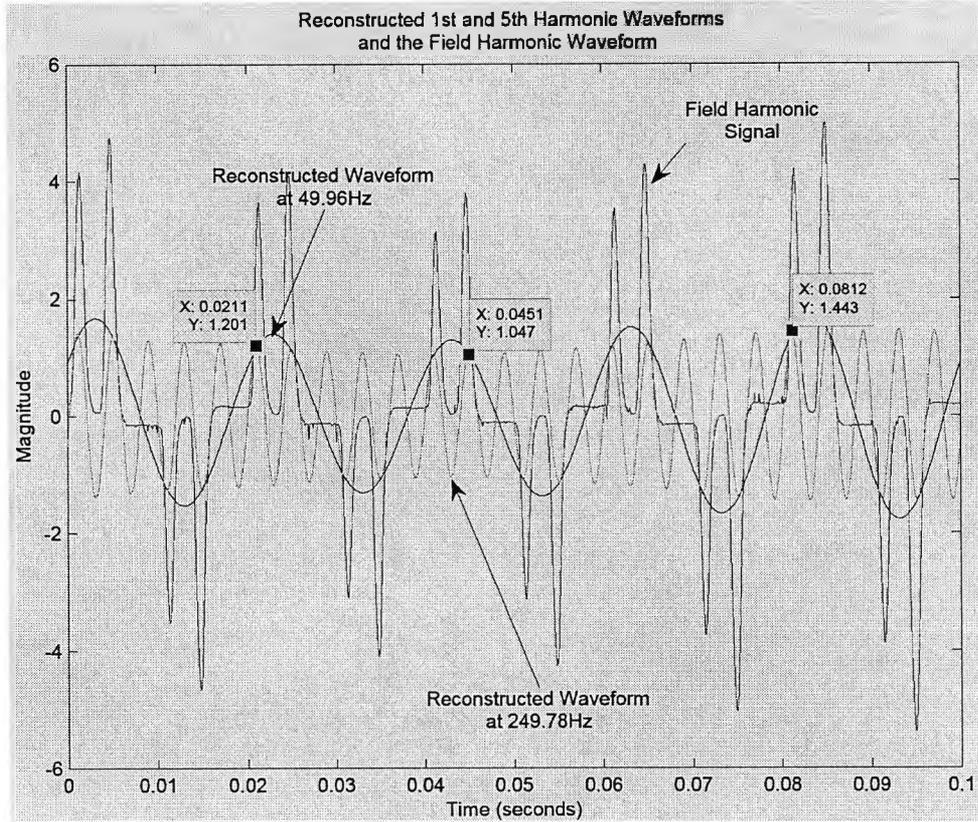
Fig. 9.12 Field harmonic signal vs. reconstructed fundamental
& 5th harmonic waveform

It can be seen from Fig. 9.12 that the reconstructed 5th harmonic waveform coincides with the peaks of the field harmonic waveform. The reconstruction algorithm is able to represent the variations in amplitude of the 5th harmonic waveform.

9.6.2   Single-Phase Non-linear Loads

From Section 8.3.2, the input current of a single-phase supply to a group of single-phase loads contained the fundamental current and 3rd harmonic current as shown in Table 9.5.

Table 9.5 Estimated fundamental & 5th harmonics of field harmonic signal
(Section 8.3.2)

	Fundamental Current	3rd Harmonic Current
Frequency	50.03 Hz	150.08 Hz
Amplitude	10.3274 A	1.4587 A
Initial Phase	34.52°	56.71°

Fig. 9.13 shows the reconstructed current waveform at fundamental frequency and the 3rd harmonics current waveform together with the field harmonic waveform.
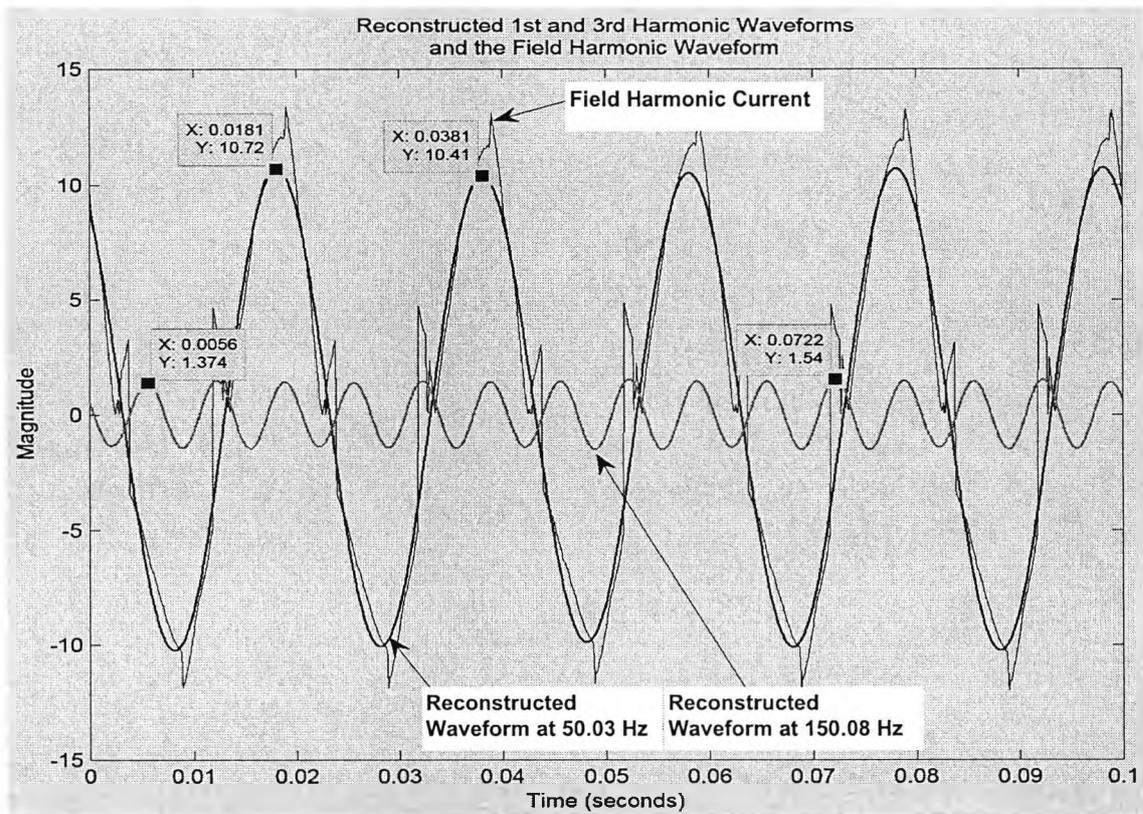
Fig. 9.13 Field harmonic signal vs. reconstructed fundamental & 3rd harmonic waveform

It can be seen from Fig. 9.13 that the reconstructed current waveform at the fundamental frequency coincides exactly with the field harmonic signal in terms of time location and frequency of oscillation. The reconstruction algorithm is able to represent the variations in amplitude of the fundamental frequency waveform and the 3rd harmonic waveform.

9.7 Conclusion

A WT-based dynamic waveform reconstruction algorithm is proposed to reconstruct the harmonic waveforms from the complex CWT coefficients. This is useful for identifying the amplitude variations of the harmonic frequency over the estimation period. The WT-based reconstruction algorithm is time-invariant and therefore is able to preserve the time and

phase information of the harmonic waveform. The proposed WT-based waveform reconstruction algorithm is tested vigorously by both synthesized waveforms and field harmonic waveforms. DWT is also used to reconstruct the synthesized waveforms and it was found that the proposed algorithm is better than DWT in waveform reconstruction. The tests revealed that the algorithm is able to reconstruct any harmonic waveforms accurately. Due to the properties of the modified CMW, only small errors are found at negative peaks. The WT-based reconstruction algorithm is able to represent waveform variations of one cycle short.

Chapter 10

Conclusions

10.1 Overall Conclusions

With the advance of power electronics technologies and the increasing number of equipment being supplied by power electronic devices, power harmonics are drawing ever more attentions from engineers and researchers. Nowadays power harmonics include integer harmonics, sub-harmonics and inter-harmonics. The identification of power harmonics includes the estimation of frequencies, amplitudes and phases. The harmonics are time-invariant if the electrical power system is supplying a steady electrical load and the configuration of the electrical power system is not altered. This is a rare condition; therefore power harmonics analysis involves time-invariant as well as time-variant harmonics. A new power harmonics analysis needs to be developed which should be able to identify harmonic frequencies, amplitudes and phases in regardless of whether the harmonics are integer harmonics, sub-harmonics or inter-harmonics. Moreover the harmonic signal length required for the analysis should be very short such that the analysis results would not be fooled by variations in the harmonics amplitudes due to dynamic load changes and other power system configuration alternations.

Having identified the limitations of the existing DFT-based harmonic analysis in modern applications, a new method based on wavelet transform was developed for harmonic analysis. Given the properties of wavelet transform which is able to represent a time signal in the time-frequency plane, it is most suitable for harmonic analysis. In particular, the complex continuous wavelet transform (CWT) was used because of its property to preserve phase information.

In wavelet transform, the wavelet should be chosen with regard to the problems to be explored. The choice of a right mother wavelet is instrumental in extracting the right information from a signal. In Chapter 5, the simplified complex Morlet wavelet (CMW) was chosen for harmonic analysis. The shape of the CMW is smooth and harmonic-like. The CMW has the smallest Heisenberg box area; which means that it can achieve the best time-frequency localization. The CMW therefore is able to extract frequency information of a harmonic signal with the shortest signal length. The time-frequency localization of a CMW can be altered by the Q-factor of the wavelet which in turn is determined from its centre frequency and bandwidth parameter. The normalization factor of the CMW was modified for detecting harmonics of very small amplitudes. Wavelet ridges were employed to extract frequency and amplitude information of harmonic components in a harmonic signal. For a given setting of the modified CMW, the CWT has high frequency localization at low frequency and low frequency localization at high frequency. This is not a desirable feature for harmonic analysis. It was suggested in Chapter 5 that the centre frequency of the CMW would be adapted to the harmonic frequencies to be estimated so that the same frequency localization would be maintained for all harmonic frequencies.

The filter banks generated by dilating the modified CMW have finite bandwidths. To avoid aliasing due to overlapping of the filters in frequency domain, Chapter 6 presented a necessary condition for the discrimination of adjacent harmonic frequencies, by suitably choosing the Q-factor of the modified CMW. With the modified CMW, it was found that the minimum sampling frequency required without aliasing is dependent on the Q-factor of the modified CMW, which lies in the range of 2 to 2.9 times the highest harmonic frequency under investigation. The minimum signal length required for the harmonic analysis was then determined based on the support and the Q-factor of the modified CMW. The procedures of estimating initial phase information from the wavelet coefficients were presented.

A WT-based harmonic analysis algorithm was developed in Chapter 7. The proposed algorithm is implemented with FFT for fast and efficient computation. Computational formulae for estimating the centre frequency of the modified CMW for discriminating adjacent frequencies, minimum sampling frequency, minimum harmonic signal length, maximum scale and minimum scale were presented. It was suggested for accurate harmonic frequency estimation to determine scale dilation increments from the required

frequency resolution. Practical issues of computation of the proposed algorithm including edge effect and signal data number required for phase estimation were taken into account in deriving the computation algorithm.

In Chapter 8, the WT-based harmonic analysis algorithm was tested vigorously by synthesized harmonic signals and field harmonic signals respectively. From the results of the synthesized harmonic signal tests, the proposed algorithm was found to able to identify exactly the frequencies, amplitudes and initial phases of any harmonic signals with a very short signal length. The robustness and reliability of the WT-based harmonic analysis algorithm was verified by the field harmonic signal tests. DFT-based algorithm was also used for the tests in Chapter 8 for comparison.

A WT-based dynamic waveform reconstruction algorithm was then developed in Chapter 9 which is able to reconstruct the amplitude variations of the harmonic components in the harmonic signal with very high accuracy. The proposed algorithm was tested with synthesized waveforms and field harmonic waveforms respectively. From the results of the synthesized harmonic waveform tests, the proposed algorithm was able to reconstruct the harmonic waveform amplitude variations with error not greater than 3% in the worst case. The robustness and reliability of the proposed waveform reconstruction algorithm was verified by the field harmonic signal tests. Discrete wavelet transform based algorithm was also used for the tests in Chapter 9 for comparison of the reconstruction of the fundamental waveform.

Overall the WT-based harmonic analysis algorithm and dynamic waveform reconstruction algorithm are very effective and accurate in solving harmonic problems presented in this thesis. The only drawback of the algorithms is the computation time required. The proposed algorithms were implemented in Matlab standard software in Windows platform. The computation time would be effectively shortened by developing the computation algorithm in C++ language.

10.2 Areas for Further Research

Many researches can be developed based on the studies presented in this thesis.

Upon solving the problem on computation time, a prototype power harmonics measurement device would be developed based on the proposed WT-based algorithms for real time power harmonics monitoring.

In [3], the trial IEEE Std. 1459-2000 proposes new definitions for the measurement of electric power quantities under sinusoidal, nonsinusoidal, balanced or unbalanced conditions. The new standard gives due considerations to the proliferation of nonlinear loads, and addresses their effects on the electrical power system and traditional power measurement instruments. New definitions of power quantities are suggested in the trial standard for appropriate instrumentation design. The WT-based harmonic analysis and waveform reconstruction algorithms proposed in this thesis is able to extract frequency and time information from the harmonic signal; these provide means for the estimation of instantaneous powers under sinusoidal and nonsinusoidal conditions. The new definitions suggested in the trial standard would be further developed based on wavelet coefficients.

Although the main objective of the thesis is to develop a new power harmonics analysis algorithm based on wavelet transform, the algorithm suggested has the important feature that can be further developed for the analysis of oscillatory transients, which are typically caused by line switching, capacitor switching and load switching. An integrated approach would also be developed based on the WT-based harmonic analysis and waveform reconstruction algorithms suggested in this thesis and DWT-based power disturbance analysis algorithm for comprehensive power quality analysis.

References

1   John Stones and Alan Collinson, "*Power quality*," Power Engineering Journal, IEE, pp. 58-64, April 2001.

2   *IEEE Recommended Practice for Monitoring Electric Power Quality*, IEEE Std 1159:1995.

3   *IEEE Trial-Use Standard, Definitions for the Measurement of Electric Power Quantities under Sinusoidal, Nonsinusoidal, Balanced, or Unbalanced Conditions*, IEEE Std 1459-2000.

4   *Voltage Characteristics of Electricity Supplied by Public Distribution Systems*, BSEN50160:2000.

5   *IEEE Recommended Practices and Requirements for Harmonic Control in Electrical Power Systems*, IEEE Std.519-1992.

6   Carbone R., Testa A., Menniti D., Morrison R. E. and, Delaney E. "Harmonic and inter-harmonic distortion in current source type inverter drives," IEEE Trans. Power Delivery, Vol.. 10, No. 3, pp. 1576-1583, July 1995.

7   Leon M. Tolbert, Harold D. Hollis and Peyton S. Hale, Jr., "*Evaluation of harmonic suppression devices*," IEEE, 1996 Industry Applications Society annual meeting, pp. 2340-2347, Oct 1996.

8   Jih-Sheng Lai and Thomas Key, "*Effectiveness of harmonic mitigation equipment for commercial office buildings*," IEEE, 1996 Industry Applications Society annual meeting, pp. 2340-2347, Oct 1996.

9   Robert L. Almonte, "*Harmonics at the utility industrial interface: a real world example*," IEEE Trans. Ind. Appli., Vol. 31, No. 6, Nov 1995.

10   Conroy E., *"Power monitoring and harmonic problems in the modern building,"* Power Engineering Journal, IEE, April 2001.

11   Arrillaga, J., Bradley, D. A., Bodger, P. S., *Power system harmonics*, John Wiley and Sons, 1985.

12   Leszek S. Czarnecki and Tadeusz Swietlicki, *"Powers in nonsinusoidal networks: their interpretation, analysis and measurement,"* IEEE Trans. Instru. And Meas., Vol. 39, No. 2, pp. 340-345, April 1990.

13   V. E. Wagner, *"Effects of harmonics on equipment, report of the IEEE task force on the effects of harmonics on equipment,"* IEEE Trans. on Power Delivery, Vol. 8, No. 2, April 1993.

14   IEEE Task Force on the Effects of Harmonics on Equipment, *"Effects of Harmonics on Equipment,"* IEEE Trans. Power Delivery, Vol. 8, No. 2, pp. 672-680, April 1993.

15   Alexander E. Emanuel, John A. Orr, David Cyganski and Edward M. Gulachenski, *"A survey of harmonic voltages and currents at the customer's bus,"* IEEE Trans. Power Delivery, Vol. 8, No. 1, pp. 411-421, January 1993.

16   Guy Lemieux, *"Power system harmonic resonance - a documented case,"* IEEE Trans. Industry Applications, Vol. 26, No. 3, pp. 483-488, MayJune 1990.

17   Brozek J.P., *"The Effects of Harmonics On Overcurrent Protection Devices,"* IEEE Trans. IAS, pp. 1965-1967, 1990.

18   Douglas S. Dorr, Thomas M. Gruzs, M. Brent Hughes, Robert E. Jurewicz, Gurcharn Dang and John L. McClaine, *"Interpreting recent power quality surveys to define the electrical environment,"* IEEE, 1996 Industry Applications Society annual meeting, pp. 2251-2258, Oct 1996.

19   Weon-Ki Yoon and Michael J. Devaney, *"Reactive power measurement using the wavelet transform,"* IEEE Trans. Instrument & Measurement, Vol. 49 No. 2, pp. 246-252, April 2000.

20 Larry G. Durante and Prasanta K. Ghosh, "*Active power measurement in nonsinusoidal environment*," IEEE Trans. Power Systems, Vol. 15, No. 3, pp. 1142-1147, Aug. 2000.

21 IEEE working group on nonsinusoidal situations, "*Practical definitions for powers in systems with nonsinsoidal waveforms and unbalanced loads: a discussion*," IEEE Trans. Power Delivery, Vol. 11, No. 1, pp. 79-101, Jan 1996.

22 Thomas S. Key and Jih-Sheng Lai, "*Costs and benefits of harmonic current reduction for switch-mode power supplies in a commercial office building*," IEEE Trans. Industry Applications, Vol. 32, No. 5, pp. 1017-1025, Sept/Oct 1996.

23 Barhara B Hubbard, "*The world according to wavelets*," A K Peters Ltd., Wellesley, MA, 1996.

24 Y Meyer, "*Ondeletts, ondeletts et operateurs*," Paris: Hermann, 1990.

25 Stephane Mallet, *A wavelet tour of signal processing*, Academic Press, 1998.

26 Chan Y. T., *Wavelet basics*, Royal Military College of Canada, Kluwer Academic Publishers, 1995.

27 Gilbert Strang and Truong Nguyen, *Wavelets and Filter Banks*, Wellesley-Cambridge Press, Wellesley, MA, January, 1996.

28 Teolis, A., *Computational signal processing with wavelets*, Birkhauser, 1998.

29 Daubechies I., *Ten lectures on wavelets*, SIAM, Philadelphia, Pennylvania, 1992.

30 Amara Graps, "*Introduction to wavelets*," IEEE Computational Sciences and Engineering, 2(2), pp. 50-61, 1995,
URL:http://www.cis.udel.edu/~amer/CISC651/IEEEwavelet.pdf.

31 Robi Polikar, "*The story of wavelets*," In Physics and Modern Topics in Mechanical and Electrical Engineering (ed. N Mastorakis), pp. 192-197, World Scientic and Eng. Press,
URL:http://engineering.rowan.edu/%7epolikar/WAVELETS/WTutorial.ht.

32   Misiti, M., Misiti, Y., Oppenheim, G.: *"Wavelet Toolbox for use with Matlab,"* (The Mathworks Inc., March 1996), pp. 6-43.

33   Simonovski and M. Boltezar, *"The norms and variances of the Gabor, Morlet and general harmonic wavelet functions,"* Journal of Sound and Vibration, Academic Press, Elsevier Science Ltd., Vol. 264 pp. 545-557, 2003.

34   Christopher Torrence and Gilbert P. Compo, *"A practical guide to wavelet analysis,"* Bulletin of the American Meteorological Society, Vol. 79, No. 1, pp. 61-78, Jan 1998.

35   Chien-Hsing Lee, Yaw-Juen Wang and Wen-Liang Huang, *"A literature survey of wavelets in power engineering applications,"* Proc. Natl. Sci. Counc. ROC(A), Vol. 24, No. 4, pp. 249-258, 2000.

36   Chul Hwan Kim and Raj Aggarwal, *"Wavelet transforms in power systems, part 1 - general introduction to the wavelet transforms,"* Power Engineering Journal, IEE, pp. 81-87, April 2000.

37   Chul Hwan Kim and Raj Aggarwal, *"Wavelet transforms in power systems, part 2 - examples of application to actual power system transients,"* Power Engineering Journal, IEE, pp. 193-202, August 2001.

38   Shyh-Jier Huang, Cheng-Tao Hsieh, *"Application of continous wavelet transform for study of voltage flicker-generated signals,"* IEEE Trans. Aerospace and Electronic Systems, Vol. 36, No. 3, pp. 925-932, July 2000.

39   Zhang C., Y. Huang, X. Ma, W. Lu and G. Wang, *"A new approach to detect transformer inrush current by applying wavelet transform,"* The 1998 International Conference on Power System Technology, pp. 1040-1044, Beijing, P.R.C.

40   Pandey S. K. and L. Satish, *"Multiresolution signal decomposition: a new tool for fault detection in power transformers during impulse tests,"* IEEE Trans. Power Delivery, 13(4), pp. 1194-1200, 1998.

41   Terwiesch P., S. Menth and S. Schmidt, *"Analysis of transients in electrical railway networks using wavelets,"* IEEE Trans. Industrial Electronics, 45(6) pp. 955-959,

1998.

42   Chung J. and E. J. Powers, "*Variable rate power disturbance signal compression using embedded zerotree wavelet transform*," The 1999 IEEE/PES Winter Meeting, New York, NY, USA, 1999.

43   Santoso S., E. J. Powers, W. Grady and A. Parsons, "*Power quality disturbance waveform recognition using wavelet-based neural classifier, part 1: theoretical foundation*," The 1997 IEEE/PES Winter Meeting, New York, NY, USA, 1997.

44   Santoso S., E. J. Powers, W. Grady and A. Parsons, "*Power quality disturbance waveform recognition using wavelet-based neural classifier, part 2: application*," The 1997 IEEE/PES Winter Meeting, New York, NY, USA, 1997.

45   Santoso S., E. J. Powers and W. M. Grady, "*Power quality disturbance data compression using wavelet transform methods*," IEEE Trans. Power Delivery, 12(3), pp. 1250-1257, 1997.

46   Surya S., W. Mack Grady, E. J. Powers, J. Lamoree, S. C. Siddharth, "*Characterization of distribution power quality events with Fourier and wavelet transforms*," IEEE Trans. Power Delivery, Vol. 15, No. 1, pp. 247-254, Jan. 2000.

47   Santoso S., E. J. Powers, and W. M. Grady and P. Hoffman, "*Power quality assessment via wavelet transform analysis*," IEEE Trans. Power Delivery, 11(2), pp. 924-930, 1996.

48   Angrisani L., P. Daponte, M. D' Apuzzo, and A. Testa, "*A method based on wavelet networks for the detection and classification of transients*," IEEE Instrumentation Measurement Technology Conference, pp. 903-908, St. Paul, MN, USA.

49   L. Angrisani, P. Daponte, M.D' Apuzzo and A. Testa, "*A measurement method based on the wavelet transform for power quality analysis*," IEEE Trans. Power Delivery, Vol. 13, No. 4, pp. 990-998, Oct. 1998.

50   L L Lai, W L Chan, C T Tse and A T P So, "*Real-time frequency and harmonic evaluation using artificial neural networks*," IEEE Trans. on Power Delivery, Vol. 14, No. 1, January 1999, pp. 52-59.

51   W L Chan, A T P So and L L Lai, *"Harmonics load signature recognition by wavelets transforms"*, Proceedings of the International Conference on Electric Utility Deregulation, Restructuring and Power Technologies DRPT2000, IEEE Catalog Number 00EX382, April 2000, pp. 666-671.

52   Chaari O. M. Meunier and F. Brouaye, *"Wavelets: a new tool for the resonant grounded power distribution systems relaying*," IEEE Trans. Power Delivery, 11(3), pp. 1301-1308, 1996.

53   Islam Md. S., A. H. Samra and J. Andrian, *"Wavelet transform analysis arrestor voltage in surge motor protection,"* The 1996 IEEE Southern Bringing together Education, Science and Technology, pp. 305-308, Tampa, FL., USA.

54   Gomes-Morgante M. and D. W. Nicollete, *"A wavelet based differential transformer protection,"* The 1999 IEEE/PES Winter Meeting, New York, NY, USA, 1999.

55   Lee C. H., J. S. Lee, J. O. Kim and S. W. Nam, *"Feature vector extraction for the automatic classification of power quality disturbances,"* The 1997 IEEE International Symposium on Circuits and Systems, pp. 2681-2684, Hong Kong, PRC, 1997.

56   Galli A. W., *"Analysis of electrical transients in power systems via a noel wavelet recursive method,"* Ph.D Dissertation, Purdue University, Purdue, IN, USA.

57   Meliopoulos A. P. S. and C. H. Lee, *"Power disturbance analysis via wavelet domain equivalents,"* The 1998 International Conference on Harmonics and Quality of Power, pp. 388-394, Athens, Greece.

58   Weon-Ki Yoon and Michael J. Devaney, *"Power measurement using the wavelet transform,"* IEEE Trans. Instrument & Measurement, Vol. 47 No. 5, pp. 1205-1210, Oct. 1998.

59   Johan L. J. Driesen and Ronnie J. M. Belmans, *"Wavelet-based power quantification approaches,"* IEEE Trans. Instrument & Measurement, Vol. 52 No. 4, pp. 1232-1238, Aug. 2003.

60   V. L. Pham and K. P. Wong, *"Wavelet-transform-based algorithm for harmonic analysis of power system waveforms,"* IEE Proc. - Gener. Transm. Distrib., Vol. 146, No. 3, May 1999.

61   Paul S Addison, *The Illustrated Wavelet Transform Handbook*, Institute of Physics Publishing Ltd., Bristol and Philadelphia, 2002.

62   Steven W. Smith, *Digital signal processing: a practical guide for engineers and scientists*, Newnes, 2002.

63   Robert W. Ramirez, *The FFT : fundamentals and concepts*, Englewood Cliffs, N.J., Prentice-Hall, 1985.

64   Xie Ming and Ding Kang, *"Corrections for frequency, amplitude and phase in a fast Fourier transform of a harmonic signal,"* Mechanical Systems and Signal Processing (1996) 10(2), pp. 211-221.

65   Adly A. Girgis, *"A Quantitative Study of Pitfalls in the FFT,"* IEEE Trans. Aerospace & Electronic Systems, Vol. AES-16, No. 4, pp. 434-439, July 1980.

66   Oppenhem, A. V. and Schafer, R. W., *"Discrete-time signal processing,"* Prentice Hall Inc., Englewood Cliffs, New Jersey, 1989.

67   Z. L. Qiu and A. K. Tieu, *"A method to obtain exact frequency characteristics of harmonic signals,"* Mechanical Systems and Signal Processing (1999) 13(3), pp. 523-529.

68   D. Kang, X. Ming and Z. Xiaofei, *"Phase difference correction method for phase and frequency in spectral analysis,"* Mechanical Systems and Signal Processing (1999) 14(5), pp. 835-843.

69   Shyh-Jier Huang, Cheng-Tao Hsieh and Ching-Lien Huang, *"Application of morlet wavelets to supervise power system disturbances,"* IEEE Trans. On Power Delivery, Vol. 14, No. 1, Jan., 1999.

70   N. G. Kingsbury, *"Complex wavelets for shift invariant analysis and filtering of signals,"* Journal of Applied and Computational Harmonic Analysis, Vol. 10, No. 3,

pp. 234-253, 2001.

71 Norman C. F. Tse and L. L. Lai, "*Wavelet-based algorithm for signal analysis*," EURASIP Journal on Advances in Signal Processing, Vol. 2007, Article ID 38916.

72 John Sadowsky, "*Investigation of signal characteristics using the continuous wavelet transform*," Johns Hopkins APL Technical Digest, Vol. 17, No. 3, pp. 258-269, 1996.

73 René A. Carmona, Wen L. Hwang and Brun Torrésane, "*Characterization of signals by the ridges of their wavelet transforms*," IEEE Trans. Signal Processing, Vol. 45, No. 10, pp. 2586-2590, Oct. 1997.

74 D. E. Newland, "*Ridge and phase identification in the frequency analysis of transient signals by harmonic wavelets*," Journal Vibration and Acoustics, ASME, Vol. 121, pp. 149-155, April 1999.

75 Heng Liu, Alexander N. Cartwright and Cemal Basaran, "*Moire interferogram phase extraction: a ridge detection algorithm for continuous wavelet transforms*," Applied Optics, Vol. 43, No. 4, pp. 850-857, Feb. 2004.

76 R. Carmona, W.L. Hwang, and B. Torrésani. "*Characterization of signals by the ridges of their wavelet transform*," IEEE Trans. on Signal Processing, 45(10):2586, 1997.

77 Norman C F Tse, "*Practical application of wavelet to power quality analysis*", Proceedings of the 2006 IEEE Power Engineering Society General Meeting, IEEE Catalogue Number 06CH37818C, June 2006, CD ROM.

78 D. Jordan, R. W. Miksad and E. J. Powers, "*Implementation of the continuous wavelet transform for digital time series analysis*," Rev. Sci. Instrum. 68(3), pp.1484-1494, March 1997.

79 Rene A. Carmona, Wen L. Hwang and Bruno Torresani, "*Multiridge detection and time-frequency reconstruction*," IEEE Trans. on Signal Processing, Vol. 47, No. 2, Feb., 1999.

80   Norman C F Tse and L. L. Lai, "*Wavelet-based algorithm for detection of voltage fluctuation,*" The 6th International Conference on Advances in Power System Control, Operation and Management, IET Hong Kong APSCOM2006, CD-ROM (Paper - APSCOM2006-509).

81   V. L. Pham and K. P. Wong, "*Antidistortion method for wavelet transform filter banks and nonstationary power system waveform harmonic analysis*" IEE Proc. - Gener. Transm. Distrib., Vol. 148, No. 2, March 2001

82   Math H. J. Bollen, "*Voltage sags: effects, mitigation and prediction,*" Power Engineering Journal, IEE, pp. 129-135, June 1996.

83   Karen L. Butler-Purry and Mustafa Bagriyanik, "Characterization of transients in transformers using discrete wavelet transforms," IEEE Trans. Power System, Vol. 18, No. 2, pp. 648-656, May 2003.